JOURNAL OF CAVE AND KARST STUDIES

December 2021
Volume 83, Number 4
ISSN 1090-6924
A Publication of the National Speleological Society

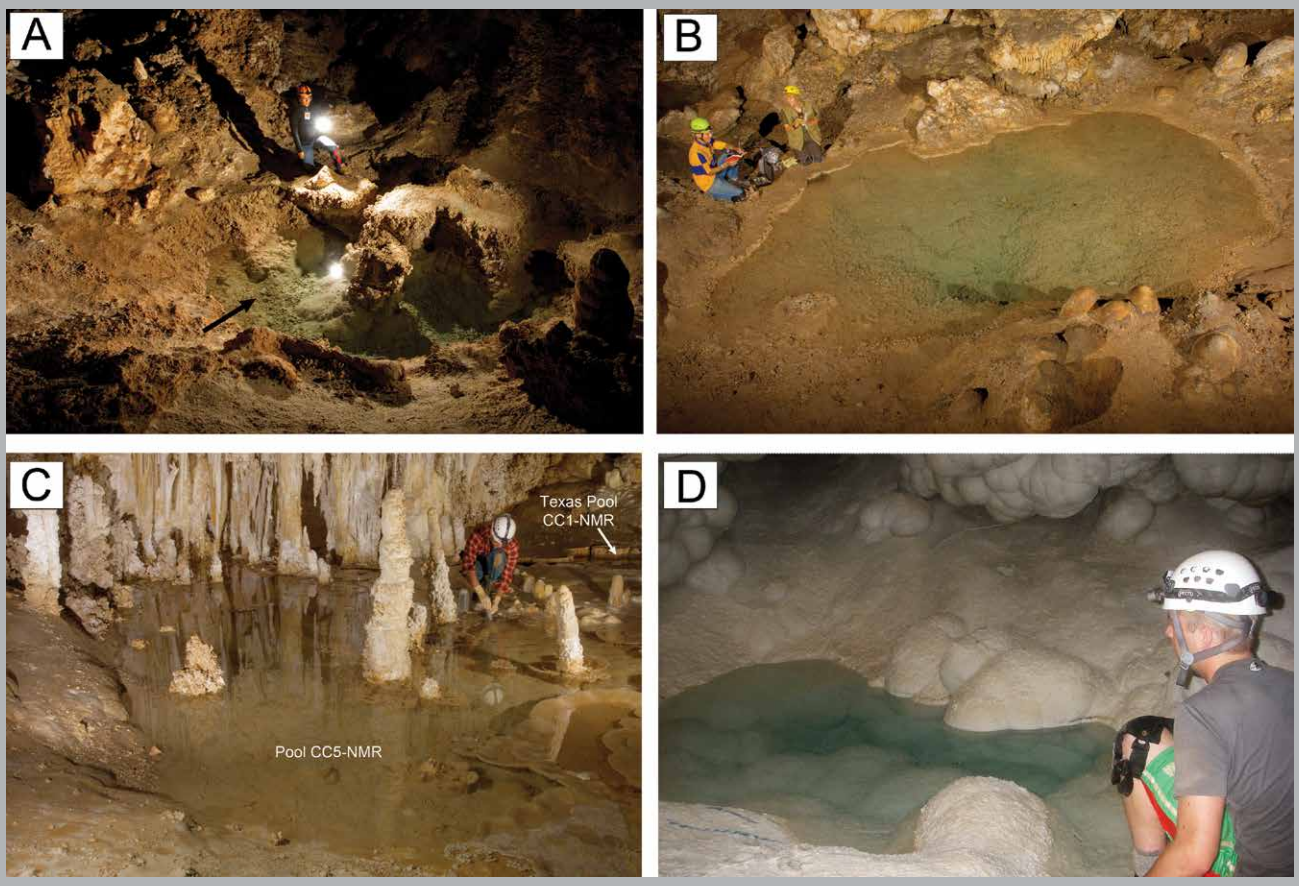

DEDICATED TO THE ADVANCEMENT OF SCIENCE, EDUCATION, EXPLORATION, AND CONSERVATION

Published By
The National Speleological Society

http://caves.org/pub/journal

Office
6001 Pulaski Pike NW
Huntsville, AL 35810 USA
Tel:256-852-1300
nss@caves.org

Editor-in-Chief
Malcolm S. Field
Washington, DC
703-347-8601
field.malcolm1@gmail.com

Production Editor
Scott A. Engel
Knoxville, TN
225-281-3914
saecaver@gmail.com

The *Journal of Cave and Karst Studies* , ISSN 1090-6924, CPM Number #40065056, is a multi-disciplinary, refereed journal published four times a year by the National Speleological Society. The *Journal* is available by open access on its website, or check the website for current print subscription rates. Back issues are available from the NSS office.

POSTMASTER: send address changes to the National Speleological Society Office listed above.

The Journal of Cave and Karst Studies is covered by the following ISI Thomson Services Science Citation Index Expanded, ISI Alerting Services, and Current Contents/Physical, Chemical, and Earth Sciences.

Front cover: Representative cave pools in the study by Read et al. in this issue.

Alexandra Tsalickis, Matthew N. Waters, and Joshua W. Campbell. Methods and analysis of bat guano cores from caves for paleoecology. *Journal of Cave and Karst Studies*, v. 83, no. 4, p. 141-150. DOI:10.4311/2020ES0104

METHODS AND ANALYSIS OF BAT GUANO CORES FROM CAVES FOR PALEOECOLOGY

Alexandra Tsalickis[1,C], Matthew N. Waters[1], and Joshua W. Campbell[2]

Abstract

Whereas bat guano is gaining viability in accurately reconstructing local paleoenvironmental and climatic conditions, overall reviews of methods for analyzing and collecting bat guano cores have received less attention. Guano cores have been collected from several locations (e.g., United States, Romania, Philippines, and southeast Asia), and the processing and collection methods are quite similar despite a lack of standardized techniques. Physical, chemical, and elemental analyses on guano samples have focused on the interpretation of precipitation changes over time, with additional applications from stable isotope analysis being used for other paleoenvironmental conditions. We obtained three bat guano cores from Alabama and Tennessee to evaluate the collecting and processing techniques of guano. Climatic temperature changes were not analyzed in this study. The purpose of this investigation was to summarize multiple techniques and approaches used to process and analyze bat guano cores with a focus on reconstructing paleoclimate in cave environments throughout the globe. From these three cores, we describe challenges and make recommendations for improving guano analysis.

INTRODUCTION

Traditional methods of assessing paleoclimate include analyzing samples from lacustrine sediments, ice, pollen, and even soils. However, these sample types are limited to specific geographic areas. For example, glacial lakes can provide Holocene climatic histories but are limited to upper latitudes or high altitudes. In areas such as the southeastern United States, glacial lakes do not exist. Ice cores can only be obtained from ice-covered regions such as polar areas and high-altitude glaciers and cannot provide local climate histories (Jouzel and Masson-Delmotte, 2010). Furthermore, lakes tend to occur clustered in specific regions, thus limiting extensive distribution. Similarly, caves are clustered in specific regions and provide variable conditions for habitation by bats and for the accumulation and preservation of guano deposits. Some species such as *Myotis grisescens* (gray bats), roost in the same caves each year depositing annual laminations of guano into mounds (Martin, 2007). Insectivorous bat guano has been useful in paleoecological studies by tracking moisture and precipitation through stable isotope analysis, elements, nutrients, and radiocarbon dates (Bird et al., 2007; Wurster et al., 2008, 2010; Onac et al., 2014; Forray et al., 2015; Choa et al., 2016; Cleary et al., 2016, 2018, 2019). Thus, bat guano can be key for reconstructing the paleoclimate in areas where traditional methods are not available.

Insectivorous bat guano is comprised of multiple constituents such as bat-associated materials (pollen, bat hair, skin cells, feces, and dander), as well as extraneous materials (guanivorous and fungivorous invertebrates that burrow through the guano, the invertebrates frass, fungal hyphae and spores, and microbes that grow in the guano) making analysis indirect and complicated. Bat hair accumulates in guano piles through grooming during roosting activity. Insectivorous gray bats produce chitin-rich guano, which decomposes over time causing older deposits to lack discernible chitin that is more prevalent in younger deposits. Ambient pollen grains stick to bat hair as they fly in search for insects to consume, which themselves carry pollen (Maher, 2006). While roosting on cave ceilings, pollen falls off bat hair and into guano piles. Bats also ingest pollen, which passes through their intestinal tract via grooming or consuming pollen-laden insects. Pollen, hair, and chitin can provide individual data when analyzed alone; bat hair provides phylogenetic insight; stable isotopes in chitin provide information about local vegetation and precipitation; and pollen provides information on local vegetation changes. Collectively, these tools create a robust paleoclimatic record.

Bat guano has been shown to track moisture regimes and changes in local vegetation over the duration of the Holocene (11,650 YBP) and even into the Pleistocene (2.6 Ma – 11,700 YBP) (Wurster et al., 2008, 2010; Campbell et al., 2017). Although bat guano has only recently been exploited as a paleoclimate tool, more studies are utilizing its potential in providing information about local paleoenvironmental conditions that are both reliable and reproducible (Shahack-Gross et al., 2004; Onac et al., 2014; Forray et al., 2015; Choa et al., 2016; Campbell et al., 2017, Gallant, et al., 2020). Bat guano found inside caves is protected from surficial weathering, providing a uniquely unaltered data source (Onac et al., 2014; Cleary et al., 2016). Bat guano can sometimes provide high-resolution age-depth models

[1]Department of Crop, Soil, and Environmental Sciences, Auburn University, Auburn, AL
Current Affiliation: Clemson University, Department of Forestry and Environmental Conservation, 261 Lehotsky Hall Box 3403317, Clemson, SC
[1]Department of Crop, Soil, and Environmental Sciences, Auburn University, Auburn, AL
[2] USDA-ARS, Northern Plains Agricultural Research Laboratory, Sidney, MT
[C]Corresponding author: atsalic@g.clemson.edu

with constant deposition rates as maternity colonies and/or hibernacula of bats roost in the same caves each year (Martin, 2007). To further guano research and expand on paleoclimatic records, we present the physical, chemical, and biological characteristics of three guano cores and potential methods to provide a reproducible procedure for processing guano. In the first portion of this paper, we will review methods and analyses performed in other bat guano studies (Table 1), and in the second portion we discuss methods and analyses used on our three bat guano coring experiments with recommendations for challenges confounding guano interpretation.

METHODS REVIEW

Field Collection Methods

Various extraction procedures have been utilized when coring bat guano. Wurster et al. (2010) used two 1 m length pieces of PVC (polyvinyl chloride) that had a diameter of 5 cm. The PVC pipes were driven into the guano pile and sealed causing the pipes to be removed with no excavation. It is ideal to avoid excavation to preserve the remaining guano pile and prevent any further disturbance to the natural cave setting. Similarly, Campbell et al. (2017) used aluminum tubes to core by manually pushing them into a guano pile. One drawback for these methods is compaction of the guano during collection. Campbell et al. (2017) noted compaction of the guano core by 59 % and Wurster et al. (2010) noted compaction of the guano core by 65 %. Compaction can cause the temporal resolution to alter and may negatively impact analysis when producing an age-depth model. One benefit of using PVC pipes or aluminum tubes to core guano is that it is a less expensive alternative to some other methods described further.

A standard Livingstone piston sampler has also been used in guano studies (Maher, 2006). To use a standard Livingstone piston sampler, the piston cable is anchored, and the corer is pushed into the guano mound. Maher (2006) wrapped the core barrel in plastic foil when it was removed to avoid handling adhering feces. Maher (2006) does note compaction (50 %) occurring with this type of corer. Additionally, a large coring system such as a piston sampler could be difficult to transport to the sample site in some cave systems.

A Russian peat corer is another method used to sample guano (Geantă et al., 2012; Forray et al., 2015; Cleary et al., 2016). Forray et al. (2015) notes their corers were one meter long and five cm in diameter. Studies that have used Russian peat corers for guano collection do not comment on any compaction that occurs. Therefore, to prevent compaction, a Russian peat corer could be ideal provided the system can be transported through the cave as mentioned above.

Sample Processing and Handling Methods

Different sampling preparations have been used in guano studies and all have been successful. Wurster et al. (2010) brought guano cores to the laboratory where they were later opened and sectioned by wetting the guano with deionized water to prevent mixing during the sampling process. Their guano cores were sectioned at four- and eight-mm intervals. Campbell et al. (2017) stored guano cores at -80°C until they were ready for sampling and sectioned their cores at 2 cm intervals. While some sampling methods occurred in laboratories (Mizutani et al., 1992; Maher 2006; Wurster et al., 2010; Campbell et al., 2017), other sampling methods occurred right after guano core extraction in the cave (Cleary et al., 2016) to reduce potential contamination of the core during transport. Forray et al. (2015) and Cleary et al. (2016) both sectioned guano cores at two cm intervals.

Table 1. Comparison of methods from existing literature.

Literature Explored	Core Collection	Isotopes Analyzed	Number of ^{14}C dates	Pollen Analyzed?	Oldest ^{14}C Date (YBP)
Cleary et al., 2019	Russian peat corer	$\delta^{13}C$, $\delta^{15}N$	12	Yes	810
Cleary et al., 2018	Russian peat corer	$\delta^{13}C$, $\delta^{15}N$	20	Yes	1,069
Campbell et al., 2017	Aluminum tubes	$\delta^{13}C$, $\delta^{15}N$	5	Yes	5,950
Royer et al., 2017	Excavation of cave floor	$\delta^{13}C$, $\delta^{15}N$	16	No	34,640
Cleary et al., 2016	Russian peat corer	$\delta^{15}N$	3	No	940
Forray et al., 2015	Russian peat corer	$\delta^{13}C$, $\delta^{15}N$	12	Yes	940
Royer et al., 2015	Plastic film placed below bat roosts	$\delta^{13}C$, $\delta^{15}N$	0	No	N/A
Onac et al., 2014	Excavated floor below bat roost	$\delta^{13}C$	3	No	670
Geantă et al., 2012	Russian peat corer	None	10	Yes	855
Wurster et al., 2010	PVC pipes	$\delta^{13}C$, $\delta^{15}N$, and δD	2	No	15,300
Bird et al., 2007	Excavated floor below bat roost	$\delta^{13}C$, $\delta^{15}N$	2	No	29,990
Wurster et al., 2007	Scooped surface of guano mound	$\delta^{13}C$, $\delta^{15}N$	0	No	N/A
Maher, 2006	Livingstone piston sampler	None	1	Yes	2,890

Prior to sample analysis methods, guano typically requires pre-treatments for various measurements. Most studies used dried guano samples and homogenized them in an agate mortar (Forray et al., 2015; Cleary et al., 2016; Campbell et al., 2017). Mizutani et al. (1992), used two different methods to dry guano: 1) samples were dried at 60 °C for 24 hours soon after collection; and 2) samples were dried after 17 days at ambient temperature by using a Labconco FDC-8 freeze dryer. Mizutani et al. (1992) noted neither drying method affected isotope values. Wurster et al. (2010) provides several different detailed extraction procedures used in their study to isolate organic matter components from bulk guano. Overall, the simplest way to prepare guano samples for analysis is to combine freeze drying with grinding in an agate mortar.

Sample Analysis Methods

Methods for Stable Isotopes

Isotopic analysis is important for determining changes in paleoenvironmental conditions. $\delta^{13}C$ and $\delta^{15}N$ are used to show changes in vegetation type through time while δD is used to show changes in hydrologic conditions over time. Some bat guano studies only performed isotopic analysis on $\delta^{13}C$, $\delta^{15}N$, or both (Mizutani et al., 1992; Forray et al., 2015; Royer et al., 2015; Cleary et al., 2016; Campbell et al., 2017; Royer et al., 2017; Cleary et al., 2018, 2019) while other studies performed isotopic analysis on all three isotopes $\delta^{13}C$, $\delta^{15}N$, and δD (Wurster et al., 2010). Some studies performed isotopic analyses at their own laboratory such as Wurster et al. (2010) using continuous-flow-isotope-ratio mass spectrometry (CF-IRMS) to determine $\delta^{13}C$ and $\delta^{15}N$. They used a ThermoFinnigan Flash 1112 Elemental Analyzer coupled by a ConFlo III to a ThermoFinnigan Delta XL Plus mass spectrometer. $\delta^{13}C$ and $\delta^{15}N$ values were determined for each section in the guano core. They also determined δD by using high-temperature flash pyrolysis CF-IRMS using a ThermoFinnigan High Temperature Conversion Elemental Analyzer (TC/EA) coupled through a ThemoFinnigan ConFlo III to a ThermoFinnigan Delta XL Pluss mass spectrometer. Other studies mailed subsampled sections of guano to other laboratories to be analyzed (Forray et al., 2015; Campbell et al., 2017).

Methods for ^{14}C

Obtaining ^{14}C values is necessary for determining the age of guano and creating an age-depth profile. ^{14}C values is something all guano studies have in common, however, what is not uniform is the quantity of radiocarbon dates collected. Wurster et al. (2010) collected only two ^{14}C dates: one at the surface of their guano core and the other at the bottom depth of 1.3 meters. Samples were sent to Beta Analytic (Miami, Florida). Campbell et al. (2017) used five samples from their core to establish a dating model with Beta Analytic performing the analysis. The five samples were chosen depending upon color changes or abrupt changes in guano texture. Forray et al. (2015) used twelve guano samples to obtain ^{14}C dates. While no set number is required, a greater number of samples analyzed provides a more robust dating model, but due to the cost of ^{14}C analysis, a minimum of three is recommended so that a trend line can be established showing age-depth relationships through time.

Methods for Elements/Nutrients

Elements and nutrients are not analyzed in every bat guano study. Those that do typically measure for C:N and N:H elemental ratios (Wurster et al., 2010) or TC (Total Carbon), TN (Total Nitrogen), and TP (Total Phosphorus) (Campbell et al., 2017). Campbell et al. (2017) measured bulk density by drying and weighing five mL aliquots of raw guano. They also measured loss on ignition by burning dried guano samples at 550 °C for three hours**.** Elemental analyses are typically measured on dried and homogenized guano.

Methods for Minerals

Few guano studies have thoroughly analyzed minerals in bat guano. Detailed methods for mineral analysis are explained in Giurgiu and Tămaş (2013). Giurgiu and Tămaş (2013) used X-ray diffraction, scanning electron microscopy, and electron dispersive spectroscopy to analyze mineral samples. Their analyses revealed the presence of multiple phosphate minerals: brushite, hydorxylapatite, leucophosphite, taranakite, variscite, gypsum, calcite, and illite-group minerals and quartz. Forray et al. (2015) analyzed minerals in their study by using a Bruker D8 Advance diffractometer with cobalt anode ($CoKa_1$ with ¼ 1.78897), Fe filter for the Kb line, and a one-dimensional LynxEye detector, using corundum (NIST SRM1976a) as the standard for instrument alignment.

Methods for Chitin Analysis

Chitinous insect fragments can be separated from guano to use for analysis and Wurster et al. (2010) provides a thorough description of their methods. They created solvent-extracted guano from bulk guano and neutralized the guano in H_2O. After neutralization, the guano was washed once in methanol and three times in chloroform/methanol with a 2:1 ratio. Finally, samples were lypholized. Wurster et al. (2010) used Fourier-Transform Infrared Spectroscopy to investigate chitin. Chitin can also be used to obtain stable isotope values, but no studies were found that performed such analysis.

Methods for Pollen

Pollen provides evidence for local vegetation types and can remain preserved for millions of years (Whitehead, 1973; Delcourt, 1980; Geantă et al., 2012). The pollen that accumulates in guano needs to be separated out from the other constituents through rinsing and repeated centrifugation (Rich, 1979). After pollen separation is complete, the pollen grains must be stained for slide preparation and identification under a microscope (Halbritter et al., 2018). Identifying pollen grains is a difficult task and should be accomplished by a trained individual. Pollen was not identified in guano cores collected for this project, but pollen analysis has been successfully applied to guano cores from the southeastern United States (Campbell et al. 2017). However, less is known concerning pollen delivery and the link between local vegetation and pollen occurrence is still needed.

Campbell et al. (2017) describes the typical routine of pollen analysis includes counting at least 300 identifiable grains and calculating percentages of individual taxa based on that sum. However, not all guano core samples will have abundant pollen, so a compromised version can be performed. To prepare guano samples for pollen analysis, Campbell et al. (2017) placed guano samples in 10 % KOH and immersed them in a boiling water bath for 10 minutes and then washed clean of water-soluble humic substances using distilled water and centrifugation. Once completed, residues were mixed with glycerine jelly and prepared on slides.

According to Maher (2006), guano can be processed as if it were lake sediment using standard palynology procedures without using the 10 % HCl and 10 % NaOH treatments because the guano is too acidic to contain much carbonate. This method has successfully been used in several guano studies (Geantă et al., 2012; Cleary et al., 2018, 2019). Maher (2006) recommends washing guano in warm water containing a trace amount of dish-washing detergent, followed by 5 to 10 minutes of acetolysis solution in a boiling water bath, staining, and mounting in glycerine.

Methods for Charcoal

Charcoal can be used to determine the presence of fire. We did not analyze microcharcoal in this experiment, however, it has been successfully analyzed in other bat guano studies (Forray et al., 2015). To analyze charcoal, add 5−10 mL of KOH to one gram of guano and then centrifuge for three minutes. Discard supernatant and dilute with H_2O_2 (4−6 %) and allow it to settle overnight. Mix and sieve through a 125µm sieve and rinse with deionized water. The sieve containing the guano is kept in a drying oven until all moisture is removed. Contents are emptied into a petri dish with graph paper underneath to visually inspect and count charcoal pieces under a binocular microscope. Charcoal accumulates in caves via water, wind, and bats (Forray et al., 2015). In congruence with a pollen record, charcoal can be used to assess fire histories, changes in vegetation structure, anthropogenic activities, and local climate (Forray et al., 2015). Additionally, Campbell et al. (2017) found evidence of Woodland Indian campfires within a guano core.

Data Analysis Methods

Age-Depth Model

A critical component to paleoclimate studies is to construct accurate age models from radioisotopic measurements. Radiocarbon dating provides an effective way to age a guano core since guano usually does not date back farther than 40,000 YBP. However, there are a few exceptions to this generalization: (1) ^{14}C dates cannot be obtained in brushite or mineral layers because dates will not be in a chronologic order and will show an inversion, and (2) as ^{14}C dates cannot date past 40,000 YBP, guano cores cannot be dated beyond this time limit, deeming ^{14}C ineffective.

Forray et al. (2015) used an age-depth model based on linear interpolation between all ^{14}C dates using the clam package in R software. Age-depth models can also be extended to the full length of the core, even if ^{14}C dates were not collected at the bottom of cores. Once ^{14}C dates are obtained, the Bayesian accumulation history (BACON) age-depth modelling package in R software can be used to project ages throughout guano cores with a 95 % confidence interval (Blaauw and Andrès, 2011). BACON works by dividing a core into multiple vertical sections and subsequently uses millions of Markov Chain Monte Carlo iterations to estimate the accumulation rate for each section in years/cm (Blaauw and Andrès, 2011).

CORING EXPERIMENT

To provide examples and compare the efficacy of a majority of the analyses mentioned above, three guano cores collected from the southeastern United States were analyzed to demonstrate the diversity of paleoenvironmental data in guano deposits. The three guano cores were collected from: (1) Cave Springs Cave in Priceville, Alabama, (2) Cripps Mill Cave in Cookeville, Tennessee, and (3) Nunley Mountain Cave in McMinnville, Tennessee.

Core Collection

Access for caves was granted by private landowners or filling out permits for access to protected caves on government property. The gray bat, *Myotis grisescens*, is the primary species in the three caves visited during this study in northern Alabama and Tennessee. Locations within each cave for guano coring were chosen based on availability and height of the guano pile. Ideal height for guano coring for this study was about two meters. Prior to coring, driving a

thin metal rod or wooden dowel was used to test depth of a guano pile, or ground penetrating radar, if available. Once chosen, one-meter sections of PVC pipes were hammered into the pile with a mallet. Diameter of the PVC pipes were about five cm to provide enough guano material for the analytical techniques applied to each sample. A minimum of five cm in diameter is our recommended size for core tubes. To decrease disturbance, guano core sections were dug out so as not to compromise lower guano core sections and to limit modern guano from falling into the core hole. In addition, hammering PVC pipe caused compaction. A Russian peat corer was not used in our studies, but it has proven to be successful in other studies (Geantă et al., 2012; Forray et al., 2015; Cleary et al., 2016). Cores must be kept upright after collection and frozen until ready to section, which can be challenging if cores are obtained long distances from cave entrances. Thus, extraneous material (e.g., newspaper, cotton, etc.) may be used to fill portions of the coring container that are unoccupied by guano to limit movement of the top sections of loose guano.

Core Processing

We stored our guano cores in a walk-in freezer to maintain their integrity and prevent any contamination. PVC pipes were cut open by using a circular saw and sliced down the pipe on opposing sides. Our cores were sectioned at one cm intervals. Based on our literature review, one cm is the smallest scale typically used in sectioning bat guano (Wurster et al., 2010; Geantă et al., 2012; Forray et al., 2015; Cleary et al., 2016; Campbell et al., 2017; Royer et al., 2017). If possible, a smaller scale can be used to create a higher resolution in the radiocarbon dating model and isotopic profile, but limitation of material could occur based on the number of analyses performed. Before sectioning the guano core, radiocarbon dates were chosen observationally in each of the guano cores. We picked samples at the top and bottom of each of the cores to retrieve the best age estimates. Our guano samples were analyzed by Beta Analytic Laboratories for radiocarbon dates.

Once sectioned, each centimeter was analyzed for organic matter as loss on ignition (LOI) when heated to 550 °C for four to five hours. Bulk density was calculated as (g dry cm^{-3} wet) using the proportion of dry/wet mass and organic/inorganic content like methods performed in limnology studies by Brenner et al. (1999) (Fig. 1). For chemical analyses one cm sections were freeze dried, ground with a mortar and pestle, and sent to Waters Agricultural Laboratories (Camilla, Ga.) for elemental and nutrient data using an ARL ICP instrument. Dried and ground guano samples were sent to UC Davis Stable Isotope Facility (Davis, CA) for $\delta^{13}C$ and $\delta^{15}N$ isotopes and to Cornell University Stable Isotope Laboratory (Ithaca, NY) for δD isotopes.

Sample Analysis

Methods for Insect Separation

To separate insect chitin, one gram of guano was put in a vial along with 10 mL of a 1 % solution of detergent to break apart the guano. The vial was then put on a vortex mixer for 10 seconds followed by a hot water bath for 10 minutes and sonication for 10 minutes. After this, the guano solution sat for 24 hours and the following day was sieved through a 120 µm screen with hot water followed by deionized water. After samples dried in an oven, they were brushed out of sieves and placed in petri dishes for separation using forceps under a dissecting microscope (Fig. 2). While this method could be used to reconstruct insect consumption through time by volume of identified chitin fragments recovered from samples and species (if able to identify from chitin pieces), it appears that application is limited to modern guano samples. Degradation of deeper insect samples showed a decomposition of insect parts where individual parts were not recognizable. Chitin fragments were not identified in this study but may be able to be identified to Order level in the top portion of cores where less degradation occurred. Not all types of

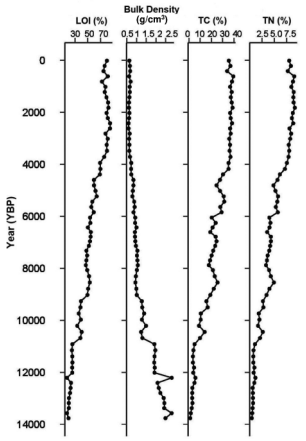

Figure 1. Organic matter content analysis in Cave Springs core. Bulk density increases with depth. Total carbon (TC), Total nitrogen (TN), and loss on Ignition (LOI) decrease with depth.

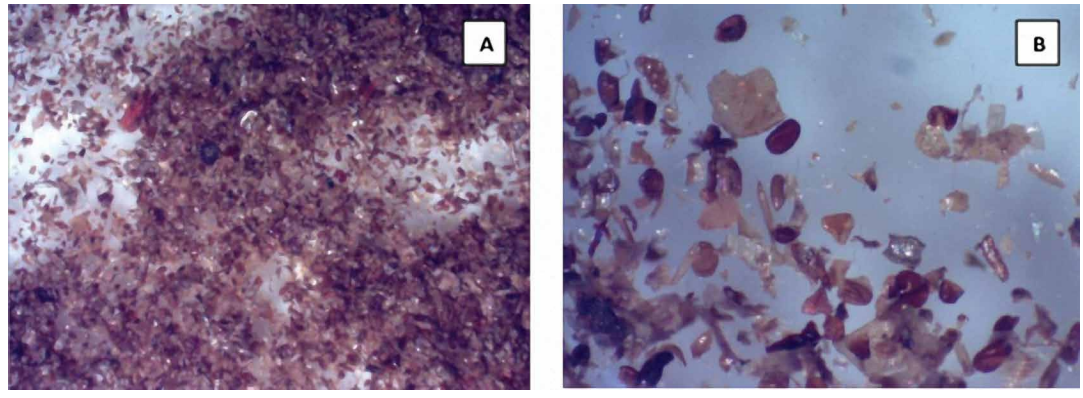

Figure 2. Insect chitin in bat guano. Pictures are taken under a dissecting microscope A) 20× magnification and B) 40× magnification.

insects were equally preserved and equally recognizable by isolated body parts, but undoubtedly, many soft-bodied insects are completely digested and will not leave any traces behind. This phenomenon may differ in caves in other regions that have a different climatic history or invertebrate fauna.

Climatic Temperature Analysis

While many studies have utilized bat guano as a proxy for moisture regimes (Wurster et al., 2007, 2010; Forray et al., 2015; Choa et al., 2016; Cleary et al., 2016; Campbell et al., 2017; Gallant et al., 2020), none have reconstructed paleotemperature conditions. It may be possible to use $\delta^{13}C$ in combination with a pollen record to determine the local vegetation type over time and what the temperature requirements would have been for those plants to thrive. In our studies, we have identified distinctions between C_3 and C_4 plant dominance throughout time by using $\delta^{13}C$ values. C_3 plants are between −32 ‰ and −20 ‰, C_4 plants are between −17 ‰ and 9 ‰, and CAM plants range between the two from −14 ‰ to −33 ‰ (Bender et al., 1973; Choa et al., 2016; Des Marais et al., 1980).

RESULTS AND DISCUSSION

Physical Characteristics of Guano Cores

Bat guano cores vary in their physical and elemental components. The Cave Springs Cave guano core contained many colored striations that varied from tan to dark brown (Fig. 3). The Cripps Mill guano core from Tennessee showed no striations in color and was consistently dark brown even though it was equal in length to Cave Springs Cave (87 cm) (Fig. 4). The Nunley Mountain guano core had many color striations as well. The bottom of the core was gold in color while becoming darker shades of brown towards the top (Fig. 5). Variation in colors is caused by differences in mineral composition. Cores commonly have a pellet-like consistency towards the top and become denser and more clay-like with depth due to compaction. Bulk density increased with depth in the Cave Springs guano core while total carbon (TC) and total nitrogen (TN) decreased (Fig. 1). Even though Cave Springs and Cripps Mill cores were around the same length ~87 cm, they had dramatically different ages (Table 2). Compaction of guano also occurs over time resulting in the bottom portion to be more densely compacted than the top of a guano pile. Cave Springs guano was dated from radiocarbon to ~9000 YBP whereas radiocarbon dating showed Cripps Mill guano to be modern—showing length of guano cores alone do not provide an accurate measure of age. Guano from Nunley Mountain Cave was dated from radiocarbon to ~36,000 YBP (Fig. 5).

Elemental Composition Analysis

In each guano core, tan-colored material with a clay-like consistency was found at the bottom and was determined to be a mineral called brushite ($Ca(HPO_4)\cdot 2H_2O$) (Giurgiu and Tamas, 2013; Stahle et al., 2019). It is thought that brushite forms from reaction with guano calcite and clay at low pH values (Anthony et al. 2000). Calcium and phosphorus rapidly increase at a

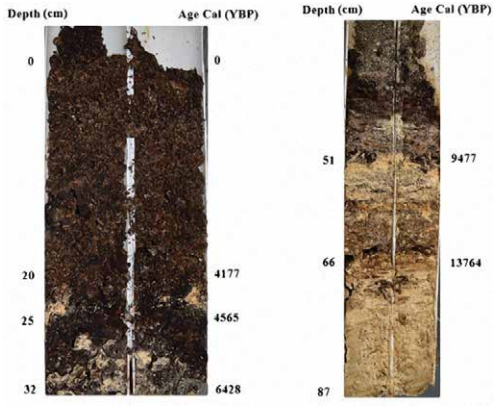

Figure 3. Cave Springs Cave guano core. Cave Springs Cave is located in Priceville, Alabama. Left: The top 0−32 cm the portion of the core is pellet-like and dark brown. Right: The bottom 33−87 cm portion of the core has many colored striations with layers of brushite intermixed with the guano. Guano core was 87 centimeters in total length.

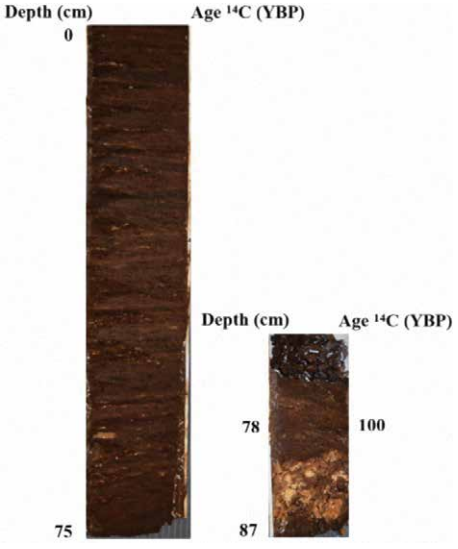

Figure 4. Cripps Mill guano core. Cripps Mill is located in Cookeville, Tennessee. Left: The top (0−86 cm) is consistent in texture and color. Right: The bottom (81−87 cm) indicates brushite. Guano core was 87 centimeters in total length.

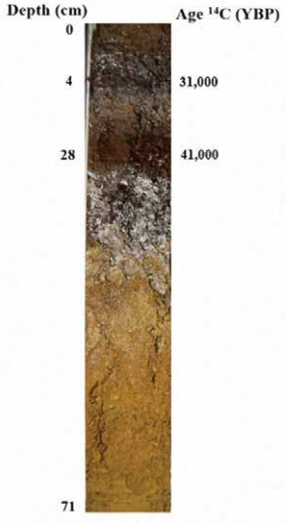

Figure 5. Nunley Mountain Cave guano core. Nunley Mountain Cave is located in McMinnville, Tennessee. The top (0−28 cm) is a dark brown color with some white deposits in between. The middle of the core (30−36 cm) contains white deposits while the bottom of the core (37−71 cm) is cave sediment. Guano core was 71 centimeters in total length.

Table 2. Comparison of ^{14}C dates and core lengths for each collected guano core. Basal ^{14}C dates listed are uncalibrated.

Cave and Location	Basal Age ^{14}C date (YBP)	Length of Core (cm)
Cave Springs Priceville, AL	8,440 ± 30	87
Nunley Mountain Cave McMinneville, TN	36,430 ± 130	71
Cripps Mill Cave Cookeville, TN	100 ± 20	87

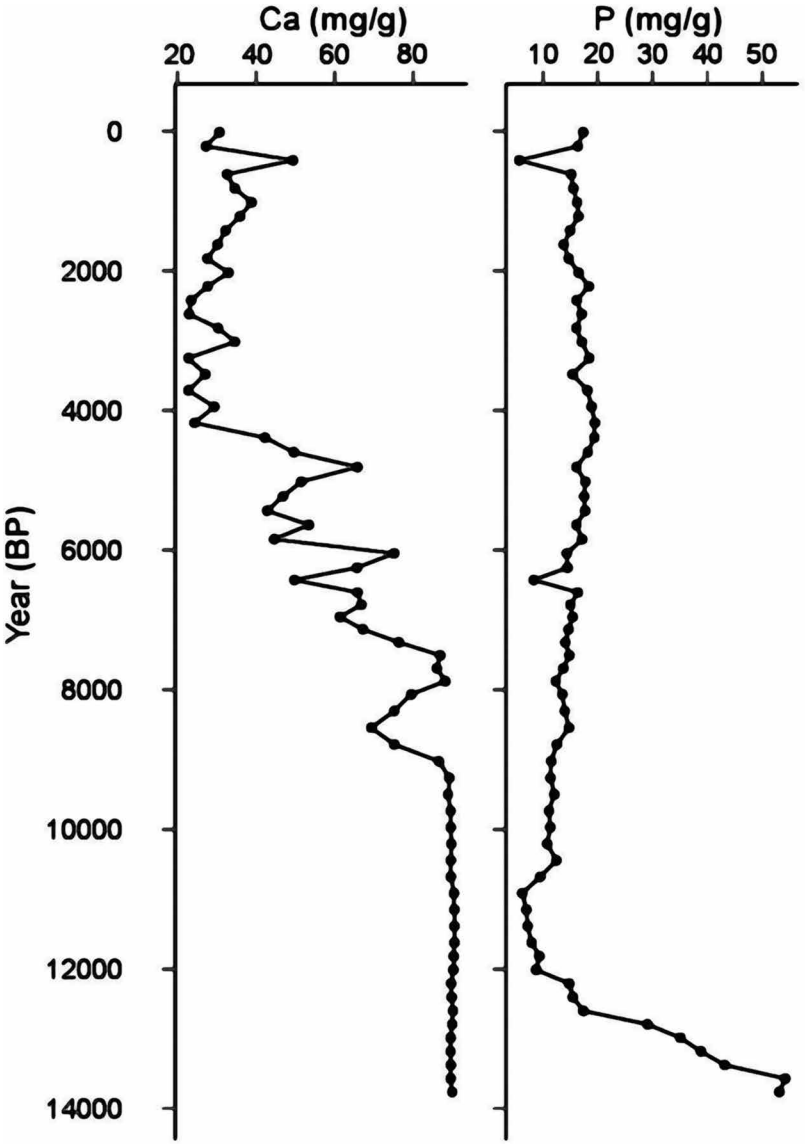

Figure 6. Elemental concentrations measured throughout Cave Springs guano core. Both elements rapidly increase at the bottom of the core, but at different times. Calcium peaks at 9,024 YBP and phosphorus peaks at 12,794 YBP. Increases in both elements indicate brushite.

the bottom of guano cores in congruence with the presence of brushite (Fig. 6). Brushite and other cave minerals contain high amounts of phosphorus and calcium and form after long periods of time (hundreds to thousands of years). However, due to the lack of organic material in the brushite zones of the cores, these portions are not ideal for paleoenvironmental reconstructions.

From our collected cores, brushite was found at the bottom of those extending throughout the Holocene, which indicates it is commonly occurring. Even though brushite has been found in older cores collected from this project, those samples do not produce accurate radiocarbon dates and resulted in inversions of the dating model. As a result, brushite cannot establish chronology in guano cores and was not included in any geochemical analyses.

Stable Isotopes Analysis

Stable isotopes (e.g., $\delta^{13}C$, $\delta^{15}N$, and δD) do not decay as radio isotopes do, allowing them to be quantified throughout a core despite their age. In addition, the stable isotope composition (i.e., isotopic ratio) of a material is the result of differences in the behavior of individual isotopes in response to natural processes. $\delta^{13}C$ isotopes provide information on the local vegetation type of a landscape due to the specific photosynthetic pathways that plants use (Des Marais et al., 1980). With $\delta^{13}C$ isotopes it can be determined whether C_3, C_4, or CAM plants dominated a region at a specific time, and this can give insight into the moisture content as C_3, C_4, and CAM plants each require unique water levels to survive (Cleary et al., 2016). Cleary et al. (2016) proposed that $\delta^{15}N$ accumulates from N gains/losses, N pool mixing, and isotope fractionations which may vary depending on local environment and climatic regimes. The interpretation of $\delta^{15}N$ isotopes from bat guano has changed over time. Recent contributions in the literature of $\delta^{15}N$ isotopes have built upon previous studies resulting in the now accepted interpretation from Cleary et al. (2016) suggesting low $\delta^{15}N$ values indicate periods of dry or arid climate. δD isotopes from bat guano are a common, standard, and accurate way to determine moisture levels of local environments (Wurster et al., 2010). δD values of insect chitin reflects metabolic and drinking water sources and they are correlated with δD values in local precipitation (Gröcke et al., 2006; Wurster et al., 2010).

For these guano core experiments, we only analyzed δD isotopes. Isotopes were compared with a paired t-test between bulk guano and insect chitin alone from Cave Springs Cave for the first 20 cm of the core to determine if insect chitin provides the same or distinct δD values compared to bulk guano (Fig. 7). No difference between the bulk guano

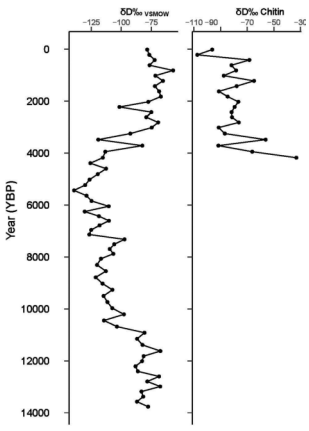

Figure 7. δD values of bulk guano (left) and insect chitin (right) from Cave Springs core. YBP measurements are calibrated years. Fewer values were obtained from older chitin due to degradation.

and insect chitin was detected (t = −0.34, df = 20, p = 0.74) despite some deviating values (e.g., −119.15δD ‰ bulk guano and −56.19δD ‰ insect chitin at 3,480 YBP). Deviating values may indicate hydrogen isotope fractionation which has not been analyzed in other studies reconstructing paleoclimate from guano cores (Bird et al., 2007; Wurster et al., 2008, 2010; Onac et al., 2014; Forray et al., 2015; Choa et al., 2016; Cleary et al., 2016). We suggest less negative δD indicates wet hydroclimatic periods while more negative δD values indicates dry hydroclimatic periods, thus, isotopes are coeval with precipitation over time. Results from the paired t-test are also unique to the limited number of samples (n = 20) and isotopes from Cave Springs Cave and may vary when analyzed from guano cores collected from other locations. One drawback of performing analyses on insect chitin alone is the degradation of chitinous material. Distinguishable insect chitin pieces were not found throughout the entirety of the core due to degradation making analysis only possible for the top to middle of the core, depending on the age. Older guano cores will have less chitin and possibly none at the bottom of the cores while cores that are modern should be consistent in quantity. Therefore, analyzing isotopic values of bulk guano may be the most efficient and productive method.

Age-Depth Models

Each of the three collected cores had unique dating structures. We sampled five radiocarbon dates from Cave Springs Cave and the oldest calibrated age at 67 cm was 12,380 YBP (Fig. 3). The BACON model was applied to this core and had linear correlation lines that indicate sedimentation rates were constant over time. The Cripps Mill Core was sampled at the bottom of the core (78 cm) for a radiocarbon date and revealed a modern age throughout the core (Fig. 4). Nunley Mountain Cave had the oldest radiocarbon date of 36,000 YBP (Fig. 5). However, Nunley Mountain Cave experienced a hiatus in bat presence as there were no modern or recent ages towards the top of the core when calibrated using the BACON model. Hiatuses can occur when bats undergo migratory changes or population changes.

Currently, it is not possible to date modern guano deposits since limnological dating methods such as 210 Pb and 137 Cs are not effective when used independently (McFarlane and Lundberg 2021). However, ^{137}Cs could be a possible method to date recent guano deposits, although it has not been tested.

CONCLUSIONS AND FUTURE IMPROVEMENTS

From three guano cores collected in various locations of Alabama and Tennessee, we analyzed physical, chemical, and elemental components. All three cores showed varying results and ages were drastically different despite having similar lengths. The goal of this study was to provide results for multiple guano cores and review methods and findings from other studies to allow advancement for studying bat guano.

With the potential to determine paleoclimatic and paleoenvironmental conditions, bat guano will gain notice as an accurate and viable proxy. As more studies of bat guano are being implemented around the globe, the interpretations of stable isotope ratios will become a more widely accepted method of paleoclimatic change throughout history, and a comprehensive procedural analysis may be created. Attention still needs to be focused on pollen pathways and potential δD isotope fractionations in bat guano. Currently, isotopic analysis has been favored over biological remains. In the future, biological aspects of guano may also be studied to determine paleoclimatic conditions. Guano studies have already been used across the globe in countries such as Romania (Onac et al., 2014), Guadeloupe (Royer et al., 2015), the Philippines (Choa et al., 2016) and the United States (Mizutani et al., 1992; Wurster et al., 2010; Campbell et al., 2017) and would be a useful tool for filling data gaps where paleoclimatic records currently do not exist.

ACKNOWLEDGEMENTS

We thank the Tennessee Nature Conservancy and Cory Holliday for being a guide through many Tennessee caves. We thank Julianne Ramsey for permitting us access to Nunley Mountain Cave, acting as our guide, collecting a guano core, and financial support for C^{14} analysis. We thank Wheeler National Wildlife Refuge for granting us access to Cave Springs Cave. We also thank the National Speleological Society for providing funding for isotopic analysis.

REFERENCES

Anthony, J.W., Bideaux, R.A., Bladh, K.W., and Nichols, M.C., Eds., 2003, Handbook of Mineralogy: Mineralogical Society of America, Chantilly, VA 20151−1110, USA, http://www.handbookofmineralogy.org/.

Bender, M.M., Rouhani, I., Vines, H.M. and Black Jr, C.C., 1973, 13C/12C ratio changes in Crassulacean acid metabolism plants. Plant Physiology, v. 52, no. 5, p.427−430, https://doi.org/10.1104/pp.52.5.427.

Bird, M., Boobyer E., Bryant C., and Lewis H., 2007, A long record of environmental change from bat guano deposits in Makangit Cave, Palawan, Philippines: Earth and Environmental Science Transactions of the Royal Society of Edinburgh, p. 59−69, https://doi.org/10.1017/

S1755691007000059.
Blaauw, M., and Andrés C., 2011, Flexible paleoclimate age-depth models using an autoregressive gamma process: Bayesian Analysis, v. 6, no. 3, p. 457−474. https://doi.org/10.1214/11-BA618. https://projecteuclid.org/euclid.ba/1339616472.
Brenner, M., Whitmore, T., Curtis, J., Hodell, D., Schelske, C., 1999, Stable isotope (δ13C and δ15N) signatures of sedimented organic matter as indicators of historic lake trophic state: Journal of Paleolimnology, v. 22, no. 2 p. 205−221, https://doi.org/10.1023/A:1008078222806.
Campbell, J., Waters M., and Rich, F., 2017, Guano core evidence of palaeoenvironmental change and Woodland Indian inhabitance in Fern Cave, Alabama, USA, from the mid-Holocene to present: Boreas, v. 46, no. 3, p. 462−469, https://doi.org/10.1111/bor.12228.
Choa, O., Lebon M., Gallet X., Dizon E., Ronquillo W., Jago-On S., Détroit F., Falguères, C., Ghaleb B., and Sémah F., 2016, Stable isotopes in guano: Potential contributions towards palaeoenvironmental reconstruction in Tabon Cave, Palawan, Philippines: Quaternary International, v. 416, p. 27−37, https://doi.org/10.1016/j.quaint.2015.12.034.
Cleary, D., Feurdean, A., Tanţău, I. and Forray, F., 2019, Pollen, δ15N and δ13C guano-derived record of late Holocene vegetation and climate in the southern Carpathians, Romania: Review of Palaeobotany and Palynology, v. 265, p. 62−75, https://doi.org/10.1016/j.revpalbo.2019.03.002.
Cleary, D., Onac B., Forray F., and Wynn J., 2016, Effect of diet, anthropogenic activity, and climate on δ15N values of cave bat guano: Palaeogeography, Palaeoclimatology, Palaeoecology, v. 461, p. 87−97, https://doi.org/10.1016/j.palaeo.2016.08.012.
Cleary, D., Onac, B., Tanţău, I., Forray, F., Wynn, J., Ionita, M. and Tămaş, T., 2018, A guano-derived δ13C and δ15N record of climate since the Medieval Warm Period in north-west Romania: Journal of Quaternary Science, v. 33, no. 6, p. 677−688, https://doi.org/10.1002/jqs.3044.
Delcourt, P., 1980, Goshen Springs: late Quaternary vegetation record for southern Alabama: Ecology, v. 61, no. 2, p. 371−386, https://doi.org/10.2307/1935195.
Des Marais, D., Mitchell, J., Meinschein, W., and Hayes, J., 1980, The carbon isotope biogeochemistry of the individual hydrocarbons in bat guano and the ecology of the insectivorous bats in the region of Carlsbad, New Mexico: Geochimica et Cosmochimica Acta, v. 44, no. 12, p. 2075-2086, https://doi.org/10.1016/0016-7037(80)90205-7.
Forray, F., Onac, B. Tanţău, I., Wynn, J., Tămaş, T., Coroiu, I., Giurgiu, A., 2015, A Late Holocene environmental history of a bat guano deposit from Romania: an isotopic, pollen and microcharcoal study: Quaternary Science Reviews, v. 127, p. 141−154, https://doi.org/10.1016/j.quascirev.2015.05.022.
Gallant, L., Grooms, C., Kimpe, L., Smol, J., Bogdanowicz, W., Stewart, R., Clare, E., Fenton, M., Blais, J., 2020, A bat guano deposit in Jamaica recorded agricultural changes and metal exposure over the last > 4300 years: Palaeogeography, Palaeoclimatology, and Palaeoecology, v. 538, p. 109470, https://doi.org/10.1016/j.palaeo.2019.109470.
Geantă, A., Tanţău, I., Tămaş, T. and Johnston, V.E., 2012, Palaeoenvironmental information from the palynology of an 800-year-old bat guano deposit from Măgurici Cave, NW Transylvania (Romania): Review of Palaeobotany and Palynology, v. 174, p. 57−66, https://doi.org/10.1016/j.revpalbo.2011.12.009.
Giurgiu, A., and Tămaş, T., 2013, Mineralogical data on bat guano deposits from three Romanian caves: Studia UBB Geologia, v. 58, no. 2, p. 13−18, https://doi.org/10.5038/1937-8602.58.2.2.
Gröcke, D., Schimmelmann, A., Elias, S., and Miller, R., 2006, Stable hydrogen-isotope ratios in beetle chitin: preliminary European data and re-interpretation of North American data: Quaternary Science Reviews, v. 25, no. 15-16, p. 1850−1864. https://doi.org/10.1016/j.quascirev.2006.01.021.
Halbritter, H., Ulrich, S., Grímsson, F., Weber, M., Zetter, R., Hesse, M., Buchner, R., Svojtka, M. and Frosch-Radivo, A., 2018, Methods in Palynology: In Illustrated Pollen Terminology, p. 97−127, Springer, Cham. https://doi.org/10.1007/978-3-319-71365-6_6
Jouzel, J., and Masson-Delmotte V., 2010, Paleoclimates: what do we learn from deep ice cores?: Wiley Interdisciplinary Reviews: Climate Change, v. 1, no. 5, p. 654−669, https://doi.org/10.1002/wcc.72
Maher, L., 2006, Environmental information from guano palynology of insectivorous bats of the central part of the United States of America: Paleogeology, Paleoclimate, Paleoecology, v. 237, p. 19−31, https://doi.org/10.1016/j.palaeo.2005.11.026.
Martin, C., 2007, Assessment of the population status of the gray bat (*Myotis grisescens*); Status Review, DoD initiatives, and results of a multi-agency effort to survey wintering populations at major hibernacula: Engineer Research and Development Center, Vicksburg, Miss., Environmental Lab, https://doi.org/10.21236/ADA473199.
McFarlane, D.A., and Lundberg, J., 2021. Geochronological implications of 210 Pb and 137 Cs mobility in cave guano deposits. International Journal of Speleology, v. 50, no. 3, p.239−248.
Mizutani, H., McFarlane, D., and Kabaya, Y., 1992, Nitrogen and carbon isotope study of bat guano core from Eagle Creek Cave, Arizona, USA: Journal of the Mass Spectrometry Society of Japan, v. 40, no. 1, p. 57−65, https://doi.org/10.5702/massspec.40.57
Onac, B., 2012, Minerals, Encyclopedia of Caves, v. 2, p. 499−508, https://doi.org/10.1016/B978-0-12-383832-2.00072-4.
Onac, B., Forray, F., Wynn, J., and Giurgiu, A., 2014, Guano-derived δ 13 C-based paleo-hydroclimate record from Gaura cu Musca Cave, SW Romania, Environmental Earth Sciences, v. 71, no. 9, p. 4061−4069, https://doi.org/10.1007/s12665-013-2789-x.
Onac, B., and Forti, P., 2011, Minerogenetic mechanisms occurring in the cave environment: An overview: International Journal of Speleology, v. 20, no. 2, p. 79−98, https://doi.org/10.5038/1827-806X.40.2.1
Rich, F., 1979, The origin and development of tree islands in the Okefenokee Swamp, as determined by peat petrography and pollen stratigraphy [Ph.D. Dissertation]: State College, Pennsylvania State University.
Royer, A., Malaizé, B., Lécuyer, C., Queffelec, A., Charlier, K., Caley, T. and Lenoble, A., 2017, A high-resolution temporal record of environmental changes in the Eastern Caribbean (Guadeloupe) from 40 to 10 ka BP: Quaternary Science Reviews, v. 155, p. 198−212, https://doi.org/10.1016/j.quascirev.2016.11.010.
Royer, A., Queffelec, A., Charlier, K., Puech, E., Malaize, B., and Lenoble, A., 2015, Seasonal changes in stable carbon and nitrogen isotope compositions of bat guano (Guadeloupe): Palaeogeography, Palaeoclimatology, Palaeoecology, v. 440, p. 524−532, https://doi.org/10.1016/j.palaeo.2015.09.033.
Shahack-Gross, R., Berna, F., Karkanas, P., and Weiner, S., 2004, Bat guano and preservation of archaeological remains in cave sites: Journal of Archaeology, p. 1259−1272, https://doi.org/10.1016/j.jas.2004.02.004.
Stahle, D.W., Edmondson, J., Howard, I., Robbins, C., Griffin, R., Carl, A., Hall, C., Stahle, D.K., and Torbenson, M., 2019, Longevity, climate sensitivity, and conservation status of wetland trees at Black River, North Carolina: Environmental Research Communications, v. 1, no. 4, p. 041002, https://doi.org/10.1088/2515-7620/ab0c4a.
Whitehead, D., 1973, Late-Wisconsin vegetational changes in unglaciated Eastern North America: Quaternary Research, v. 3, no. 4, p. 621−631, https://doi.org/10.1016/0033-5894(73)90034-3.

Wurster, C., McFarlane, D., and Bird, M., 2007, Spatial and temporal expression of vegetation and atmospheric variability from stable carbon and nitrogen isotope analysis of bat guano in the southern United States: Geochimica et Cosmochimica Acta, v. 71, no. 13, p. 3302−3310, https://doi.org/10.1016/j.gca.2007.05.002.

Wurster, C., McFarlane, D., Bird, M., Ascough, P., and Athfield, N., 2010, Stable isotopes of subfossil bat guano as a long-term environmental archive: insights from a Grand Canyon cave deposit: Journal of Cave and Karst Studies, v. 72, no. 2, p. 111−121.

Wurster, C., Patterson, W., McFarlane, D., Wassenaar, L., Hobson, K., Athfield N., and Bird, M., 2008, Stable carbon and hydrogen isotopes from bat guano in the Grand Canyon, USA, reveal Younger Dryas and 8.2 ka events: Geology, v. 36, no. 9, p. 683−686.

Rachel Bosch, Dylan Ward, Aaron Bird, Dan Sturmer, and Rick Olson. A debris flow deposit in Mammoth Cave: field characterization. *Journal of Cave and Karst Studies*, v. 83, no. 4, p. 151-162. DOI:10.4311/2020ES0108

A DEBRIS FLOW DEPOSIT IN MAMMOTH CAVE: FIELD CHARACTERIZATION

Rachel Bosch[1,C], Dylan Ward[1], Aaron Bird[2], Dan Sturmer[1], and Rick Olson[3]

Abstract

This work presents an analysis of a debris flow deposit below Earth's surface in the Mammoth Cave System in Kentucky, USA, and is the first study to characterize an in-cave debris flow to this level of detail. The deposit, named Mt. Ararat by cavers, has a maximum thickness of 7 m, a head-to-tail length of 75 m, and a total volume of about 3400 m^3, as determined by terrestrial LiDAR and electrical resistivity surveys. The deposit is chaotic, angular, matrix-supported, and roughly inversely graded, with grain sizes, quantified through various grain-size distribution measuring techniques, ranging from clay through boulders larger than 1 m. The clasts are predominantly Mississippian Big Clifty sandstone, which is allochthonous in this part of the cave. The angularity of the blocks in the deposit indicate that they had not experienced significant erosion; and therefore, are determined to have been transported only a relatively short distance over a short time. The deposit profile is compound in appearance with two heads. We thus interpret this as a debris flow deposit resulting from two distinct flow events, and present a chronology of events leading to the present-day Mt. Ararat in Mammoth Cave. The findings of this work will inform further studies of karst-related erosional events, sediment transport, and deposition at different scales in karst aquifers, as well as the ways in which surface and subsurface processes interact to contribute to karst landscape evolution.

INTRODUCTION

While karst landscapes vary widely, those with extensive subterranean drainage systems are often associated with unconfined carbonate sequences overlain and underlain by more chemically-resistant beds. As erosion progresses in these landscapes, clastic sediments from the resistant layers are washed into and through subterranean conduits. Significant amounts of clastic sediment must be transported through cave conduits to keep the passages open. Like surface sediment deposits, cave sediments are classified according to grain size, sorting, and sedimentary structures. These deposits can then be interpreted in terms of the conditions of their transport and deposition.

In this study, we focus on a diamictic deposit of sandstone boulders deep under the Central Kentucky Karst landscape in Mammoth Cave. In 1971, John Wilcox noted these boulders on his map as "sandstone breakdown" (Wilcox, 1971). The deposit—later named "Mt. Ararat" by cavers—prompted further scrutiny in 2016, when Art and Peg Palmer began to investigate why this much sandstone was located so far into the cave, where the smooth, gently rounded limestone ceiling meant it could not in fact be a breakdown pile (Palmer et al., 2019). They hypothesized that it was the result of transport during a large flood.

DIAMICTON FACIES SEDIMENTATION

In discussion of the sedimentary facies concept as applied to siliciclastic sedimentation in caves, Bosch and White (2004; 2018) defined a massive, matrix-supported clay to boulder facies that is chaotic, unsorted, and unbedded with the interpretation of diamicton cave deposit as "the result of debris flows where materials of all particle sizes are taken into suspension and flow down high gradient passages" (Bosch and White, 2018).

Terrestrial (Takahashi, 1981; Pierson, 1986; Hungr, 1995) and submarine (Prior et al., 1984) debris flow deposits resulting from single-flow events were reported in field studies as simple profiles beginning with relatively fine material at the upstream "tail," increasing in thickness downstream and coarsening toward the steep front, or "head," with a boulder accumulation at the head. The geometry of debris flows was described in detail by Pierson (1986; Fig. 1) based upon his observations of deposits resulting from channelized debris flows following the 1980 eruption of Mount St. Helens, Washington, USA.

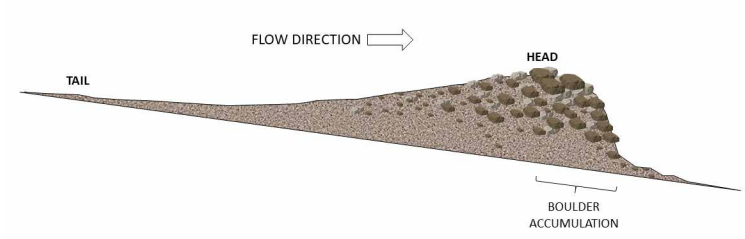

Figure 1. Schematic drawing of a single-surge debris flow in profile with major geometry names labeled (after Pierson, 1986).

Debris flows and their resulting diamicton deposits have been observed and described in caves throughout the world. Many descriptions in the litera-

[1]Department of Geology, University of Cincinnati, Cincinnati, Ohio 45221-0013 USA Current affiliation: Department of Physics, Geology, and Engineering Technology, Northern Kentucky University, Nunn Drive, SC 114, Highland Heights, KY 41099
[2]Siemens Digital Industries Software, 2000 Eastman Dr, Milford, Ohio 45150 USA
[3]Division of Science and Resource Management, Mammoth Cave National Park, Mammoth Cave, Kentucky 42259-0007 USA
[C]Corresponding author, boschr1@nku.edu

ture were written to provide detailed stratigraphy as a necessary context for anthropological or archaeological studies because catastrophic debris flows that came to be deposited in caves were also ideal for entrapment and preservation of bones from the Pliocene through the Holocene. In El Sidrón Cave in Asturia, Spain (Santamaría et al., 2010), there is a deposit described as a "Unit of poorly sorted gravels, sands and mud" which has been interpreted as "fluvial-karstic materials [that] originated from a high energy event and [were] clearly erosive in nature." Similar deposits were investigated as an archaeological complex in Scladina Cave in Belgium (Abrams et al., 2014), interpreted as having been "dominated by solifluction and debris flow." Multiple debris flows hosting archaeological materials were documented in the Great Cave of Niah in Sarawak, northern Borneo (Gilbertson et al., 2005) one of these flows being a diamicton of guano, clay clasts, and limestone boulders with a lobate planform, and another described as "diamicton composed of pink silt-sized material with variably sized white inclusions, interpreted as having resulted from a mudflow." An archaeological site particularly worthy of note, the Malapa Site located in the Cradle of Humankind World Heritage Site in South Africa (Dirks et al., 2010), contains debris flow deposits with "abundant, well-preserved macro- and micromammal fossils." This deposit is a "poorly sorted, coarse-grained sandstone . . . cemented by blocky sparite," that "contains allochthonous material (chert, shale and feldspar grains, bone fragments) mixed with cave-derived sediment, suggesting deposition as a single debris flow. . . "

Other studies have been written from an exclusively geological or geomorphological perspective. Gillieson pioneered studies of siliciclastic sediments in caves with his 1986 study of Selminum Tem in the Highlands of Papua New Guinea. In that work he noted that, "Two diamictons are present in the main passage of Selminum Tem. One attains a maximum depth of 5 m in Coprates Canyon, a 30 m high vadose canyon. . . The diamicton is a silty fine sandy pebble gravel which is matrix supported and unstratified." The Butler Cave-Sinking Creek System in Virginia, USA (Chess et al., 2010) contains extensive siliciclastic deposits, the "most remarkable" of which "are the diamicton facies. . . These are unsorted and unstratified mixtures of sand, pebbles, and cobbles. These seem to have infilled all of the side caves on the western side of the system. . . Diamicton facies implies a debris flow. . . " In a study of a modern event, Van Gundy and White (2009) detailed a volume of material that they estimated at 1800 m^3 (from before and after measurements of the sediment source area) that was transported completely into, through, and out of Mystic Cave in West Virginia, USA, during the "1985 Potomac Valley flood." The observed sediments that were discovered wedged into crevices in the cave after the storm contained a broad "range of particle sizes with a significant fraction of cobble-sized colluvium." When they divided mean-known discharges during the storm event by the cross-sectional area of smaller conduits in Mystic Cave, they arrived at an estimated water velocity of 5–9 m/s required to move that volume of water through some portions of the cave.

FIELD SETTING

Big Avenue, Noah's Way, and Fossil Avenue are adjoining cave passages formed at approximately the same elevation in the Joppa member of the Ste. Genevieve limestone in Mammoth Cave, Mammoth Cave National Park, Kentucky, USA. At the junction of Big Avenue and Noah's Way, is an unconsolidated deposit of rocks named Mt. Ararat. It is about 12–15 m wide with a maximum relief of 7 m and a 75 m long tail that extends into Noah's Way. The grains in this deposit consist of a buff-colored fine- to medium-grained quartz sandstone consistent with descriptions of the Big Clifty sandstone member of the Mississippian Golconda formation, which is stratigraphically about 60 m above the Joppa limestone (Fig. 2). Additionally, the ceiling above the pile is smooth and rounded (Fig. 3). From this evidence, Palmer et al. (2019) inferred that there had been no stoping, that is, the blocks did not break down from the ceiling. Therefore, the rocks making up this deposit were concluded to be allochthonous.

Four discrete levels are observed consistently throughout the over four-hundred miles of mapped passage in the Mammoth Cave System and have been labeled A through D by Palmer (1989) with A at about 200 m ASL, B at 177–186 m ASL, C at 166–167 m ASL, and D at 151–158 m ASL. The passages associated with the Mt. Ararat deposit correlate in elevation with other level C passages. Granger at al. (2001) performed cosmogenic radionuclide burial dating using ^{26}Al and ^{10}Be to sequence the events that resulted in these levels. During that study, they dated quartz gravels (originally from the Pennsylvanian Caseyville conglomerate) sampled from Fossil Avenue (elevation 167 m ASL), approximately 400 m from its junction with Big Avenue (elevation 166 m ASL), at 1.21 ± 0.09 Ma. Additionally, detailed observations of Mt. Ararat have revealed no Caseyville gravels, which was interpreted as the timing of fluvial deposition of these gravels; and therefore, the time at which this passage was last active as a cave stream flow route at base level. Beginning from this approximate timing of younger than 1.21 Ma, we used sedimentological analyses, terrestrial LiDAR, and geophysical data to deduce a sequence of events contributing to deposition of Mt. Ararat.

METHODS

FIELD OBSERVATIONS

Observations were made to characterize the sediment deposit named Mt. Ararat in Mammoth Cave, cave passages containing that deposit, and the geomorphology of Doyle Valley on the surface above. (Although "Doyel" is the spelling

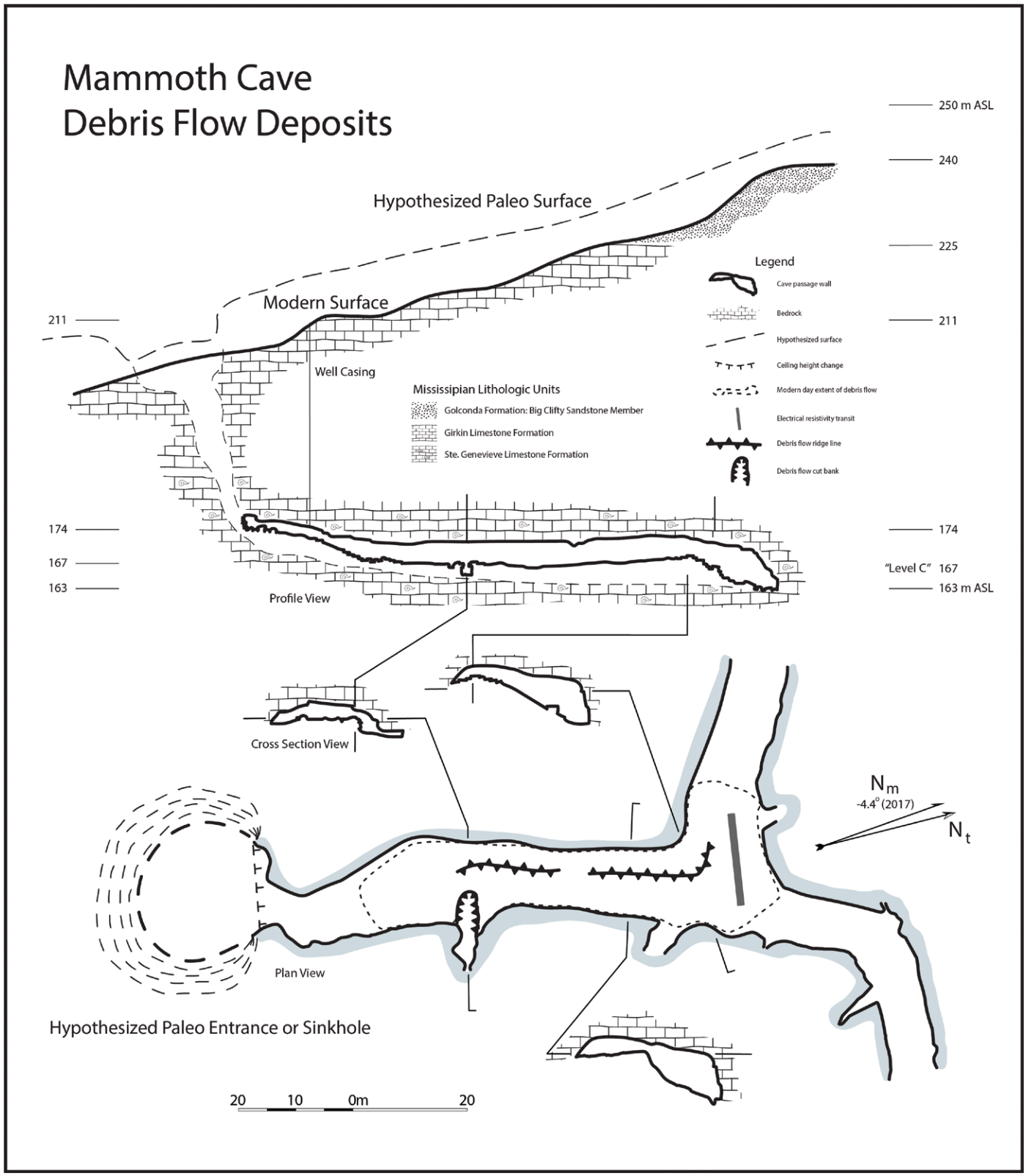

Figure 2. Study area: Mt. Ararat deposit in Noah's Way, Mammoth Cave System, Mammoth Cave National Park, Kentucky, USA. Cave cartography by Bird. (Location topographic map, USGS, 1972; Haynes, 1964; Cave Research Foundation 2010a, 2010b, 2012; Wilcox, 1971).

found on USGS maps (Haynes, 1964; USGS, 1972) and in USNPS publications (2018), Mammoth Cave area historians concur that "Doyle" is the preferred local spelling (Palmer, pers. Comm., 2019)). Field survey books and maps provided by the Cave Research Foundation (1971, 2010a, 2010b, 2012) were used as references for in-cave fieldwork and for cartography of the study area (Fig. 2). Surface field work drew upon the same Cave Research Foundation (CRF) cave data,

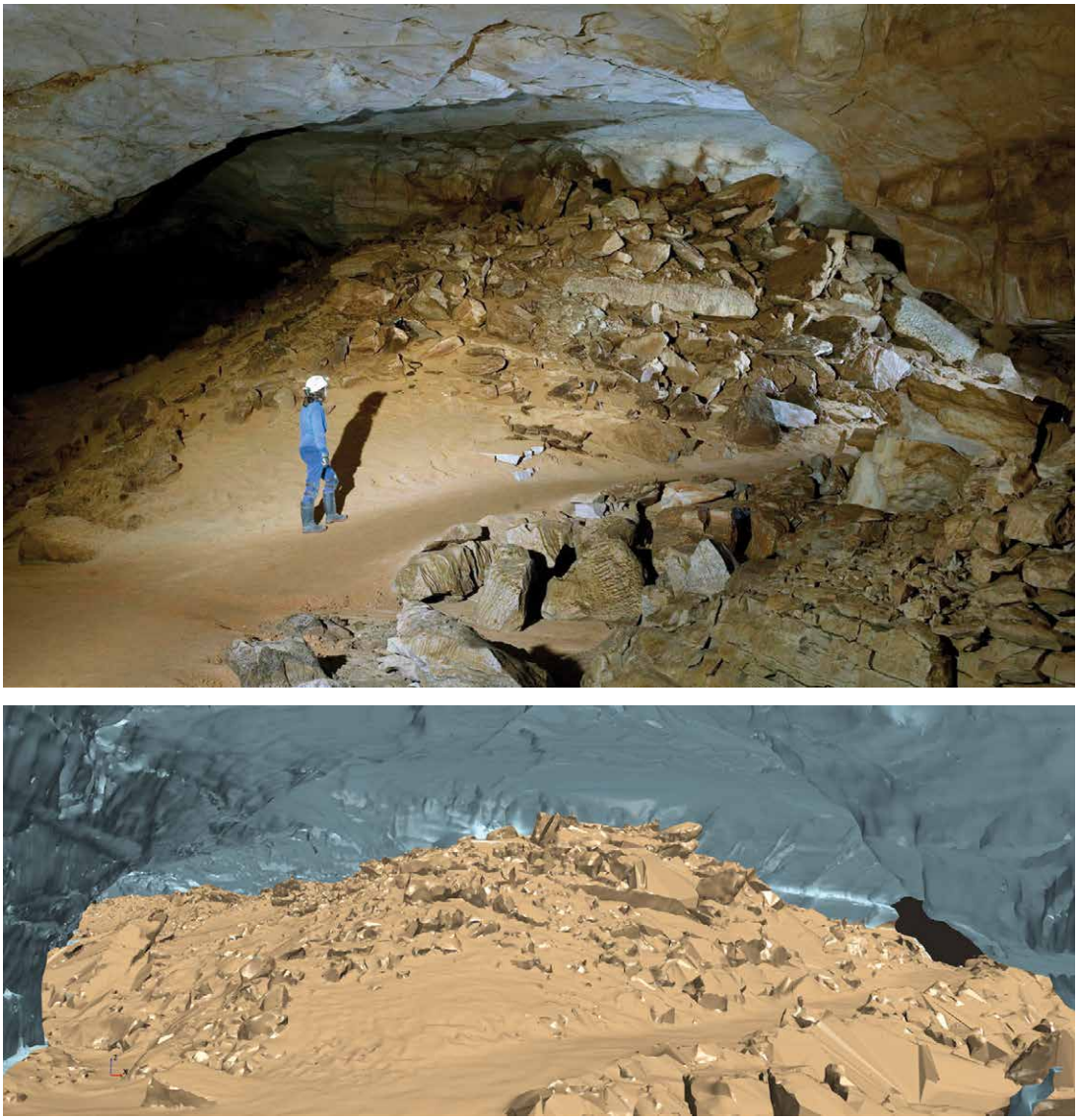

Figure 3. Head of Mt. Ararat as seen from Big Avenue, standing to the northeast of the deposit. A) Photo used with permission of the photographer, Arthur N. Palmer. B) LiDAR scan of Mt. Ararat with portions of Noah's Way and Big Avenue.

topographic and geologic maps (Haynes, 1964; USGS, 1972), and the global positioning system app for iOS, GPS Kit (2017). We defined the volume of material in Mt. Ararat using terrestrial LiDAR for the aerially exposed surface and an electrical resistivity survey to estimate the obscured portion. The facies analysis and interpretations of clastic sediment deposits in the cave were made according to the classification scheme of Bosch and White (2018).

Terrestrial LiDAR

To characterize the outer surface geometry of Mt. Ararat, Tate Jones led a surveying team from KCI Technologies to perform LiDAR scans of the deposit and its immediately surrounding cave passages. They used a *RIEGL* VZ-400i to perform four three-dimensional terrestrial LiDAR scans in the cave. The point clouds from these scans were merged to result in a high-resolution stereolithography file of the surface of Mt. Ararat (Fig. 3B). The resulting mesh comprised over 5.5 million triangles, each about 0.06 m on a side, encompassing 240 m of cave passage length with ceilings approximately 7 m high and passages widths of about 10 m throughout their length. This level of resolution was observed to accurately capture details of the caves passages and individual rocks when compared with photographic evidence and cartographic survey and therefore also realistically reconstructed the shape and structure of Mt. Ararat.

Sedimentology

To determine grain-size distribution for the entire Mt. Ararat deposit, analysis was needed at multiple scales. At the highest precision and finest scale was the fine-grained matrix of the deposit. Mt. Ararat appears to have been partially eroded on its eastern (right-lateral) side by a younger, high-gradient stream, exposing a cross-section that displays a lack of sorting and sedimentary structure in the deposit, with grain sizes ranging from clays to boulders on the order of 1 m on a side (Fig. 4). From this exposed face, we collected three sediment samples: MAXC1, MAXC2, and MAXC3. Dry-sieving of these samples was performed using methods outlined in ASTM (Smith, 2014) using stacked sieves on a mechanical shaker with mesh sizes of 8 mm, 4, mm, 2 mm, 1 mm, 500 µm, 250 µm, 125 µm, 63 µm, and 38 µm.

At the next scale larger in this deposit, a grid-square counting technique was implemented to assess grain-size analysis on the entire cross-section of the exposed face (Fig. 5) (Kellerhals et al., 1975; Ortiz et al., 1975). Each 10 cm by 10 cm grid box was labeled with either the diameter of the largest clast in that square, or if there was not a significant indi-

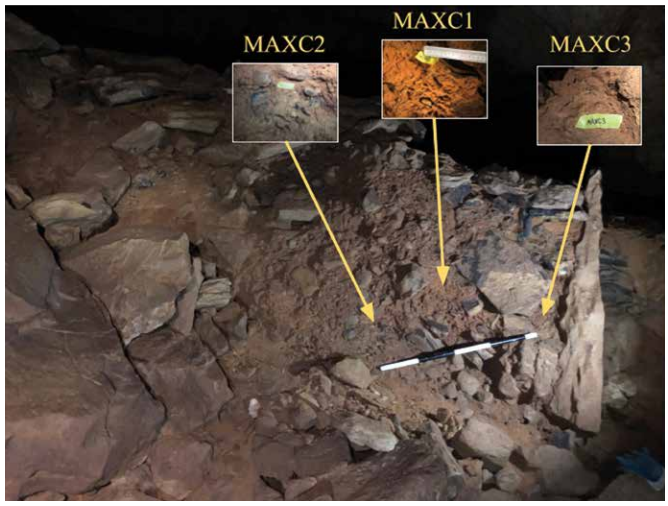

Figure 4. Exposed cross-section of Mt. Ararat. Poorly sorted, matrix-supported clastic sediments with a very wide grain-size distribution. Note the large boulders near the top of the deposit. Interpretation is a diamicton deposit resulting from a catastrophic debris-flow event. Matrix sampling locations are shown inset. Scale bar has 20-cm-long alternating white and black segments. Photo by Bosch.

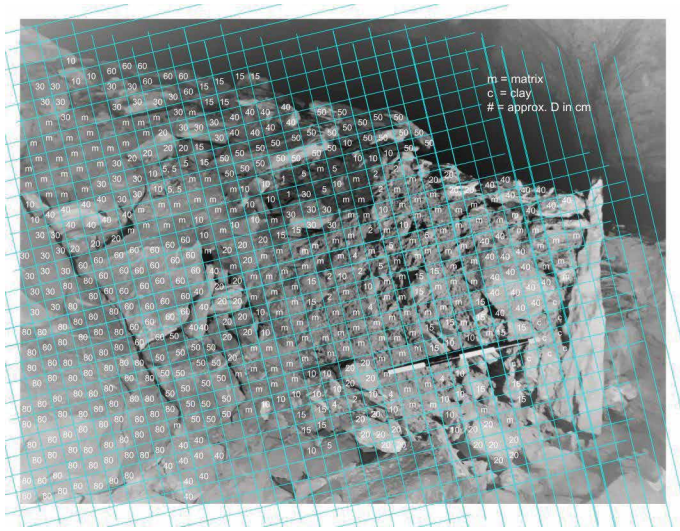

Figure 5. Grain-size analysis for exposed cross-section of Mt. Ararat. Grid-squares for grain-size distribution analysis.

vidual clast visible, the grid square was labeled m for matrix, or in the case of the few squares we identified in the field as clay-dominated, c for clay. Boxes with clasts comprised 70 % of the exposed-section surface area, while matrix- and clay-dominated boxes accounted for 30 % of the section. To construct the grain-size-distribution curve, the cumulative percentage results from sieving the matrix material were multiplied by 0.3 and the whole-clast grid-counting results were plotted relative to the entire gridded section (Fig. 6).

Electrical resistivity

Near-surface geophysics was used to approximate the subsurface stratigraphy in Big Avenue near the junction with Noah's Way (Fig. 2). Since Mt. Ararat's material covers the paleo bedrock floor of the passage, we used electrical resistivity tomography to constrain the thickness of the deposit. We used an IRIS Syscal Kid Switch24 to perform a Wenner Vertical Electrical Survey (VES) along the trail. A Wenner VES assesses the vertical resistivity profile below one point by acquiring readings on progressively longer arrays, with increased array lengths sampling deeper stratigraphy (Burger et al., 2006). We set up arrays with intervals of 0.5 m, 1 m, 1.5 m, 2 m, 3 m, 4 m, and 4.5 m. The resistivity readings from each of these arrays were used to model the vertical profile using the program ipi2WIN (Bobachev, 2002). This modeled near-surface stratigraphy was used to help constrain the three-dimensional geometry of the deposit.

Morphological analyses

A longitudinal profile and seven cross sections were measured using the Profile Tool plugin (Jurgiel, et al., 2020) in QGIS (QGIS.org, 2020) on a digital elevation model of Mt. Ararat built in CloudCompare (2020) using the point cloud obtained from the terrestrial LiDAR survey (Fig. 8). The volume of the deposit was constrained by the LiDAR-scanned topography and the position of the underlying passage floor inferred from the electrical resistivity near-surface stratigraphy model. Using the multiphysics modeling software, STAR-CCM+ (Siemens, 2020), the stereolithography mesh was imported as a geometry part. All holes in the model were then closed using the surface repair tool in STAR-CCM+. The bedrock passage floor was modeled as a plane coincident with the bedrock floor location inferred from electrical resistivity. Where the flat floor did not intersect the LiDAR surface, planes were introduced to model bedrock passage wall obscured by Mt. Ararat where the deposit contacts the western wall along Noah's Way and the southern wall of Big Avenue in the inside of the bend. Using this combination of three plane surface and the LiDAR-derived surface, a geometric model of the Mt. Ararat deposit was isolated.

RESULTS

Surface topography relative to debris flow deposit

On the cave map by John Wilcox (1971), about 75 m beyond the junction with Big Avenue, in Noah's Way, there is a note written at survey station V-11: "bore hole directly above." Upon visual inspection in the cave, we observed a small copper pipe protruding a few centimeters from the passage ceiling. Further upstream from this, the passage has limestone breakdown and travertine deposits and becomes impassible to humans. The origin and possible motivation for installing this pipe before Mammoth Cave was administered by the National Park Service is unknown. However, it provided an opportunity to robustly tie cave observations to surface observations. Using that cave map in conjunction

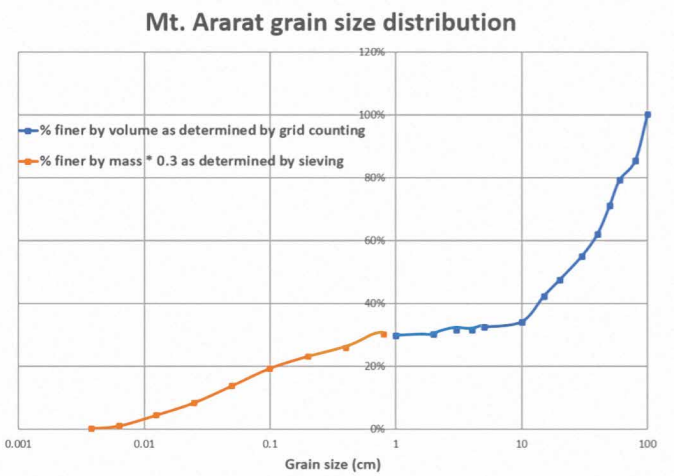

Figure 6. Grain-size distribution curve for exposed cross-section of Mt. Ararat. Finer grained matrix mass percentage determined by sieving. Coarser grained clasts volume percentage determined by grid-counting. Since this material is concluded to have derived from the Big Clifty sandstone, it is of uniform density, and these two approaches are therefore directly comparable.

with the app *GPS Kit*, the surface end of the "bore hole" was found at an elevation of 210 m ASL on the north side of Doyle Valley (Fig. 2).

The contact between Girkin Limestone Formation and Big Clifty Sandstone Member of the Golconda Formation is at about 225 m, 15 m above the borehole. At this elevation the landscape slope becomes much gentler. These are the plateau-like Jim Lee Ridge and Joppa Ridge to the north-northeast and south-southwest of Doyle Valley, respectively. Throughout Mammoth Cave National Park, there are ponds intermittently perched on the Big Clifty sandstone on the ridges (Studinski and Grubbs, 2007).

A sinkhole in the floor of Doyle Valley was found at about 140 m horizontal distance south-southwest from the bore hole and at an elevation of 200 m; it was dry when we completed our surface reconnaissance work and is indicative of the closest modern place for water to enter the Noah's Way area of Mammoth Cave. An entrance point for the material that became Mt. Ararat may have looked somewhat like this but at 2–7 m higher in elevation (Fig. 2) due to the 2–7 m/Ma erosion rate presented by Granger et al. (2001). If we add 2 m to account for the minimum estimated erosion, the shortest travel distance from the nearest modern exposure of the contact to the upstream end of Noah's Way is the resultant of the vertical offset of 62 m with the horizontal distance of about 200 m, or about 210 m of straight-line travel. This estimate is, of course a minimum, since transport would not likely be in a straight line.

Sedimentology

Table 1. Grain-size distribution of Mt. Ararat matrix material from sieve analysis.

Cumulative sediment mass (g)		Grain size (mm)		Percentage finer by weight (%)	
MAXC1	MAXC2	MAXC1	MAXC2	MAXC1	MAXC2
48.35	67.55	8	8	100	100
48.35	48.8	4	4	100	72
46.75	38.4	2	2	97	57
38.85	32.1	1	1	80	48
28.35	21.8	0.5	0.5	59	32
17.65	12.5	0.25	0.25	37	19
8.35	7.7	0.125	0.125	17	11
1.25	2.1	0.063	0.063	3	3
0.2	0.35	0.038	0.038	0	1

Grain-size distributions for samples of the deposit matrix as determined by sieving MAXC1 and MAXC2 were similar to one another (Table 1). The third matrix sample, MAXC3, was nearly 100 % clay. These were combined to create a grain-size distribution for the matrix of the cross-section exposed by erosion with a minimum grain size of 0.0038 cm, a maximum of 0.8 cm, and a D50 of about 0.05 cm. When plotted as 30 % of the total grain-size distribution, with the grid-counting results contributing the other 70 %, the maximum grain size was then 100 cm and the D50 for the entire cross-section grain-size distribution was about 20 cm (Fig. 6).

Table 2. Raw data results of electrical resistivity survey.

Depth below center of VES Array (m)	Measured resistivity (Ω·m)
0.5	175.98
1	651.29
1.5	1532.35
2	6059.78
3	2483.17
4	1961.21
4.5	1003.91

Obscured stratigraphy

Measurements recorded during the electrical resistivity tomography (ERT) survey (Table 2) represent the resistivity encountered by an electrical signal as it traveled through multiple stratigraphic layers, each with a different resistivity. The raw data then shows

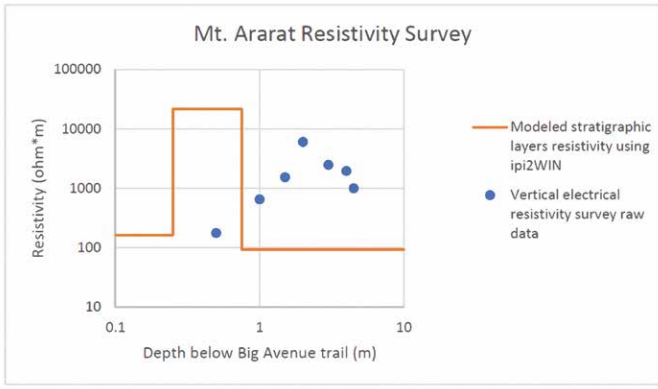

Figure 7. Raw electrical resistivity signal responses and modeled electrical resistivity strata. Data modeling indicates the trail depth below the center of the resistivity array at 0.25 m (horizon A), debris flow deposits from 0.25 m to 0.75 m in depth (horizon B), and below 0.75 m as bedrock with vugs and fractures (horizon C).

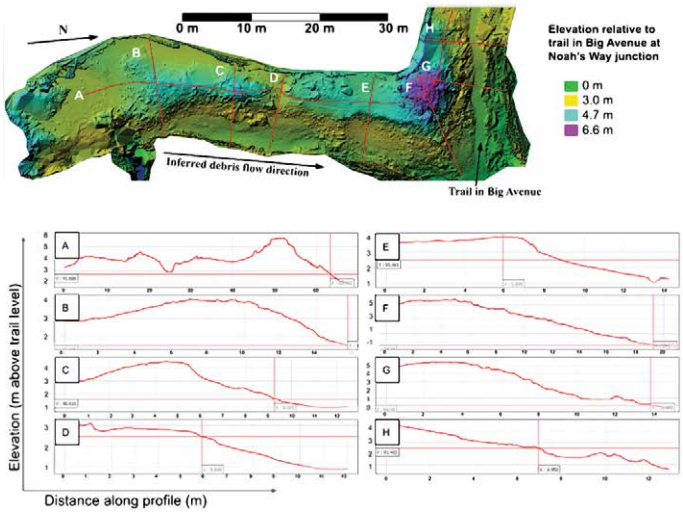

Figure 8. Digital elevation model of Mt. Ararat along the spine, A, and at seven cross-sections, B through H.

the averaged resistivity along each semicircular travel path. To determine the number and resistivities of discrete layers, the data were numerically modeled using the software package ipi2WIN (Bobachev, 2002). The data were input into the program and then inverted to generate an earth model. The initial model was manually adjusted to minimize root-mean squared error between the modeled curve generated from the earth model and the data. The number of layers required in the model is dictated by the shape of the data. Each inflection point in the curvature of the data requires another layer. The model resulting from our analysis divided the subsurface into three layers: Layer 1 from 0 m to 0.25 m below the center of the survey with a resistivity of 163 Ω·m; Layer 2 from 0.25 m to 0.75 m below the trail with a resistivity of 21,785 Ω·m; and Layer 3, 0.75 m to 4.5 m deep, with a resistivity of 93 Ω·m. Layer 1 is interpreted as human-built trail material (sand moved from deposits in other areas of the cave), Layer 2 as Mt. Ararat sand and boulders, and Layer 3 as vuggy/fractured limestone (Fig. 7). These resistivity values fall within the range observed for natural materials: sand, sandstone, and limestone, respectively (Mussett and Khan, 2000).

Deposit pile morphology

For local topography, we designated the trail elevation at the junction of Noah's Way and Big Avenue as the zero datum. Mt. Ararat, with the general form of a debris flow deposit (Fig. 1, Fig. 8), occupies most of the length and approximately one-half of the volume of Noah's Way. From the junction of Noah's Way to the south, the floor on the eastern side of Noah's Way slopes up at a gradient of about 0.05 while the ridge of Mt. Ararat slopes down from its highest point at an average gradient of −0.06.

A striking feature of Mt. Ararat is that it has two main peaks: the larger one is 7 m tall at the downstream end of the deposit near the junction, and, following the ridge along the crest of the deposit, there is a secondary peak about 4 m tall that is 35 m upstream from the taller peak (Fig. 8A). About 20 m upstream from that secondary peak, the tail of the deposit tapers off and is obscured by limestone breakdown. Along the western wall of Noah's Way, the deposit is in continuous contact with the wall. The coarsest grain sizes in Mt. Ararat, found at the taller peak, are boulders of greater than 1 m in diameter, with the second highest concentration of large grains located at the second peak.

Two areas of Mt. Ararat show evidence of surface modification postdating deposition. Along the eastern wall of Noah's Way, for about 40 m, the side of Mt. Ararat has the appearance of a cutbank at the angle of repose for silt, rising to the west from a small feature that appears to be an abandoned channel up toward the crest of the deposit (Fig. 8E). The stream, when it occupied that channel, would have drained from Noah's Way out to Big Avenue. Upstream from the large peak, about 50 m up Noah's Way, there is a side passage leading away to the east. At the entrance to this deposit, Mt. Ararat has been partially eroded through its entire vertical extent to reveal a cross-section of the deposit (Fig.4), and 10 m further down that side passage is a small, hydrologically active stream.

From the tall peak at the junction of Noah's Way and Big Avenue, the deposit makes a sharp turn to the west, into Big Avenue, with its left-lateral side remaining in contact with the cave passage wall (Figs. 8G, 8H). Slopes around that peak area of Mt. Ararat vary due to the wide range of grain sizes but are roughly at the angle of repose and continue under the human-built trail in Big Avenue toward the cave passage floor.

We used the LiDAR point cloud and resistivity depth profile to evaluate the volume of material represented by the deposit. The resistivity results indicated that the bedrock floor near the junction of Big Ave and Noah's Way lies 0.75 m below the trail at the center of the array (Fig 9). At the southeast corner of Noah's Way, bedrock is exposed where a

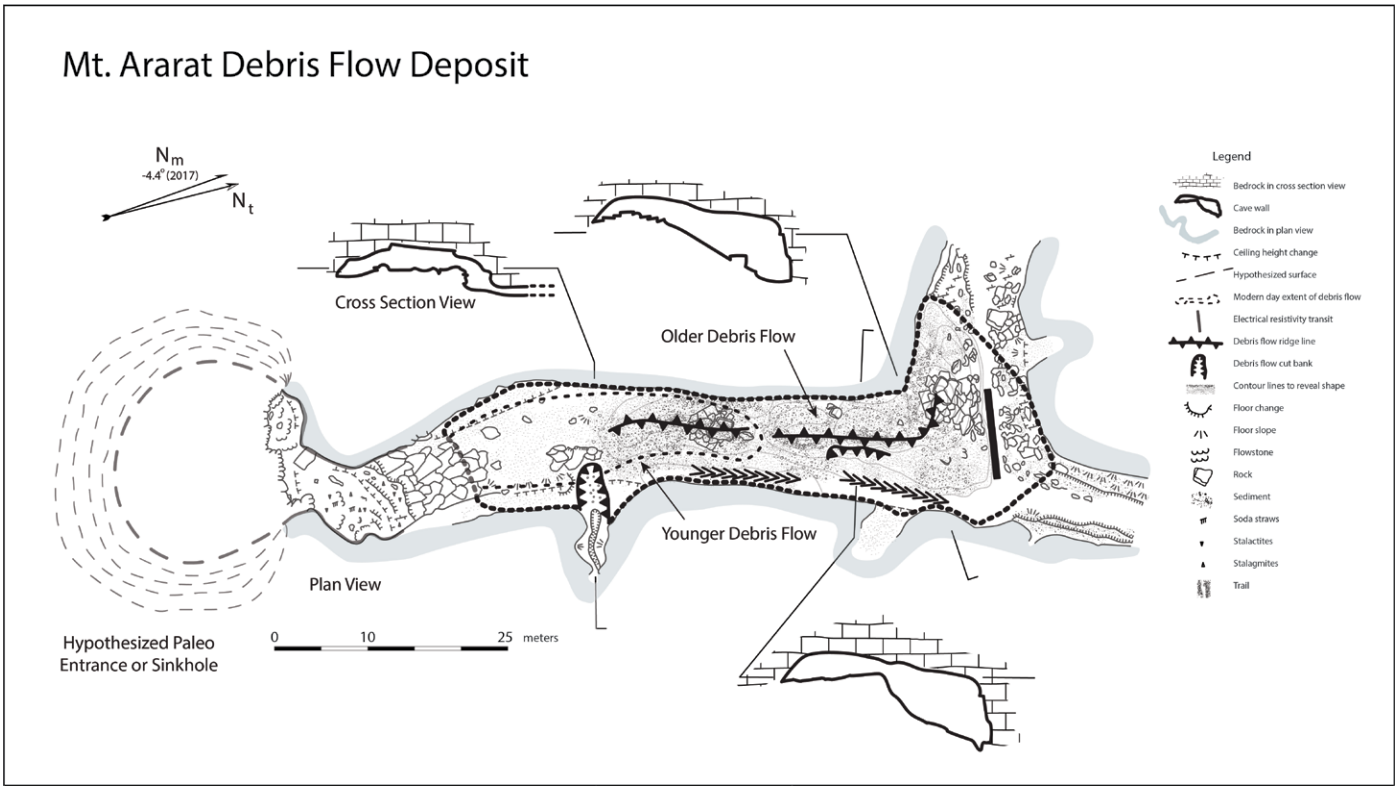

Figure 9. Geomorphological map of Mt. Ararat with sequence of depositional and erosion events as follows: 1) deposition of primary, large, debris flow; 2 or 3) fluvial erosion of primary, and perhaps also secondary, debris flow(s) along eastern wall channel; 3 or 2) deposition of secondary, smaller, debris flow; head of small debris flow marked by grain-size transition from large-gravel- to sand-dominated in the downstream direction; and 4) erosion of primary and secondary debris flow into eastern side passage. Map symbols consistent with Gustavsson et al. (2006).

smaller passage opens through the floor, and its position qualitatively supports the assumption of a roughly constant bedrock floor level along the length of Noah's Way. The exact relationship between this bedrock exposure and the Mt. Ararat deposit is obscured by a later-stage breakdown jumble. Neither the resistivity profile, nor observations of scattered alluvial cave deposits in Big Avenue and Fossil Avenue, support the premise that a significant thickness of unrelated sediment underlies Mt. Ararat. Nor is there evidence for subsequent deposition of dissimilar sediments atop the debris flow material; the sandstone-bearing facies is only apparently overlain by a few cm of weathering residuum, sporadic calcium carbonate deposits, and occasional breakdown blocks, all of proximal origin. In other words, we may assume that most of the volume of sediment in Noah's Way between the breakdown pile at the south end and the junction at the north end is related to the Mt Ararat event. This assumption means that our volume estimates will be maximum-limiting because there is little direct constraint on depth to bedrock in Noah's Way.

We isolated features of interest in plan view and measured their volume using the 2.5D Volume tool in CloudCompare (2020), using a grid size of 1 m. Volume is computed as the sum of gridded thicknesses above a reference level, here set to the inferred level of the bedrock passage floor. We measured the volume of Noah's Way enclosed by its ceiling, extending from the base of the breakdown pile in the south end, north to the junction area with Big Avenue, to be 6700 m^3, of which ~1700 m^3 is in the junction area. Measured in the same way, the present volume of the Mt Ararat deposit is ~3400 m^3. If we assume that the original deposit filled the width of the passage, the volume of material eroded along the east (right lateral) margin has been ~400 m^3. In summary, our best maximum-limiting estimate for the original deposited volume is 3800 m^3, or about 50% filling of the available passage space in Noah's Way (c.f. Fig 3).

DISCUSSION

The Mt. Ararat deposit in Mammoth Cave consists of poorly-sorted, matrix-supported, angular grains sourced from the Big Clifty sandstone and ranging from clay-sized through boulders of about 1 m in diameter, as quantified by detailed analysis of an exposed cross-section of the deposit. With over 60 % of this material having grain sizes greater than 10 cm in diameter (Fig. 6), a volume between 2280 m^3 and 4020 m^3 of sandstone must have been directly sourced from the Big Clifty Sandstone Member. These sedimentological results support our interpretation of Mt. Ararat as a debris flow deposit originating from a mass-wasting or flood-like event in Doyle Valley, although the specific nature of the event occurring on the surface remains unclear. A conservative interpretation is that it represents a period of flash

flooding in the Doyle Valley watershed that mobilized sandstone colluvium and temporarily accessed a now-obscured entrance to Noah's Way.

Further analysis provides estimates on flow velocities that would be needed to transport these grains as bedload either initially from the surface or later when eroding material away from the deposit. To estimate a high-end water speed for grains transported as bedload with water as the only fluid, we performed a calculation balancing the forces on an individual grain at the moment of incipient transport (Allen, 1985),

$$\tau_{cr} = \frac{2D(\alpha-\rho)g}{3\cos\beta}\tan(\alpha-\beta) = \rho u_*^2, \quad (1)$$

where τ_{cr} is the critical shear stress at the threshold of entrainment (N m^{-2}), D is the diameter of the grain size to be transported, σ is the density of that grain (in this case, 2650 kg m^{-3}), ρ is the density of the fluid (1000 kg m^{-3}), g is the acceleration due to gravity (9.8 m s^{-2}), α is the angle between a line normal to the streambed and a line from the center of the grain to a grain-to-grain contact, β is the angle of inclination of the streambed, ρu_*^2 is the definition of shear stress, and u_* is the shear velocity.

This calculation was performed for the median grain size of 0.2 m and the largest of 1 m. To further simplify, we assumed that each transported grain was in contact with grains of identical dimensions and was transported by water. Fluids in debris flows can have a range of higher densities than water that would then result in a lower We then used a streambed slope of 0.05 (2.5 m / 50 m; Fig. 8) to calculate a shear velocity needed to entrain each of these grains. The resulting estimated average streamflow velocities were determined from the shear velocities,

$$u = \frac{u_*}{\kappa}\ln\left(\frac{z}{z_0}\right), \quad (2)$$

where κ, 0.40, is the von Karman constant (Bailey, et al., 2014), and z/z_0 is the roughness factor, which has been found to be about 9 for rough cave floors and walls through simulation of cave flow conditions (Bird et al., 2009). The calculated average velocities were 5.43 m s^{-1} for 0.2 m diameter cobbles and 12.15 m s^{-1} for 1 m diameter boulders.

Besides sediment grain size, other flow indicators in Noah's Way and Big Avenue include 1 cm to 2 cm scallops sculpted into limestone walls. Although geochronological tools do not currently exist to date the formation of scallops and it is not possible to determine when they developed in relation to the deposition of Mt. Ararat, they do represent flow conditions at some point in the period when these passages were hydrologically active. Palmer (2007) used these scallop lengths and the experimentally-derived relationship of Curl (1974) to estimate mean water speeds in this passage of about 1.25 m s^{-1} to 2.5 m s^{-1}. The flows calculated using these two approaches are on the same order of magnitude and correlated well with the estimated velocities provided by Van Gundy and White (2009) of 5–9 m s^{-1}. They thus provide an estimate of the paleoflow conditions present in Noah's Way. These calculations assume particle motion in water, so velocities are likely higher than would be needed for transport of these grain sizes in a debris flow.

We may use a similar calculation to evaluate whether the scallop-based estimate of flow velocity would be a strong enough flow to result in the partial erosion observed as a channel along the eastern flank of Mt. Ararat. Entering our slowest estimated flow velocity into Equations (1) and (2), a stream flow of 1.25 m s^{-1} in Noah's Way would be sufficient to entrain material with a median grain size of 5 mm, which is larger than that of the fine-grained matrix of Mt. Ararat.

To interpret the depositional conditions for Mt. Ararat, we referred to studies by Takahashi (1981), Pierson (1986), Hungr (1995), and Prior et al. (1984), which independently presented the simplest case of debris flow deposits resulting from single-flow events (Fig. 1). The physics behind channelized subsurface debris flows in karst conduits with a free upper surface, such as those leading to Mt. Ararat, was assumed to be similar to that of channelized surface debris flows. Assuming the simplest case, Mt. Ararat could have been deposited by a single debris flow event. This single event could have either (a) filled the entire passage of Noah's Way or (b) produced one large debris flow deposit with a classic single debris flow deposit profile (Fig. 1). A third possible scenario is that (c) two debris flows occurred, either as two surges resulting from the same event on the surface or as two flows from two discrete surface events.

Considering the possibility of event (a), had the Noah's Way passage at one time been completely full with sediment and then three-quarters of that been removed, we would expect to see residual staining on the ceiling and walls of the passage. Since the ceiling and upper walls are very cleanly exposed limestone, it is likely that this passage was never completely filled with siliciclastic sediments.

Scenario (b) would require a unique set of erosional events to sculpt a single debris flow into the basis for the modern profile of Mt. Ararat (Fig. 8A). Specifically, when we examined the morphology and grain-size distribution surrounding the secondary peak, it seemed unlikely that this shape was produced by erosion of a single debris-flow deposit. The shape of this peak is rounded, like that of the large peak and like that in the generalized sketch (Fig. 1). That peak also contains the second greatest concentration of coarse grains in Mt. Ararat. Immediately downstream of the second peak, grain sizes are fine (silts and sands) and then begin to coarsen again in the downstream direction.

This evidence favors scenario (c). Having two heads of classic debris-flow deposit morphology, the smaller of the two superposed on the tail of the larger flow, this deposit appears likely to have resulted from multiple flow events (Fig. 8A). More data would be needed to determine whether these two depositional events were triggered by two surges from the same surface event or by two different surface events and to deduce how closely timed these events were. Considering paleoflow indicators, sedimentological evidence, and the morphology of Mt. Ararat, we conclude that the sedimentation chronology included two depositional events and two erosional events (Fig. 9):

1. Deposition of the large, 75-meter long, primary debris flow.
2. Fluvial erosion of the right-lateral side as evidenced by the channel cutting through the large flow. We were unable to conclude from field evidence as to whether it also affected the smaller overlying one. If it also eroded the second deposit, this would be event 3.
3. Second debris flow deposition covering about 25 meters of upstream end of primary flow. If this deposit has been eroded by the stream, then this deposition would have been event 2.
4. Fluvial erosion into a side passage at location 50 m into Noah's Way from the junction at Big Avenue. This eroded material from both the first and second deposits, resulting in a clean exposure of the entire debris flow cross-section.

Future numerical modeling studies could use the results of this study to evaluate the hydraulic conditions that resulted in Mt. Ararat. Further detailed field investigation of Doyle Valley and the downstream reaches of Big Avenue could provide further evidence for paleo topography on the surface above the cave and the overall sedimentation history of Mammoth Cave. Geochronology studies in the sinkholes of Doyle Valley and the sediments in and near Mt. Ararat could strengthen the chronology of sedimentation events in the region. Finally, future investigations may want to extend these findings and techniques as they apply to other debris flows in Mammoth Cave and in other caves.

CONCLUSIONS

In this work, we have provided a detailed characterization of the deposit named Mt. Ararat in Mammoth Cave. The combination of sedimentological, geophysical, and digital imaging data presented in this work supported the interpretation of the Mt. Ararat deposit as resulting from debris flow event(s) and enabled the calculations of the current volume of this deposit at approximately 3400 m^3. Stratigraphic relationships with established Mammoth Cave system chronologies placed the age of the deposit at younger than 1.2 Ma. The evidence in this work supports the hypothesis of sandstone-floored-pond collapse(s) or valley-wall landslide(s) that initiated two debris flow surges into a now-obscured sinkhole entrance in the paleo Doyle Valley floor releasing a total more than 3800 m^3 of material into the cave system. The sediment was deposited taking the form of Mt. Ararat with most of the material coming to rest at the junction of Noah's Way and Big Avenue, and a secondary volume of material coming to rest on top of the tail of the first debris flow. Material was partially eroded from the eastern side via a north-flowing stream either after or between the two deposition events, and later down a steep side passage. The findings of this work will inform further studies of karst-related erosional events, sediment transport, and deposition at different scales in karst aquifers as well as the ways in which surface and subsurface processes interact to contribute to karst landscape evolution.

ACKNOWLEDGEMENTS

Research in Mammoth Cave National Park was conducted under research permit # MACA-2017-SCI-0020. This paper is dedicated to Colleen Olson of the Mammoth Cave Guide Force, a guiding light and inspiration to so many. Much gratitude goes out to Mary and Chuck Schubert, John Andersland, Tate Jones, JoAnn Jones, Christopher Chiros, Abby Kelly, Matt Covington, Missy Eppes, Chris Sheehan, Sam Berberich, Diana Garza, Reza Soltanian, Reza Ershadnia, Mark Passerby, Charles Fox, Karen Willmes, Bob Osburn, Karen Bird, Zach Bosch-Bird, Tyler Bosch-Bird, Samuel Bosch-Bird, and two anonymous reviewers who contributed useful insights. Additional thanks to the University of Cincinnati, Department of Geology, Siemens Digital Industries Software, Mammoth Cave National Park, the National Park Service, the Cave Research Foundation, and the University of Cincinnati 1819 Innovation Hub Groundfloor Makerspace. This work would not have been possible without the motivation and encouragement of Art and Peg Palmer, and Roger Brucker.

REFERENCES

Abrams, G., Bello, S.M., Di Modica, K., Pirson, S., and Bonjean, D., 2014, When Neanderthals used cave bear (*Ursus spelaeus*) remains: Bone retouchers from Unit 5 of Scladina Cave (Belgium): Quaternary International, v. 326, p. 274–287. https://doi.org/10.1016/j.quaint.2013.10.022.

Allen, J.R.L., 1985, Principles of Physical Sedimentology: London, George Allen & Unwin, 272 p. https://doi.org/10.1007/978-1-4613-2545-1.

Bailey, S.C.C., Vallikivi, M., Hultmark, M., and Smits, A.J., 2014, Estimating the value of von Kárman's constant in turbulent pipe flow: Journal of Fluid Mechanics, v. 749, p. 79–98.

Bird, A.J., Springer, G.S., Bosch, R.F., and Curl, R.L., 2009, Effects of surface morphologies on flow behavior in karst conduits, Proceedings of the 15th International Congress of Speleology, p. 1417–1421.

Bobachev, C., 2002, IPI2Win: A Windows Software for an Automatic Interpretation of Resistivity Sounding Data [Ph.D. Dissertation]: Moscow, Moscow State University, 320 p.

Bosch, R.F., and White, W.B., 2004, Lithofacies and transport of clastic sediments in karstic aquifers: *in* Studies of Cave Sediments: Springer, p. 1–22.

Bosch, R.F., and White, W.B., 2018, Lithofacies and transport for clastic sediments in karst conduits: *in* Karst Groundwater Contamination and Public Health: Springer, p. 277–281. https://doi.org/10.1007/978-3-319-51070-5_32.

Burger, H.R., Sheehan, A.F., and Jones, C.H., 2006, Introduction to Applied Geophysics: Exploring the Shallow Subsurface: New York, WW Norton, 554 p.

Cave Research Foundation, CRF Field Survey Book 526, 1971, Used with written permission of Cave Research Foundation and National Park Service.

Cave Research Foundation, CRF Field Survey Book 4489, 2010a, Used with written permission of Cave Research Foundation and National Park Service.

Cave Research Foundation, CRF Field Survey Book 4495, 2010b, Used with written permission of Cave Research Foundation and National Park Service.

Cave Research Foundation, CRF Field Survey Book 4607, 2012, Used with written permission of Cave Research Foundation and National Park Service.

Chess, D.L., Chess, C.A., Sasowsky, I.D., Schmidt, V.A., and White, W.B., 2010, Clastic sediments in the Butler Cave–Sinking Creek System, Virginia, USA: Acta Carsologica, v. 39, no. 1, p. 11–26. https://doi.org/10.3986/ac.v39i1.109.

CloudCompare (version 2.10.1), 2020, https://cloudcompare.org/.

Curl, R.L., 1974, Deducing flow velocity in cave conduits from scallops: The National Speleological Society Bulletin, v. 36, no. 2, p. 1–5.

Dirks, P.H.G.M., Kibii, J.M., Kuhn, B.F., Steininger, C., Churchill, S.E., Kramers, J.D., and Pickering, R., 2010, Geological setting and age of *Australopithecus sediba* from Southern Africa: Science, v. 328, no. 5975, p. 205–208. https://doi.org/10.1126/science.1184950.

Gilbertson, D., Bird, M., Hunt, C., McLaren, S., Banda, R.M., Pyatt, B., Rose, J., and Stephens, M., 2005, Past human activity and geomorphological change in a guano-rich tropical cave mouth: Initial Interpretations of the Late Quaternary Succession in the Great Cave of Niah, Sarawak: Asian Perspectives, p. 16–41. https://doi.org/10.1353/asi.2005.0007.

Gillieson, D., 1986, Cave sedimentation in the New Guinea Highlands: Earth Surface Processes and Landforms, v.11, no. 5, p. 533–543.

GPS Kit (version 8.0.4), 2017, GPS Kit - Offline GPS Tracker: The original GPS app, iOS, Gafara, LLC, https://apps.apple.com/us/app/gps-kit-offline-gps-tracker/id287909017.

Granger, D.E., Fabel, D., and Palmer, A.N., 2001, Pliocene- Pleistocene incision of the Green River, Kentucky, determined from radioactive decay of Cosmogenic 26Al and 10Be in Mammoth Cave dediments: Geological Society of America Bulletin, v. 113, no. 7, p. 825–836. https://doi.org/10.1130/0016-7606(2001)113<0825:PPIOTG>2.0.CO;2.

Gustavsson, M., Kolstrup, E., and Seijmonsbergen, A.C., 2006, A new symbol-and-GIS based detailed geomorphological mapping system: Renewal of a scientific discipline for understanding landscape development: Geomorphology, v. 77, no. 1-2, p. 90-111.

Haynes, D.D., 1964, Geology of the Mammoth Cave Quadrangle, Kentucky: USGS, https://pubs.er.usgs.gov/publication/gq351, [accessed May 21, 2019].

Hungr, O., 1995, A model for the runout analysis of rapid flow slides, debris lows, and avalanches: Canadian Geotechnical Journal, v. 32, no. 4, p. 610–623.

Jurgiel, B., Verchere, P., Tourigny, E., and Becerra, J., 2020, *Profile Tool*, https://plugins.qgis.org/plugins/profiletool/.

Kellerhals, R., Shaw, J., and Arora, V.K., 1975, On grain size from thin sections: The Journal of Geology, v. 83, no. 1, p. 79−96. https://www.jstor.org/stable/30062340?seq=1#metadata_info_tab_contents.

Mussett, A.E. and Khan, M.A., 2000, Looking into the Earth: an introduction to geological geophysics: Cambridge University Press, 470 p.

Ortiz, L.W., Ettinger, H.J., Fairchild, C.I., 1975, Calibration standards for counting asbestos: American Industrial Hygiene Association Journal, v. 36, no. 2, p. 104-112.

Palmer, A.N., 1989, Geomorphic history of the Mammoth Cave System, *in* Karst Hydrology: Springer, p. 317–337.

Palmer, A.N., 2007, Cave Geology: Dayton, Cave Books, 454 p.

Palmer, A.N., Olson, R., and Palmer, M.V., 2019, Evidence for extreme floods in New Discovery and related passages in Mammoth Cave: Cave Research Foundation Newsletter, v. 47, no. 2, p. 3–6.

Palmer, A.N., and Palmer, M.V., 2005, Hydraulic processes in the origin of Tiankengs: Cave and Karst Science, v. 32, no. 2/3, p. 101–106.

Pierson, T. C. 1986. Flow behavior of channelized debris flows, Mount St. Helens, Washington. In Hillslope Processes, Abrahams AD (ed.). Allen and Unwin: Boston; 269±296.

Pierson, T. C., 1986, Flow behavior of channelized debris flows, Mount St. Helens, Washington: *in* Hillslope Processes, Abrahams A.D. (ed.). Allen and Unwin: Boston; p. 269–296.

Prior, D.B., Bornhold, B.D., and Johns, M.W., 1984, Depositional characteristics of a submarine debris flow: The Journal of Geology, v. 92, no. 6, p. 707–727.

QGIS.org, 2020, QGIS Geographic Information System. OpenSource Geospatial Foundation Project. https://qgis.org.

Santamaría, D., Fortea, J., De la Rasilla, M., Martinez, L., Martinez, E., Cañaveras, J.C., and Sánchez-Moral, S., 2010, The Technological and typological behaviour of a Neanderthal group from El Sidrón Cave (Asturias, Spain): Oxford Journal of Archaeology, v. 29, no. 2, p. 119–148. https://doi.org/10.1111/j.1468-0092.2010.00342.x.

Siemens, 2020, Modeling Geometry *in* Simcenter STAR-CCM+ Documentation [accessed July 22, 2020], https://documentation.thesteveportal.plm.automation.siemens.com/starccmplus_latest_en/index.html?param=7vI4S&authLoc=https://thesteveportal.plm.automation.siemens.com/AuthoriseRedirect#page/STARCCMP%2FGUID-B18CC064-4DDB-4610-ADED-81B92767FF41.html%23wwconnect_header

Smith, T., ed., 2014, Manual on test sieving methods / prepared by ASTM Committee E29 as Guidelines for establishing sieve analysis procedures: West Conshohocken, PA, ASTM manual series MNL32, 71 p. https://www.astm.org/mnl32-5th-eb.html.

Studinski, J.M., and Grubbs, S.A., 2007, Environmental factors affecting the distribution of aquatic invertebrates in temporary ponds in Mammoth Cave National Park, Kentucky, USA.: Hydrobiologia, v. 575, no. 1, p. 211–220.

Takahashi, T., 1981, Debris Flow: Annual Review of Fluid Mechanics, v. 13, no. 1, p. 57–77.

USGS, 1972, Mammoth Cave National Park and Vicinity: United States Geological Survey, https://store.usgs.gov/assets/MOD/StoreFiles/DenverPDFs/24K/KY/60861_KY_Mammoth_Cave_NP_and_Vicinity.pdf. [accessed May 17, 2019].

USNPS, 2018, Mammoth Cave National Park map, https://www.nps.gov/maca/planyourvisit/maps.htm. [accessed September 23, 2020].
Van Gundy, J.J., and White, W.B., 2009, Sediment flushing in Mystic Cave, West Virginia, USA, in response to the 1985 Potomac Valley Flood: International Journal of Speleology, v. 38, no. 2, p. 103–109. https://doi.org/10.5038/1827-806x.38.2.2.
Wilcox, J., 1971, New Discovery, Mammoth Cave, Mammoth Cave National Park, Kentucky: Cave Research Foundation, 1 sheet.

Kaitlin J.H. Read, Leslie A. Melim, Ara S. Winter, and Diana E. Northup. Bacterial diversity in vadose cave pools: evidence for isolated ecosystems. *Journal of Cave and Karst Studies*, v. 83, no. 4, p. 163-188. DOI:10.4311/2020MB0120

BACTERIAL DIVERSITY IN VADOSE CAVE POOLS: EVIDENCE FOR ISOLATED ECOSYSTEMS

Kaitlin J.H. Read[1,4], Leslie A. Melim[2], Ara S. Winter[3], and Diana E. Northup[1,C]

Abstract

Microbial diversity of cave pools, especially vadose pools, has received relatively little attention. To help fill this gap, this study reports on the bacterial diversity of 17 pools in three New Mexican arid land caves: Carlsbad Cavern, Lechuguilla Cave, and Hell Below Cave. These pools are spread throughout the caves and, with two exceptions, are not connected. The pools share a basic water chemistry, with fresh water of the calcium-magnesium-bicarbonate type. These 17 pools have Chao1 values between 40 and 1738; the Shannon diversity averages 4.6 ± 1.1, ranging from 2.6 to 6.4; and the Simpson averages 0.881 ± 0.099, ranging from 0.622 to 0.981. No two pools had the same communities, even at the phylum level. *Nitrospirae*, *Alphaproteobacteria*, *Betaproteobacteria* and *Gammaproteobacteria* were found >5% abundance in nine or more cave pools. *Actinobacteria*, *Chloroflexi*, *Fibrobacteres*, *Firmicutes* and *Plantomycetes* were at >5 % in four to six pools. Of the top ten widespread bacterial genera, *Nitrospira* was found in all pools, with >5 % in eleven pools. Other common genera include *Polyclorovans*, *Propionibacterium*, *Polaromonas*, *Haliangium*, *Bacillus*, Subgroup 6 uncultured Acidobacteria, *Candidatus* Omnitrophica, and uncultured Nitrosomonadaceae. Presence of several potential nitrogen cycling bacteria (e.g., *Nitrospira*) in the study pools suggests that nitrogen cycling may be an important bacterial role. There is some evidence of human contamination, particularly in the heavily visited Big Room, Carlsbad Cavern, but it is not the dominant control. Rather than a single stable cave pool community, adapted to the cave pool ecosystem, the data show 17 different communities, despite relatively similar conditions. The data support the hypothesis that each pool is a unique, isolated ecosystem, with differences likely caused more by the isolation of each pool than by variable chemistry. Thus, the common habit of grouping samples, while useful for some questions, may not capture the diversity present in cave ecosystems.

INTRODUCTION

Karst caves, those found in limestone or dolomite, are recognized as potential windows into subsurface ecosystems (Engel, 2010). Microorganisms are an important part of these ecosystems, but understanding of their diversity is incomplete (Engel, 2010). The bacterial diversity of karst caves is a function of the physicochemical and nutrient setting, which varies widely between and within caves (e.g., Barton and Northup, 2007; Engel, 2010). These local conditions are, in turn, a function of the larger geological and ecological setting of the caves (Jones and Bennett, 2017; Brewer and Fierer, 2018; Alonso, et al., 2019). Because of interest in their unusual ecosystems, some of the best-studied caves are those with chemolithoautotrophy based on sulfur and/or methane (e.g., Movile Cave, Sarbu et al., 1996; Chen et al., 2009; Porter et al., 2009; Kumaresan et al., 2018; Cueva de Villa Luz, Hose et al., 2000; Hose and Rosales-Lagarde, 2017; Lower Kane Cave, Engel et al., 2004a, 2004b; Frasassi Cave, Macalady et al., 2006, 2007, 2008; Jones et al., 2016; and a semi-artificial mineral spring cave in Germany, Karwautz et al., 2018). Other caves also have ecosystems based on oxidation of iron and manganese, resulting in the formation of ferromanganese deposits (FMDs) (Northup et al., 2003; Spilde et al., 2005; Carmichael et al., 2013a, 2013b; Carmichael and Bräuer, 2015; Estes et al., 2017). The Nullarbor caves, Australia, have been shown to have a chemolithoautotrophic system based on nitrite oxidation (Holmes et al., 2001). The majority of karst caves, however, lack an obvious source of chemolithoautotrophy and are generally considered dependent on organic matter from the surface via water, air, or macrofauna transport (Goldscheider et al., 2006; Simon et al., 2007; Griebler and Lueders, 2009). However, karst caves in arid to semiarid regions are more isolated from surface inputs and are more likely to have chemolithoautotrophy (Ortiz et al., 2013, 2014).

Even with this limitation, karst caves are increasingly recognized as containing diverse microbial ecosystems. As a result, there are a growing number of studies in caves looking at the microbial communities on speleothems (Barton et al., 2007; Ikner et al., 2007; Legatzki et al., 2011, 2012; Engel et al., 2013; Yun et al., 2016a, Leuko et al., 2017, Thompson et al., 2019), wall rock (Porca et al., 2012; Carmichael et al., 2013a, 2013b; Carmichael and Bräuer, 2015; Wu et al., 2015; Lavoie et al., 2017; Sauro et al., 2018), cave sediment (Rusterholz and Mallory, 1994; Chelius and Moore, 2004; Adetutu et al., 2012; Wu et al., 2015; Brannen-Donnelly and Engel, 2015; Sauro et al., 2018; Thompson et al., 2019), and cave streams (Brannen-Donnelly and Engel, 2015; Plese et al., 2016). There are fewer studies on cave pools, which are

[1]Department of Biology, University of New Mexico
[2]Department of Earth, Atm. & GIS, Western Illinois University
[3]Bosque Ecosystem Monitoring Program, Department of Biology, University of New Mexico
[C]*Corresponding Author* dnorthup@unm.edu
[4]*Current address,* Nanoscience and Microsystems Engineering, College of Engineering, University of New Mexico

areas of standing water in caves (Shabarova and Pernthaler, 2010; Shabrova et al., 2013, 2014; Hershey et al., 2018; Sauro et al., 2018).

Studies of microorganisms in groundwater and cave streams have shown that the attached community is different from the planktonic community (Goldscheider et al., 2006; Brannen-Donnelly and Engel, 2015; Savio et al., 2018). A number of studies looking specifically at the planktonic community in karst aquifers through sampling of springs have identified an autochthonous microbial endokarst community (or AMEC) that is stable over time, particularly in aquifers with longer residence times (Farnleitner et al., 2005; Pronk et al., 2009; Savio et al., 2018). This community is disrupted during recharge with transient microorganisms from the surface, which then decrease over time (Savio et al., 2018, 2019; Wegner et al., 2019). Shabarova et al. (2013; 2014) looked at epiphreatic karst cave pools where seasonal rise of the water table completely flushed the pools. They found that each flood reintroduced the AMEC from the groundwater, which then rapidly lost diversity and abundance within weeks of residence time, such that the full AMEC was no longer present (Shabarova et al., 2013, 2014). The results from these AMEC studies suggest three possible microbial communities with different conditions: a surface community adapted to soil conditions, the AMEC adapted to groundwater conditions, and a cave pool community adapted to the conditions of the cave pool.

Cave pools in the vadose (unsaturated) zone are separate from the karst aquifer as they are perched above the water table. These pools collect infiltrated water, often within days to weeks of rainfall events (Williams, 1983; Oster et al., 2012). However, based on oxygen isotopic and tritium studies (Even et al., 1986; Chapman et al., 1992; Turin and Plummer, 1995, 2001; Williams and Fowler, 2002), residence time for water in the vadose zone is generally much longer. In temperate climates, residence times range from <1 year up to several years (Spötl et al., 2005; Genty et al., 2014; Mischal et al., 2015). In arid climates, residence times are longer, up to several decades (Chapman et al., 1992; Turin and Plummer, 1995, 2001; Kaufman et al., 2003). Depth of the cave is also a factor, with shallow caves often having shorter residence times of weeks to months (Oster et al., 2012). One of the longest residence times (17-36 years) documented is for Carlsbad Cavern, which is both deep and in an arid climate (Chapman et al., 1992). Thus, water entering most karst caves is not usually from the current rain event, but rather from the rain infiltrating from the surface pushing water out into the cave from a reservoir of water in the vadose zone (Fairchild and Baker, 2012; Genty et al., 2014).

This idea of a reservoir within the vadose zone has implications for the microbial community entering the cave with the water. Particularly for caves where drip water has a long residence time within the vadose zone, the soil microbial community from the surface is unlikely to survive unchanged. Even within karst aquifers, the soil community does not persist (Savio et al., 2019; Wegner et al., 2019). Most studies of karst habitats have indeed found cave microbial communities as distinct from the surface communities (e.g., Engel, 2010; Ortiz et al., 2013; Lavoie et al., 2017). Cave pools, however, are almost unstudied. Data on the bacterial diversity of vadose pools is limited to one study that sampled the planktonic community in two deep (~700 m below the entrance) vadose pools in a Swiss Alpine cave (Shabarova and Pernthaler, 2010). These two pools contained very diverse bacterial communities based on comparisons of the 16S rRNA gene sequencing. These pools were dominated by *Betaproteobacteria* (*Oxalobacteraceae*), and *Actinobacteria*. One of the pools also had abundant *Candidatus Omnitrophica* (originally named *OP3*) (Rivas-Marı and Devos, 2018, Kirs et al., 2020). Out of 109 operational taxonomic units (OTUs) identified in the two pools, only five were shared (two affiliated with Oxalobacteraceae; one affiliated with *Acinetobacter*, one with *Rhodoferax*, and one with *Nitrosomonadaceae*). Shabarova and Pernthaler (2010) suggest the large differences between the two pools relatively close to each other is related to differences in chemistry, since one pool has higher SO_4^{2-} and Mg^{2+}, and possibly to different microbial inputs with incoming drips.

Thus, questions remain for the microbial diversity of cave pools, particularly vadose cave pools isolated from the local aquifer. This study reports on the diversity of planktonic bacteria from 17 vadose pools from three karst caves in the Guadalupe Mountains of New Mexico, including nine pools from Carlsbad Cavern, six pools in Lechuguilla Cave, and two pools from Hell Below Cave. This study uses this larger, more diverse dataset to better explore the suggestion raised by Shabarova et al. (2010) that vadose pools each contain unique communities.

METHODS

Cave Setting and Geologic History

The three karst caves sampled, Carlsbad Cavern, Lechuguilla Cave, and Hell Below Cave, are located in the Guadalupe Mountains of New Mexico and Texas, U.S.A., at the northern edge of the Chihuahuan Desert (Fig. 1). These caves are in the Upper Permian Capitan Reef Complex, mainly in the reef and forereef facies of the Capitan Limestone, but they also extend into the time-equivalent backreef facies of the Seven Rivers, Yates, and Tansill Formations (Hill, 1987; Jagnow, 1999). The backreef facies are dolomite with interbedded sandstones, while the reef and forereef are partly dolomitized limestone (Dunham, 1972; Jagnow, 1979; Melim and Scholle, 2002; Budd et al., 2013; Frost et al., 2013).

The caves of the Guadalupe Mountains are hypogene caves dissolved by reactions with rising waters producing H_2SO_4 at the water table (Hill, 1987; Jagnow et al., 2000; Engel et al., 2004; Hose and Macalady, 2006; Palmer, 2006,

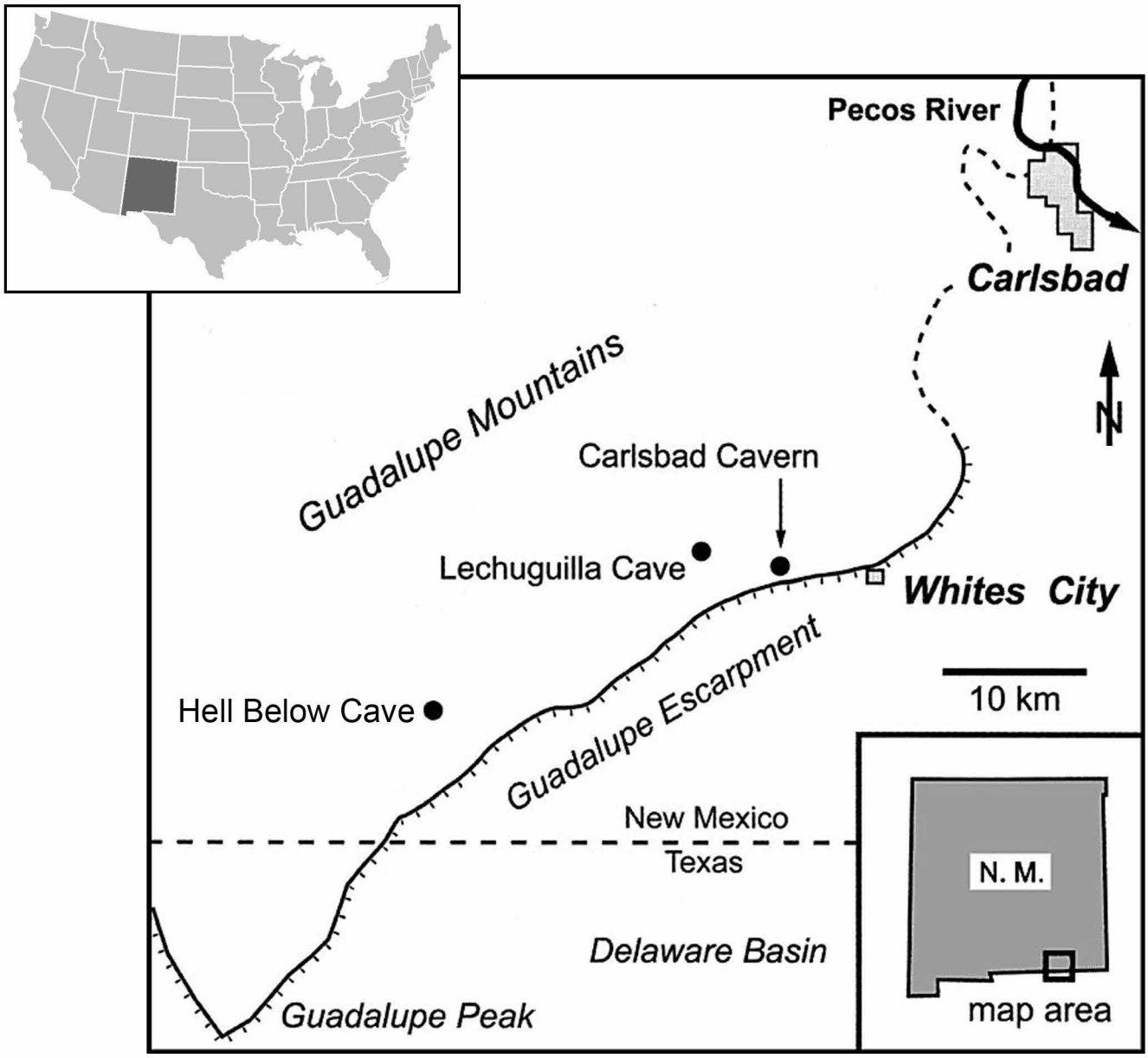

Figure 1. Location map of the three sampled caves, New Mexico, U.S.A. (After Palmer and Palmer, 2000).

2007; Kirkland, 2014). Speleogenesis started in the higher elevation caves (including Hell Below Cave) at ~11.3 Ma and continued during uplift through the upper reaches of Lechuguilla Cave at 6.0 to 5.7 Ma, and finally the lowest dated level, the Big Room in Carlsbad Cavern at 4.0 Ma to 3.9 Ma (Polyak et al., 1998). Since H_2SO_4 is a very strong acid, these karst caves contain unusually large rooms (such as the Big Room at over 3.3 hectares, 8.2 acres), often with flat floors that contain perched cave pools (Hill, 1987; Jagnow et al., 2000). Carlsbad Cavern and Lechuguilla Cave are very large and very deep caves (~64 km long and ~315 m deep; ~242 km long and ~484 m deep respectively, (Gulden 2020). Hell Below Cave is much smaller and more shallow (<400 m long; ~60 m deep) than the other two caves.

The water table in the region is ~960-970 m elevation, well below the elevation of the sampled pools (Hill, 1990; Ingraham et al., 1990; Turin and Plummer, 2000; Land and Burger, 2008; Palmer and Palmer, 2012). Each pool is fed by ceiling drips and loses water by a combination of leaking and evaporation (Ingraham et al., 1990; Forbes, 2000; Turin and Plummer, 2000). With a few exceptions, the pools are not full to the spill point under current climate conditions, but show paleo-water lines that indicate wetter conditions in the past (Melim et al., 2006; Polyak et al., 2012). Dating of shelfstone in the Big Room, Carlsbad Cavern, suggests drying started by 13.5 ka during the transition from cool, wet glacial conditions to the warm, dry Holocene (Polyak et al., 2012). In the current arid climate, water infiltrates during infrequent heavy rains (Williams, 1983; Van der Heidje et al., 1997) and spends considerable time in the vadose zone. For Carlsbad Cavern, the residence time of water in the vadose zone is 17−36 years (Chapman et al., 1992), while for

parts of Lechuguilla Cave it exceeds 50 years (Turin and Plummer, 1995, 2001; Turin et al., 2001). Considering the long residence times and the thin desert soils, the seepage water is expected to have very low TOC (Shen et al., 2015; Blyth et al., 2016; Lechleitner et al., 2017); which has been confirmed for seepage into Lechuguilla Cave (Turin and Plummer, 2000; Levy, 2007b).

Geochemical studies on pools in Lechuguilla Cave (Turin and Plummer, 2000; Levy, 2007a) and Carlsbad Cavern (Chapman et al., 1992; Forbes, 2000) have identified a 'typical pool water' that is fresh (Total dissolved solids, 200-500 mg/L) and of the calcium-magnesium-bicarbonate type, suggesting that leakage balances inflow, and evaporation is less important. Exceptions occur near gypsum deposits (where sulfate exceeds bicarbonate) and in a few pools with minimal leakage where evaporation has concentrated the water to a brine (Forbes, 2000; Turin and Plummer, 2000; Levy and Amrhein, 2011). However, there is considerable chemical variation among pools, even nearby pools, attributed to the complexity of infiltration, evaporation, and rock interaction for each pool (Forbes, 2000; Turin and Plummer, 2000; Levy, 2007a). Combining the chemical variation with the fact that pools do not currently connect via outflow suggests that these pools are completely isolated systems. How long they have been isolated is difficult to determine, but for some it could date back to the time when Big Room pools dried up at 13.5 ka during the terminal Pleistocene drought (Polyak et al., 2012).

Data on total organic carbon (TOC) and nitrate are available for drips and pools in Carlsbad Cavern (Brooke, 1996; Van der Heidje et al., 1997) and Lechuguilla (Turin and Plummer, 2000; Levy, 2007a, 2007b), albeit not for the specific pools sampled in this study. The highest TOC values (20−40 mg/L) were found in the eastern portions of Carlsbad and attributed to a combination of bat guano and a leaky sewage line (Brooke, 1996; Van der Heidje et al., 1997). Big Room and New Mexico Room pools have values between <1 (detection limit) and 15 mg/L; Lower Cave pools are similar except for one pool with 18 mg/L (Van der Heidje et al., 1997). Higher values are near trails used by visitors and Van der Heidje et al., (1997) suggest trail maintenance, including washing, is the source of contamination. TOC values from Lechuguilla are uniformly low (<1.7 mg/L, with the exception of Briny Pool at 11 mg/L; Turin and Plummer, 2000; Levy, 2007a, 2007b). Briny Pool is a very unusual pool that is highly concentrated by evaporation (Levy and Amrhein, 2011).

Nitrate values in Carlsbad are similar to TOC values: higher in eastern portions of the cave (36−238 mg/L), and low in the Big Room, New Mexico Room and Lower Cave (2−22 mg/L), except for one value of 30 mg/L from the Rookery (Brooke, 1996; Van der Heidje et al., 1997). Nitrate values collected by Turin and Plummer (2000) for Lechuguilla Cave are more variable, with 82% below 10 mg/L and 5 % over 30 mg/L. The average for the 95 % of pools with <30 mg/L is 6 mg/L. Levy (2007a, 2007b) reported lower average values for Lechuguilla Cave (<1.7 mg/L).

Sample Sites

A total of 17 pools were analyzed including nine pools from Carlsbad Cavern, six pools in Lechuguilla Cave and two pools in Hell Below Cave. The diversity of sample sites is greater than suggested by just three caves as Carlsbad Cavern and Lechuguilla Cave are very large caves and the sample sites are widely spaced (Figs. 2 and 3).

Three rooms from Carlsbad Cavern were sampled, the Big Room, Lower Cave and the New Mexico Room (Fig. 2). These are all in Hydrologic Domain 2 of Van der Heidje et al., (1997), which they characterized as having diffuse infiltration with recharge in Bat Cave Draw and have no significant nitrate concentrations. The Big Room is over 3.3 ha and ~200 m beneath the surface (Hill, 1987). It is the most developed area in the cave with asphalt paved trails and ~500,000 visitors/year. It is also the most impacted historically with extensive off-trail damage dating back to private ownership (pre-1923). The floor is very irregular with abundant stalagmites and many pool basins (mostly dry). Four widely spaced pools were sampled in the Big Room: BR17, BR25, BR30 and BR44 (Fig. 2). Pool BR17 is ~0.4 m deep pool and is located ~3 m from the public trail (Fig. 4A). Although not visited today, the area around the pool was heavily trampled in the past and loose debris from the surrounding area covers the pool spar on the bottom of the pool. Pool BR25 is also 2−3 m from the public trail, but is separated from the trail by several large stalagmites. BR25 is currently ~0.6 m deep, but has a well-developed shelfstone water line indicating a paleo depth >2 m. This area shows little evidence of past traffic. Pool BR30 is <2 m from the public trail and is the only sampled Big Room pool that is nearly full (Fig. 4B). The maximum depth is ~0.8 m, which is <5 cm from the overflow level. Pool BR44 is under the edge of Crystal Springs Dome, a rare (for Carlsbad) active stalagmite located adjacent to the public trail. The pool is currently up to 1 m in depth, but the paleo-water line suggests a maximum depth of >2 m in the past. Although the closest of the Big Room pools to the public trail (<1 m), this pool sits under an overhang that protects it from direct contact. However, water entering the pool runs off of Crystal Springs Dome that is in reach of visitors.

Lower Cave sits underneath the Big Room at a depth of ~240 m beneath the entrance (Hill, 1987). Visitation to Lower Cave is restricted to ranger-guided tours (12 person limit) on marked trails but not paved as in the Big Room. Three pools were sampled in Lower Cave: LC5, CC2-LC, and CC7-LC (Fig. 2). LC5 is in The Rookery, an area of active drips and many cave pearl nests (Hill, 1987; Melim and Spilde, 2018). This pool is ~4 cm deep in a very flat area of the cave. The guided trail is immediately adjacent to this pool but is elevated on plastic platforms to keep visitors from walking in the water. Pool CC2-LC is the largest pool in Lower Cave (~1 m deep), and the guided trail crosses it on a low bridge.

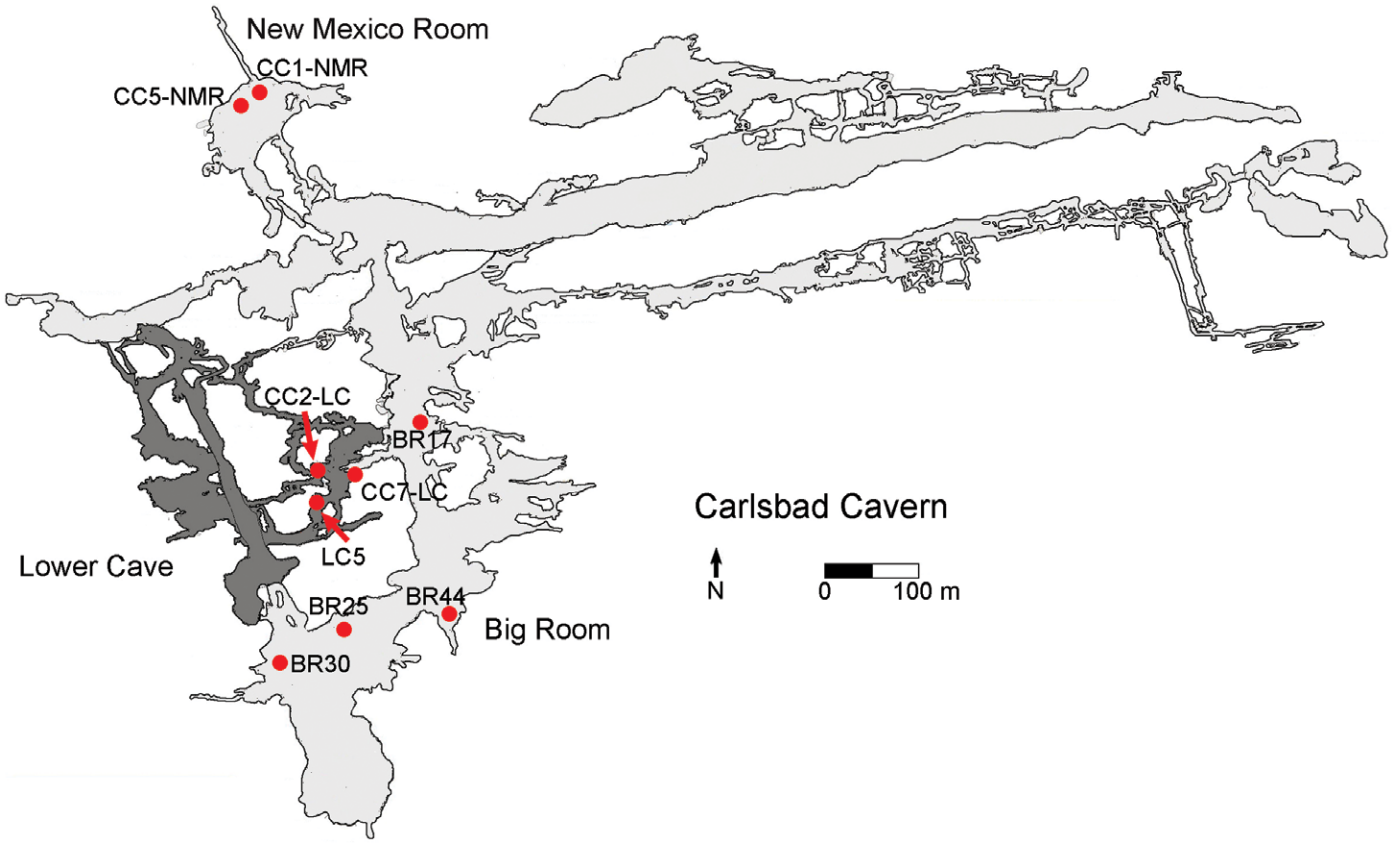

Figure 2. Map of Carlsbad Cavern showing the location of the sampled pools. Map courtesy of the Cave Research Foundation.

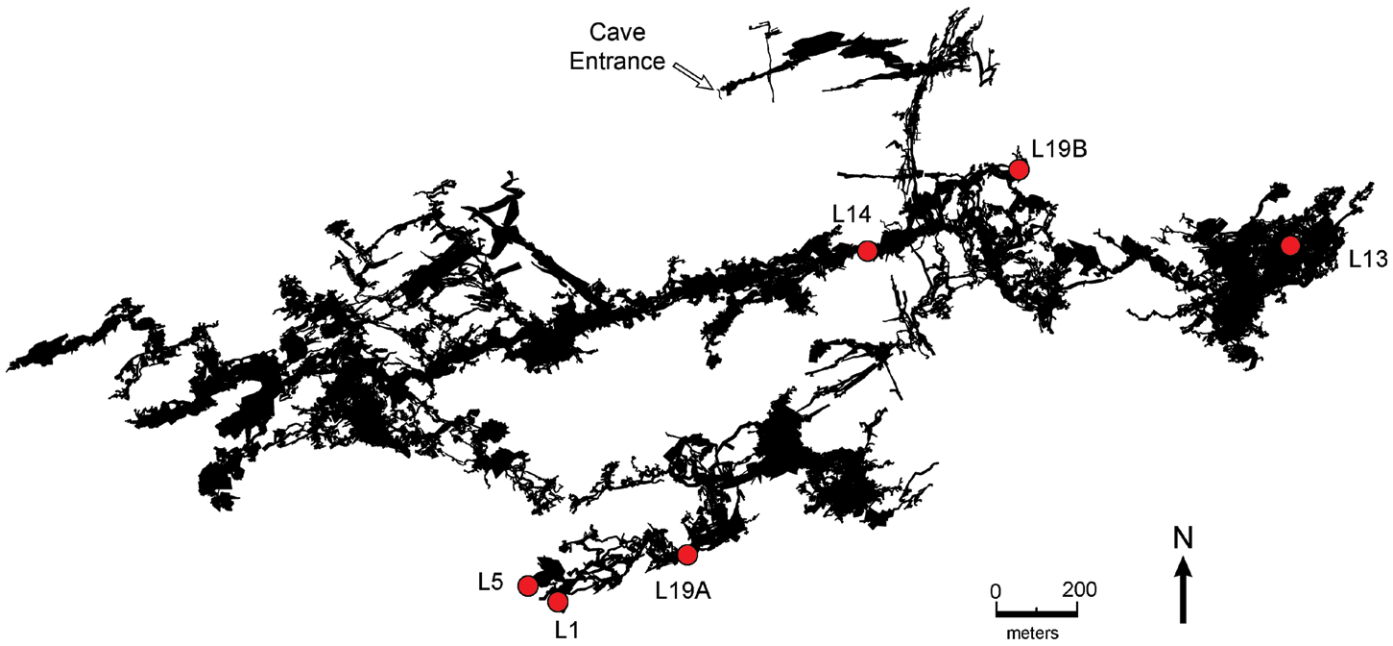

Figure 3. Map of Lechuguilla Cave showing the location of the sampled pools. Map courtesy of the National Park Service.

Like the nearby Rookery, this area has many active drips and the pool is full, or nearly so. CC7-LC, in contrast, is a small pool in an offshoot passage ~50 m from the active trail in an area almost never visited.

The final sample area in Carlsbad Cavern is the New Mexico Room, an offshoot of the main cave at approximately the same elevation as the Big Room (Hill, 1987). It was never developed for visitors and is rarely visited today. Private visits were more common in the past, but never in large numbers like in the Big Room or Lower Cave. Two adjacent

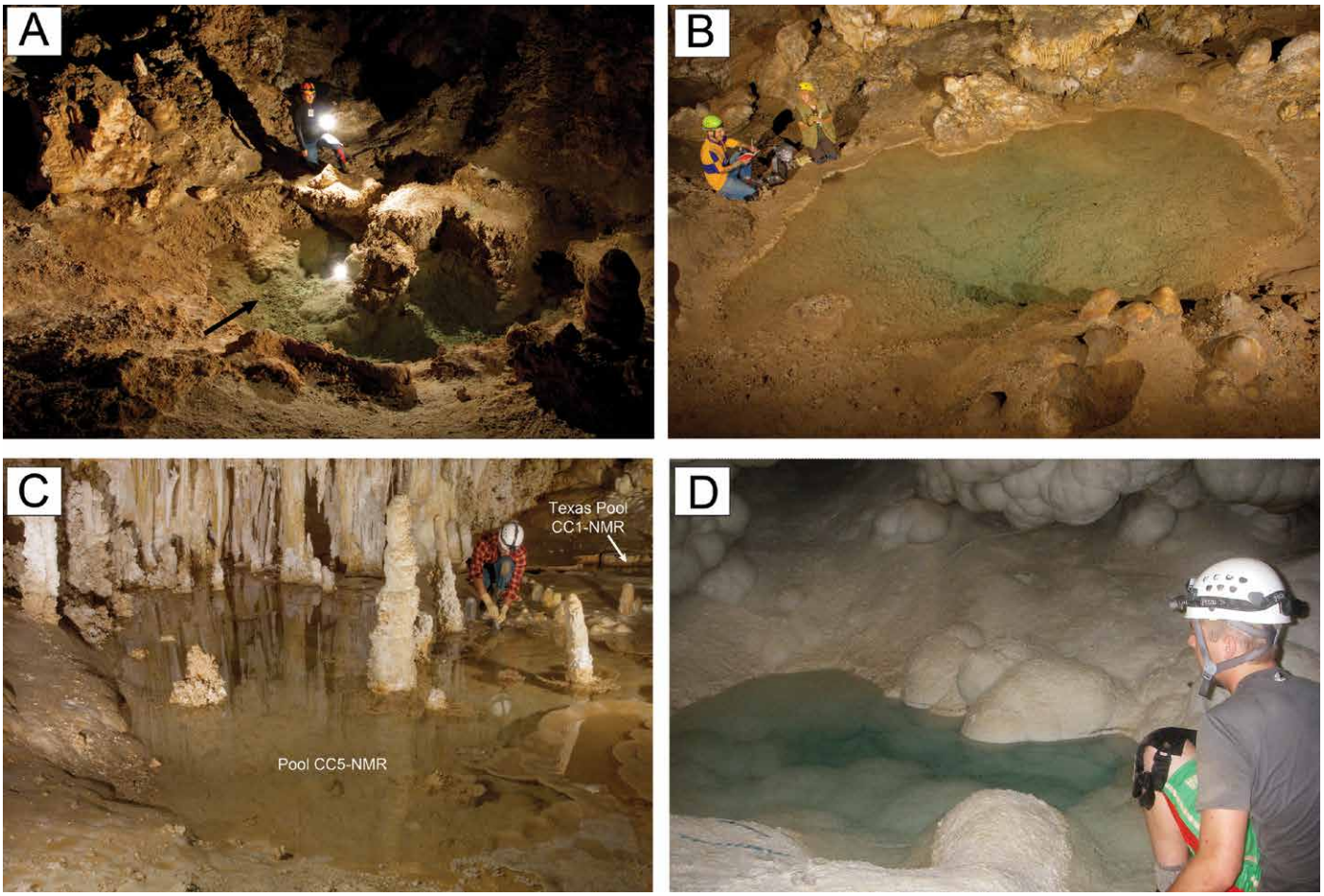

Figure 4. Representative cave pools in this study. A) Carlsbad Cavern, Big Room pool BR17. Photo taken from trail. Note loose debris in the bottom of the pool (arrow), which includes debris from the trail. B) Carlsbad Cavern, Big Room pool BR30, one of the few pools in Carlsbad that is nearly full. C) Carlsbad Cavern, New Mexico Room pools CC5-NMR and CC1-NMR. Note that CC5-NMR drains into CC1-NMR when it is full. D) Lechuguilla Cave pool L14. Photo credits: A-C, Kenneth Ingham; D, Pat Cicero.

pools were sampled, CC1-NMR and CC5-NMR (Figs. 2 and 4C). CC1-NMR is Texas Pool, a shallow (~0.2 m) pool outlined in overhanging shelfstone, which defines a paleo-depth of ~0.4 m. CC5-NMR is a larger pool that is nearly full today. When it overflows, it drains into CC1-NMR. Currently, however, CC1-NMR only collects water from drips and flowstone. The marked trail goes by both pools.

Lechuguilla Cave is also located in the Carlsbad Caverns National Park, about 5.8 km northwest of Carlsbad Cavern (Fig. 1). Access to Lechuguilla Cave is limited by permit, with 50−100 research/exploration visitors per year for the whole cave. Six pools were sampled in Lechuguilla Cave (Fig. 3). Pool L1 is a drinking water source (so more visited than some) near an underground campsite. It is 17 m × 14 m, ~12 m deep, and full. The pool is coated in pool spar and fed by several areas of flowstone on one side. Pool L5 is an irregular pool coated in yellowish pool spar, instead of the more common white, in the Vesuvius area of Lechuguilla Cave. It is shallow (~20 cm) with maximum dimensions of 4 m × 6.5 m in a T-shape. The pool is full to the water line marked by minor areas of shelfstone. However, most of the pool edge is flowstone coming in from surrounding stalagmites. Pool L13 is ~2 m × 5 m and ~1.5 m deep, but is the remnant of a larger pool up to 11 m deep. The larger pool is completely covered in pool spar and pool fingers. There is no evidence of a mineral water line at the current depth. Pool L14 is in the Deep Secrets area of Lechuguilla (Fig. 4D). The pool is a small (2 m × 4 m, <0.5 m deep) remnant of a much larger pool (>3 m deep) coated in pool spar clouds. There is a faint mineral water line near the current water line, suggesting Pool L14 has been stable at this depth for some time. Pool L19A is a small (0.5 × 1 m; ~10 cm deep) oval pool perched on a shelf in an area of continuous flowstone in the Tower Place area. The pool floor is coated in pool spar and the pool is full. L19B is a pool in the Nirvana area of Lechuguilla. No description is available for this pool.

Hell Below Cave is located in southeastern New Mexico in the Guadalupe Mountains, about 60 km southwest of the town of Carlsbad (Fig. 1). The two adjacent (<1 m apart) pools sampled are in an area with minimal visitation (<10 visitors/year), approximately 60 m below the surface. Hell Below pool HB1 is larger, much deeper (>2 m), and was near

the spill level when sampled. HB2, in contrast, is small and shallow (<10 cm), was nearly full when sampled, and is fed by an active drip. HB2 likely drains into HB1 when full.

Sampling and DNA Extraction

Samples were collected under Permit #CAVE-2008-SCI-0004 (Carlsbad Caverns National Park, 2008-2013), issued to Northup, and Forest Service Permit #FS-2700-4 (10/09) (Hell Below Cave, 2011-2030) issued to Melim. Approximately one liter of water from pools was filtered through a sterile Sterivex syringe (Millipore, Billerica, MA) via a micropore 0.2ul filter, to capture microbial cells on the filter. Sucrose lysis buffer (0.5 mL) (Giovannoni et al., 1990) was added aseptically to break open cells and stabilize the DNA. Sterivex filters were capped with the syringe and a pipette tip and were then transported to the lab on ice where they were stored in a −80 °C freezer until DNA extraction. DNA released into the sucrose lysis buffer was extracted using MoBio Power Water DNA extraction kit using the manufacturer's protocol (MoBio, Carlsbad, CA) with bead beating instead of vortexing and elution in 30 µL rather than 50 µL of Buffer EB. Purified, extracted DNA was amplified with the polymerase chain reaction (PCR), using 46F (5'-GCYTAAYACATGCAAGTCG-3') as the forward primer and 1409R 5'-GTGACGGGCRGTGTGTRCAA-3') (Northup et al. 2010) as the reverse primer and AmpliTaq LD (Applied Biosystems) with an MJ thermal cycler as follows: 4 min denaturation at 94 °C, followed by 35 cycles of 45 s annealing at 55 °C, 2 min at 72 °C (extension), and 30 s at 94 °C (denaturation), with a final 45 s 55 °C annealing and 20 min 72 °C extension step after cycling was complete.

Sequencing and Quality Control

Samples were analyzed with next-generation sequencing of the 16S SSU gene bacterial V1-3 region (primer 27F, Lane, 1991) using Roche FLX and Titanium 454 technology conducted by MR DNA, Shallowater, TX (http://www.mrdnalab.com/). All 454 data were processed in QIIME 1.9.1 (Caporaso et al., 2010). Quality control and trimming of the 454 dataset were done using the split_libraries.py command with a lower length (−L) of 100 bp and an upper length (−L) of 500. A quality score (−s) of 30 was chosen. Removal of erroneous sequences (denoising) and OTU clustering were done using pick_de_novo_otus.py pipeline with the sumaclust option (Mercier et al., 2013). The sumaclust algorithm is mainly useful to detect the 'erroneous' sequences created during amplification and sequencing protocols. OTUs were clustered at the 97% similarity level using sumaclust. The pick_de_novo command also picks the representative set and assigns taxonomy using uclust (Edgar, 2006) against the Silva 1.28 database (McDonald et al., 2012). Chimera checking was done using USEARCH to detect artifacts created during sequencing. Good's coverage showed that we were successful in getting nearly all of the diversity from our samples (Table 1). Values ranged from 87.13 % to 99.11 % with an average value of 94.98 %. Archaea were not analyzed.

Taxonomic Analysis

Bacterial taxonomies were assigned from the phylum to genera levels. OTUs unassigned to a phylogenetic level that passed chimera checking were consolidated into an *Unassigned* category. The ten most abundant bacterial phyla or *Proteobacteria* class by percentage were displayed; the remaining assigned phyla/proteobacterial classes were condensed into an *Other* category. The same method was used to categorize bacterial genera.

Diversity Analysis

Community dissimilarity was visualized using the phyloseq package (McMurdie and Holmes, 2013) and ggplot2 (Wickham, 2009) in R (R Development Core Team, 2012). Alpha diversity was analyzed using observed OTUs, Shannon, Simpson's Index of Diversity (1-D), and Chao1 indices in the phyloseq package. Alpha diversity measures were carried out on the raw data as recommended (McMurdie and Holmes, 2013). Observed OTUs and Simpson will scale with increasing library size; however both Chao1 and Shannon are robust measures of richness and diversity. Observed OTUs is the raw number of species OTUs present in each sample of quality controlled and clustered sequences as described above. Shannon index assumes even distribution of all OTUs, while Simpson's index is more influenced by dominated OTUs in a sample (Kim et al., 2017).

To assist in visualizing the diversity, plots and tables illustrate phyla and genera abundant in individual pools. Selection of which phyla (and genera) to illustrate is complicated by the large number present (38 phyla, 509 genera). Simply sorting by number of OTUs over-weighted the resulting lists for pools with large numbers of OTUs (mainly the Carlsbad Big Room pools). To better represent all pools, raw OTU counts were changed to Percent OTUs in each pool. Selecting only those phyla present at >5 % in any pool, 16 total phyla were plotted with less abundant phyla included as "other minor phyla" (0 % to 5 % of total) (Fig. 5). In addition, these 16 phyla are also listed in Table 2, with the more abundant phyla for each pool noted. Table 3 shows the top ten genera across all pools, selecting for those genera present in the most pools. While useful, this table leaves 23 % to 83 % of the genera in the "other genera" category, and thus misses much of the diversity. Trying the top ten genera in each pool included 88 genera, too many to plot. The final genera plot with 25 genera (Fig. 6), includes only the top two genera in each pool (by percent abundance). Between 15 % to 64 % (average 35 %) of the genera in any single pool are not detailed, but included as "other minor genera." To more fully

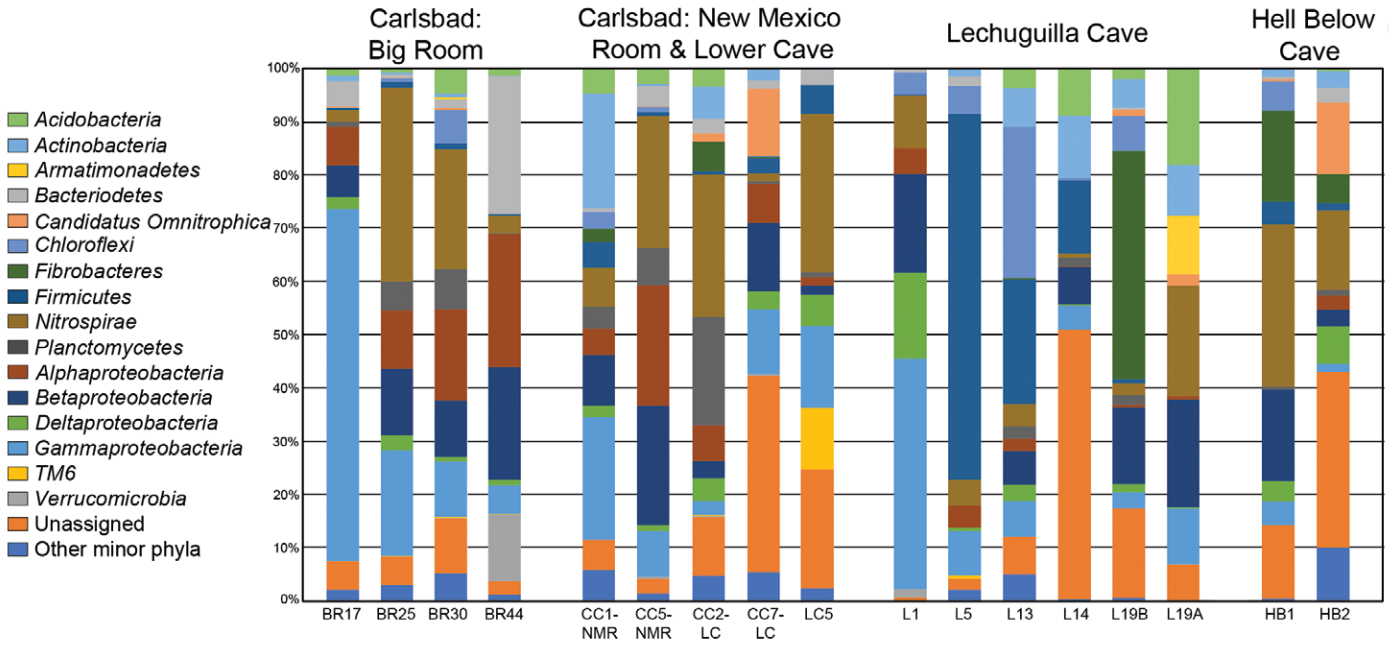

Figure 5. Top phyla/proteobacterial class distribution across pools in Carlsbad Cavern (Big Room and New Mexico Room-Lower Cave), Lechuguilla Cave, and Hell Below Cave.

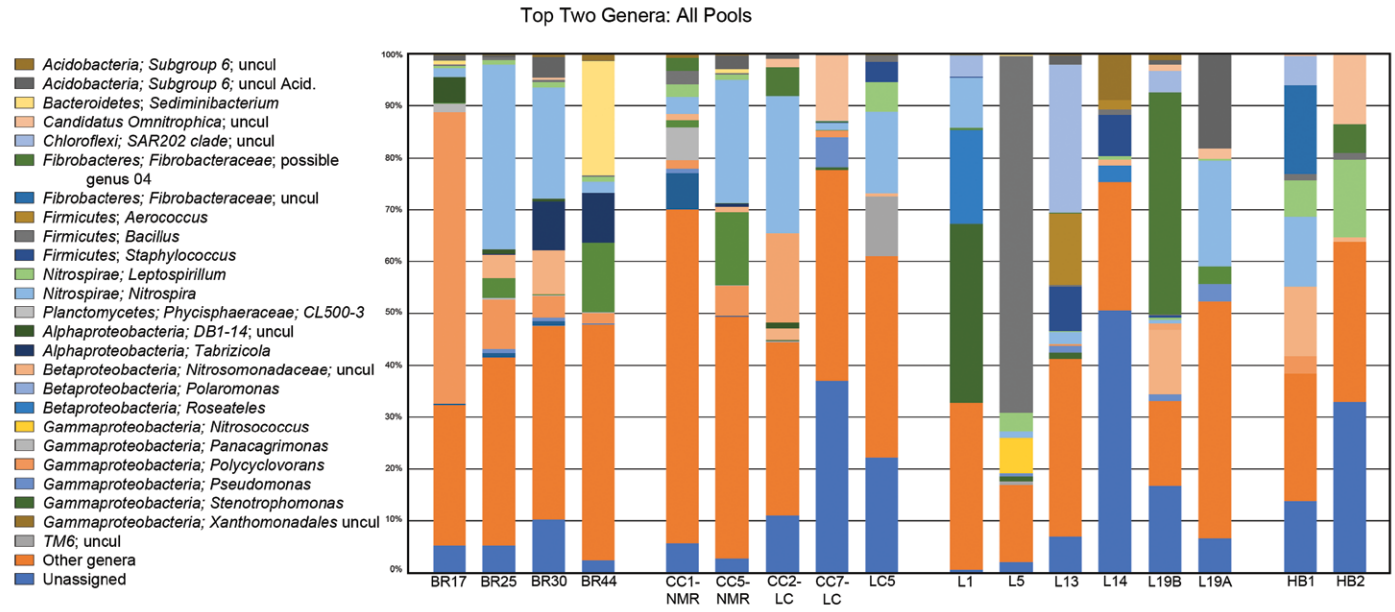

Figure 6. Distribution of the top two genera in pools in Carlsbad Cavern (Big Room and New Mexico Room-Lower Cave), Lechuguilla Cave, and Hell Below Cave.

illustrate the diversity at the genus level, all genera (total of 40) present at 5 % or more in any pool are listed in Table 4. In addition, three pairs of pools were plotted showing all genera above two percent abundance. These include one relatively low-diversity pair (BR17 – L19A, Fig. 7), and two pairs of pools that are adjacent to each other (CC1-NMR – CC5-NMR and HB1 – HB2; Figs. 8 and 9).

RESULTS

Calculated Alpha Diversity of Pools

Pools found in the Big Room of Carlsbad Cavern have the highest number of observed OTUs per pool, ranging from 231 to 925 (Table 1). The remaining pools all have a similar range of observed OTUs: pools in Carlsbad Cavern's Lower Cave and New Mexico Room have between 82 and 226; Hell Below Cave's two pools have 81 and 108, and Lechuguilla

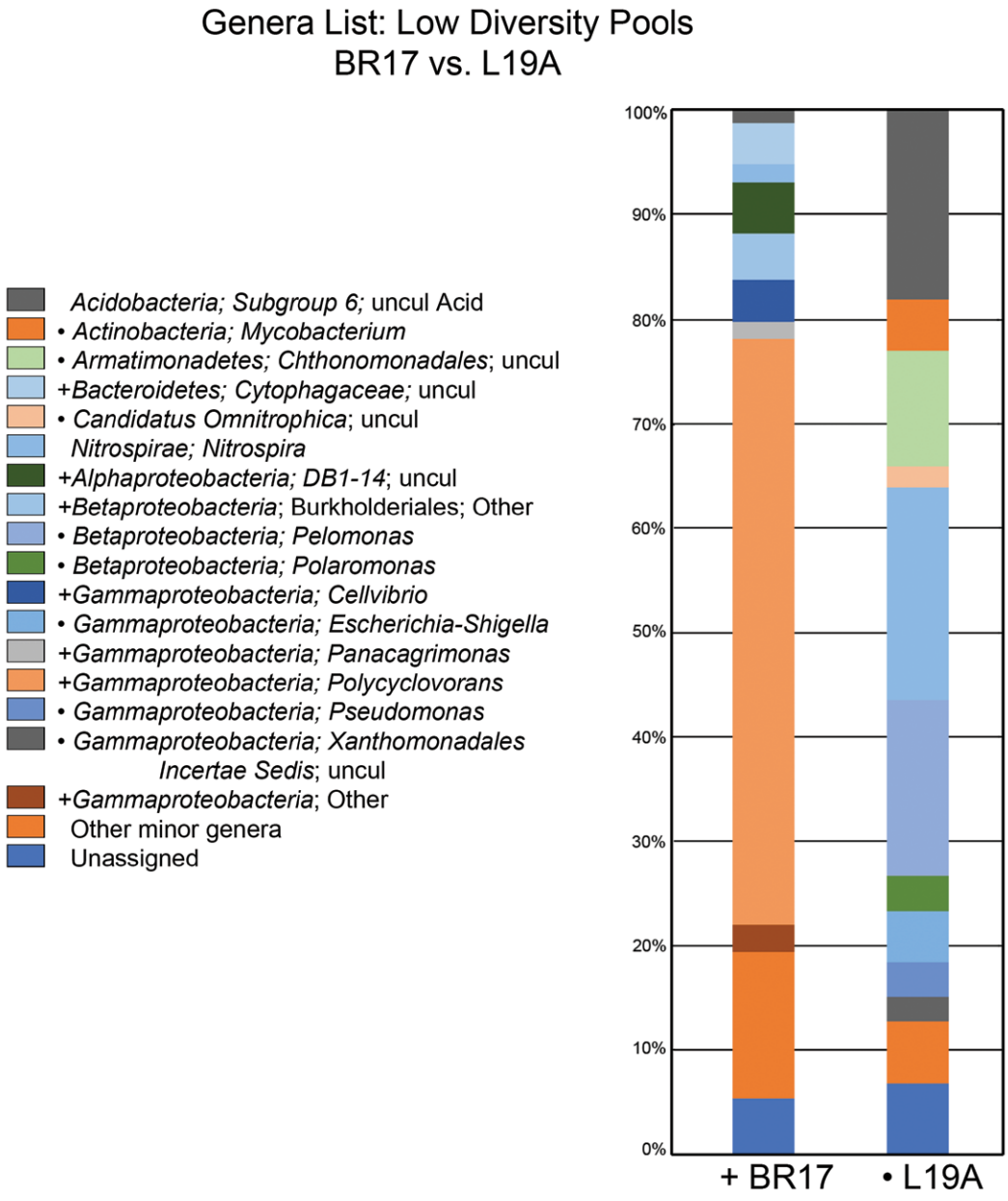

Figure 7. Comparison of genera at >2 % abundance in two relatively low diversity pools, BR17 (Simpson 0.677) and L19A (Simpson 0.881). Code: + genera present only in BR17; • genera present only in L19A.

Cave pools have the lowest value of 24 OTUs and range up to 151. Chao1 diversity scales proportionally with observed OTUs (Table 1; Fig. 10). BR25 has both the highest number of OTUs and the highest Chao1 value (1738). Lechuguilla Cave pool L1 has the lowest number of observed species and the lowest Chao1 value (31).

Shannon diversity averages 4.6 ± 1.1 and ranges from 2.6 in pool L5, Lechuguilla Cave, to 6.4 in CC1-NMR, Carlsbad Cavern. Simpson averages 0.881 ± 0.099 and ranges from 0.622 in pool L5, Lechuguilla Cave. to 0.981 in CC1-NMR, Carlsbad Cavern. Even though Simpson weighs abundant OTUs more, the two indices generally agree on the diversity (Table 1). No cave has exclusively high or low diversity values; all caves have Shannon and Simpson values that span the range of total diversity values. Lechuguilla pools are on average less diverse (Shannon of 3.7 ± 0.9; Simpson of 0.831±0.112) and include the two pools with lowest Shannon values (L1 and L5). The Big Room has higher diversity except for BR17 (Shannon of 3.5; Simpson of 0.677) that is dominated (56 %) by a single genus, *Polyclorovans*. Without BR17, the rest of the Big Room has Shannon values of 5.2 ± 0.7 and Simpson values of 0.913 ± 0.036. New Mexico Room and Lower Cave pools show slightly higher diversity values than the Big Room, with Shannon values of 5.3 ± 0.9 and Simpson values of 0.941 ± 0.042. Hell Below Cave pools are slightly lower than the Big Room, with Shannon values of 4.8 ± 0.7 and Simpson values of 0.939 ± 0.034.

Phylum Diversity

Major differences in the bacterial phyla/proteobacterial classes can be seen within caves and between caves (Fig. 4, Table 2); no two pools have the same distribution of bacteria, even those adjacent to each other in a cave. *Nitrospirae*, *Alpha-*, *Beta-,* and *Gammaproteobacteria* are the only phyla/proteobacterial classes found >5% abundance in nine or more cave pools. *Actinobacteria*, *Chloroflexi*, *Fibrobacteres*, *Firmicutes,* and *Plantomycetes* are at >5 % in 4−6 pools.

Table 1. Alpha diversity indices and Good's Coverage for the study pools.

Study Pool	Species OTUs	Chao1	Shannon	Inverse Simpson	Good's Coverage, %	Unassigned, %
Carlsbad, Big Room						
BR17	231	343	3.5	0.677	98.0	5
BR25	925	1738	5.3	0.885	97.6	5
BR30	680	1185	5.8	0.953	97.6	10
BR44	522	1065	4.5	0.899	97.4	2
Carlsbad Cavern, New Mexico Room & Lower Cave						
CC1-NMR	236	335	6.4	0.981	98.7	6
CC5-NMR	151	278	4.7	0.907	97.0	3
CC2-LC	113	141	4.5	0.888	98.6	11
CC7-LC	170	213	6.0	0.976	98.7	37
LC5	82	231	4.9	0.953	98.8	22
Lechuguilla Cave						
L1	24	31	2.9	0.809	99.3	1
L5	89	171	2.6	0.622	99.3	2
L13	71	88	5.0	0.945	96.9	7
L14	102	250	4.0	0.886	99.4	51
L19B	151	249	4.3	0.842	99.0	17
L19A	33	40	3.5	0.881	99.7	7
Hell Below Cave						
HB1	81	147	4.4	0.916	98.0	14
HB2	108	166	5.3	0.963	99.4	33

Acidobacteria, *Armatimonadetes*, Bacteroidetes, *Candidatus Omnitrophica*, *Deltaproteobacteria*, *TM6,* and *Verrucomicrobia* are found in less than four pools at >5 % abundance.

The most common phylum is *Proteobacteria*, which is common in karst caves and often dominant (Tomczyk-Żak and Zielenkiewicz, 2016). *Beta-* and *Gammaproteobacteria* are the most widespread. *Betaproteobacteria* show up in all pools except L5 in Lechuguilla Cave and vary from 2 % to 22 %. All pools have *Gammaproteobacteria*, which is the second highest phylum/class overall with 66 % in BR17, and varies across all pools from 2 % to 66 %, but with generally higher percentages in Carlsbad Cavern pools (Table 2). In six pools, *Gammaproteobacteria* are either the most abundant (BR17, CC1-NMR, L1) or the second most abundant (BR25, LC5, L5). *Alphaproteobacteria* are low in Lechuguilla Cave and Hell Below Cave pools (0−5 %, absent in two), and more dominant in Carlsbad Cavern pools (2−25 %, with four pools over 11 %). *Deltaproteobacteria* are present across all pools, but only three pools have more than 5 %.

The bacterial phylum *Nitrospirae* is also noted as common in karst caves (Tomczyk-Żak and Zielenkiewicz, 2016), but not usually in the abundance found in these cave pools. *Nitrospirae* is widespread, being found in every pool water sample, but varying from <1 % to 36 %. It is the most abundant phylum in eight pools. The highest percentage of *Nitrospirae* was observed in Carlsbad Cavern's BR25 (36 %) and it is >20 % in six pools, and >10 % in two pools (Table 2).

Of the five phyla found in 4−6 pools at >5 %, *Actinobacteria*, *Chloroflexi*, and *Firmicutes*, and *Plantomycetes* are also found in some caves worldwide, but *Fibrobacteres* is rare (Tomczyk-Żak and Zielenkiewicz, 2016). *Actinobacteria* is noted as abundant in caves, second only to *Proteobacteria*, but most commonly on surfaces (Tomczyk-Żak and Zielenkiewicz, 2016). *Actinobacteria* is present in 11 pools at >1 %, but at <5 % in five of those. In the other six, it ranges from 7 % to 22 % (Table 2). *Actinobacteria* is not the dominant phylum in any pool. *Chloroflexi* are minor constituents in several pools (1 % to 7 %, Table 2), except in Lechuguilla Cave pool L13, where it is the dominant phylum at 28 % abundance. However, five of the nine Carlsbad Cavern pools had no *Chloroflexi*, nor did one Lechuguilla pool and one Hell Below pool. *Firmicutes*, another phylum commonly found in caves (Tomczyk-Żak and Zielenkiewicz, 2016), showed the highest percentage, 69 % in Lechuguilla pool L5 (Vesuvius), of any phylum observed in any pool (Table 2). In addi-

Table 2. Distribution of phyla/Proteobacteria class in study cave pools with more common phyla in each pool highlighted. Orange, >35 %; dark blue, 20–35 %; light blue, 10–20 %.

Phyla/ Proteobacterial class	Carlsbad Cavern, Big Room, %				Carlsbad Cavern, %					Lechuguilla Cave, %						Hell Below Cave, %	
					New Mexico Room		Lower Cave										
	BR17	BR25	BR30	BR44	CC1-NMR	CC5-NMR	CC2-LC	CC7-LC	LC5	L1	L5	L13	L14	L19B	L19A	HB1	HB2
Acidobacteria	1	1	5	1	5	3	3	0	0	0	0	4	9	2	18	0	0
Actinobacteria	1	0	1	0	22	0	6	2	0	0	1	7	12	5	10	2	3
Armatimonadetes	0	0	0	0	0	0	0	0	0	0	0	0	0	0	11	0	0
Bacteroidetes	5	1	2	26	1	4	3	1	3	1	2	0	0	0	0	0	3
Candidatus Omnitrophica	0	0	0	0	0	0	2	13	0	0	0	0	0	1	2	0	13
Chloroflexi	0	1	6	0	3	1	0	0	0	4	5	28	1	7	0	6	0
Fibrobacteres	0	0	0	0	3	0	6	0	0	0	0	0	0	43	0	17	5
Firmicutes	0	1	1	0	5	1	1	3	5	0	69	24	14	1	0	4	1
Nitrospirae	2	36	22	3	7	25	27	2	30	10	5	4	1	2	21	30	15
Planctomycetes	1	5	8	0	4	7	20	0	1	0	0	2	2	2	0	1	1
Alphaproteobacteria	7	11	17	25	5	23	7	7	2	5	4	2	0	1	1	0	3
Betaproteobacteria	6	13	11	21	10	22	3	13	2	18	0	6	7	14	20	17	3
Deltaproteobacteria	2	3	1	1	2	1	4	3	6	16	1	3	0	1	0	4	7
Gammaproteobacteria	66	20	10	5	23	9	3	12	15	43	8	7	5	3	10	4	2
TM6	0	0	0	0	0	0	0	0	12	0	1	0	0	0	0	0	0
Verrucomicrobia	0	0	0	13	0	0	0	0	0	2	0	0	0	0	0	0	0
Other minor phyla	2	3	5	1	6	1	5	5	2	0	2	5	0	1	0	0	10
Unassigned	5	5	10	2	6	3	11	37	22	1	2	7	51	17	7	14	33

tion, *Firmicutes* are abundant in two other Lechuguilla pools (L13 at 24 % and L14 at 14 %). Elsewhere, *Firmicutes* are absent in four pools (BR17, BR44, L1, and L19A) and present at 1 % to 5 % in the remaining pools. *Planctomycetes* is absent to low (0 % to 2 %) in Lechuguilla Cave and Hell Below Cave pools and four Carlsbad Cavern pools, but are more present (4 % to 8 %) in the four other Carlsbad pools, reaching, 20 % in CC2-LC in Lower Cave. The *Fibrobacteres* phylum is absent from 12 pools across all three caves, present but minor (3% to 6 %) in two Carlsbad Cavern pools and one Hell Below pool, but high in two pools (43 % in Lechuguilla Cave pool L19B and 17% in Hell Below Cave pool HB1).

Acidobacteria, *Bacteroidetes* and *Verrucomicrobia* are widespread in caves (Tomczyk-Żak and Zielenkiewicz, 2016), but less so in the study cave pools (Table 2). *Acidobacteria* are present in 10 pools but at low levels (<5 %) except in two Lechuguilla Cave pools (18 % in L19A and 9 % in L14). *Bacteroidetes* is the most abundant phylum in one Carlsbad Cavern pool, with 26 % abundance in BR44. Other pools in Carlsbad Cavern contained 1 % to 5 % abundance of *Bacteroidetes*. Four of the six Lechuguilla Cave pools and one Hell Below Cave pool contained no *Bacteroidetes*. The other three pools in these two caves contained 1 % to 3 % *Bacteroidetes*. *Verrucomicrobia* is only found in two pools (at a relative abundance greater than 1 %), but makes up 13% of the microbiota in BR44.

Bacterial phyla *Armatimonadetes*, *Candidatus Omnitrophica*, and *TM6* are not known from many caves (Tomczyk-Żak and Zielenkiewicz, 2016), but each is found at >10 % in one or two pools. *Armatimonadetes* is 11% in L19A; *Candidatus Omnitrophica* is 13 % in CC7-LC and 13 % in HB2; *TM6* is 12 % in L5 (Table 2). Other minor phyla (Table 2) include phyla present at <5 % in any pool. Five of those are present at 2-5% including *Cyanobacteria*, *Gemmatimonadetes*, *Saccharibactia*, *SM2F11*, and Other Proteobacteria.

Genera Diversity

Of the top 10 most widespread bacterial genera present within these phyla/proteobacterial classes (Table 3), none were

Table 3. Distribution of top ten most widespread genera in study pools with abundances highlighted. Orange >35 %; dark blue 20–35 %; light blue 10–20 %; peach 2–10 %.

No. OTU ID	Carlsbad Cavern, Big Room, %				Carlsbad Cavern, %						Lechuguilla Cave, %						Hell Below Cave, %	
					New Mexico Room		Lower Cave											
	BR17	BR25	BR30	BR44	CC1-NMR	CC5-NMR	CC2-LC	CC7-LC	LC5		L1	L5	L13	L14	L19B	L19A	HB1	HB2
Acidobacteria; *Subgroup 6*; uncul Acid.	1	0	4	0	0	3	1	0	0		0	0	2	0	1	18	0	0
Actinobacteria; *Propionibacterium*	0	0	0	0	5	0	0	0	0		0	1	4	6	5	1	2	1
Candidatus Omnitrophica; uncul	0	0	0	0	0	0	2	13	0		0	0	0	0	1	2	0	13
Firmicutes; *Bacillus*	0	0	0	0	3	0	0	0	1		0	69	0	1	0	0	1	1
Nitrospirae; *Leptospirillum*	0	1	1	1	2	1	0	0	6		0	4	0	1	0	0	7	15
Nitrospirae; *Nitrospira*	2	36	21	2	3	24	26	1	16		10	1	2	0	1	20	14	0
Betaproteobacteria; *Polaromonas*	0	4	0	13	1	14	0	0	0		0	0	0	0	0	3	0	0
Betaproteobacteria; *Nitrosomonadaceae*; uncul	0	4	8	0	1	1	2	0	1		0	0	0	1	12	0	13	1
Deltaproteobacteria; *Haliangium*	0	0	0	0	0	0	1	1	2		16	0	0	0	0	0	1	2
Gammaproteobacteria; *Polycyclovorans*	56	10	4	2	2	6	0	1	0		0	0	0	0	0	0	3	0
Other genera	34	39	49	79	76	49	57	46	52		73	23	83	40	62	48	44	34
Unassigned	5	5	10	2	6	3	11	37	22		1	2	7	51	17	7	14	33

found in all pools. The most widespread was *Nitrospira*, a genus classified to the *Nitrospirae* phylum that was present in eight pools at >10 % (and most abundant in six of those eight, Table 4) and present above 2% in four more. *Leptospirillum*, another genus in the *Nitrospirae* phylum, was present >2 % in five pools, including two pools that lack *Nitrospira*. The *Gammaproteobacteria Polyclorovans* was the second most widespread genus, found in six of the Carlsbad pools and one pool in Hell Below Cave. In Carlsbad Cavern pool BR17, *Polyclorovans* was 56 % of the OTUs. Other widespread genera include the *Actinobacteria Propionibacterium* (five pools, 2 % to 6 %); *Betaproteobacteria Polaromonas* (4 pools, 3 % to 14 %); and *Deltaproteobacteria Haliangium* (3 pools, 2 % to 16 %). *Bacillus*, a genus in *Firmicutes* was found in only two pools over 2 %, but one of those (Lechuguilla Cave pool L5) had 69 %, the highest abundance of any genus in this study. Completing the list of the top 10 are three uncultured genera: *Acidobacteria*, *Subgroup 6*; uncultured *Acidobacteria* bacterium (four pools, 2 % to 18 %); *Candidatus Omnitrophica*, uncultured bacteria (four pools, 2 % to 13 %); and *Betaproteobacteria Nitrosomonadaceae*, uncultured (five pools, 2 % to 13 %).

Table 4 lists all genera present at ≥5 % in any pool, which is 40 genera for only 17 pools. 28 of these 40 genera (70 %) were only present in one pool at ≥5 %. Only six of these 40 genera were present at ≥5 % in three or more pools, one of which, *Nitrospira,* was present in eight pools. *Nitrospira* was also the most abundant genus in six pools (five in Carlsbad Cavern: BR25, BR30, CC5-NMR, CC2-L2, LC5, and one in Lechuguilla Cave: L19A). Each of the other 11 pools had a different most abundant genus (Table 4), including four already noted above in the top 10 most widespread genera (Carlsbad Cavern pool CC7-LC, *Candidatus Omnitrophica*, uncultured bacteria; Lechuguilla Cave pool L5, *Bacillus*; Hell Below Cave pool HB2, *Leptospirillum*; and Carlsbad Cavern pool BR17, *Polyclorovans*). Two Lechuguilla Cave pools (L13, *Chloroflexi*; *SAR202* clade; uncultured and L19B, *Fibrobacteres*; *Fibrobacteraceae*; possible genus 04) have top genera also found in other pools at ≥5 %, but in the other five pools (Carlsbad Cavern pools BR44 and CC1-NMR, and Lechuguilla Cave pools L1, L5, and L15) the most abundant genus in the pool was only found at ≥5 % in that one pool.

Since five pools have top genera found in only one pool at >2 %, a bar plot of the top two genera in each pool was done to include all of the top genera (total 25 genera; Fig. 5). Genera not included ("Other genera") range from 15 % (in Lechuguilla Cave pool L5, which has 69 % *Bacillus*) to 64 % (in Carlsbad Cavern pool CC1-NMR, the most diverse pool (Table 1)). Pools with >10 % unassigned OTUs included

Table 4. List of genera present at ≥5% in any pool. Also listed are the number of pools each is found in at that level and which (if any) pools the genus in the most abundant genus.

OTU, Genus	No. of pools >5%	Most abundant genus in pool(s)
Acidobacteria; Subgroup 6; uncul Acid	1	···
Acidobacteria; Subgroup 6; uncul	1	L14
Actinobacteria; *Propionibacterium*	3	···
Armatimonadetes; *Chthonomonadales*; uncul	1	···
Bacteroidetes; *Sediminibacterium*	1	BR44
Candidatus Omnitrophica; uncul	2	CC7-LC
Chloroflexi; *AKIW781*; uncul	1	···
Chloroflexi; *SAR202 clade*; uncul	2	L13
Fibrobacteres; *Fibrobacteraceae*; possible genus 04	3	L19B
Fibrobacteres; Fibrobacteraceae; uncul	1	HB1
Firmicutes; *Bacillus*	1	L5
Firmicutes; *Staphylococcus*	2	···
Firmicutes; *Aerococcus*	1	···
Nitrospirae; Nitrospirales; 0319-6A21; uncul	2	···
Nitrospirae; *Leptospirillum*	3	HB2
Nitrospirae; *Nitrospira*	8	BR25, BR30, CC5-NMR, CC2-LC, LC5, L19A
Planctomycetes; OM190; Other	1	···
Planctomycetes; Phycisphaeraceae; CL500-3	1	···
Alphaproteobacteria; Rhodobacter	1	···
Alphaproteobacteria; Tabrizicola	2	···
Alphaproteobacteria; Reyranella	1	···
Betaproteobacteria; Pelomonas	1	···
Betaproteobacteria; Polaromonas	2	···
Betaproteobacteria; Roseateles	1	···
Betaproteobacteria; Comamonadaceae; Other	1	···
Betaproteobacteria; *Massilia*	1	···
Betaproteobacteria; Neisseriaceae; uncul	1	···
Betaproteobacteria; *Nitrosomonadaceae*; uncul	3	···
Deltaproteobacteria; *Haliangium*	1	···
Gammaproteobacteria; Nitrosococcus	1	···
Gammaproteobacteria; Escherichia-Shigella	1	···
Gammaproteobacteria; Legionella	1	···
Gammaproteobacteria; Pseudomonas	1	···
Gammaproteobacteria; Polycyclovorans	3	BR17
Gammaproteobacteria; *Xanthomonadales*; uncul	1	CC1-NMR
Gammaproteobacteria; *Panacagrimonas*	1	···
Gammaproteobacteria; *Stenotrophomonas*	1	L1
Saccharibacteria; uncul	1	···
TM6; uncul	1	···
Verrucomicrobia; *Opitutus*	1	···
Present at ≥5% in one pool	28	
Present at ≥5% in two pools	6	
Present at ≥5% in three or more	6	
Total Genera ≥5%	40	

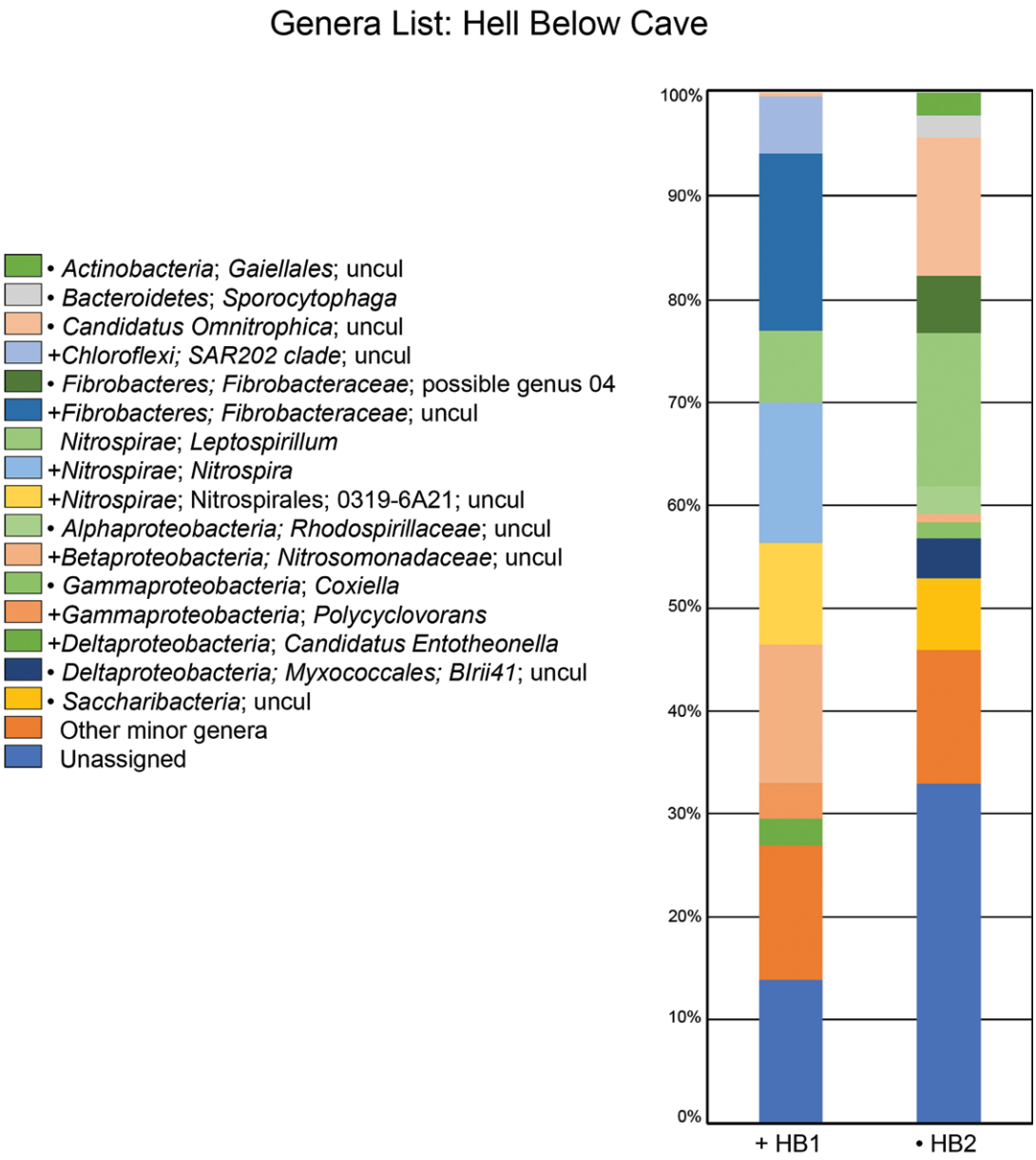

Figure 8. Comparison of genera at >2 % abundance in two relatively high diversity pools, HB1 (Simpson 0.916) and HB2 (Simpson 0.963). Pool HB2 drains into HB1 when full. Code: + genera present only in HB1; • genera present only in HB2.

four in Carlsbad Cavern (BR30, CC2-LC, CC7-LC, LC5), two in Lechuguilla Cave (L14, L19B) and both pools in Hell Below Cave (HB1, HB2). Besides the widespread genera already noted above, *Betaproteobacteria* and *Nitrosomonadaceae*, uncultured were present in five pool,s including two pools at 13 % of genera (L19B and HB1). In addition, 15 of these 25 genera were only found in one or two pools.

To illustrate the microbial diversity better, three pairs of pools were selected to show all genera above 2 % (Figs. 7, 8, and 9). Starting with relatively low diversity pools, Carlsbad Cavern pool BR17 and Lechuguilla Cave pool L19A (Fig. 7; Table 1), out of 17 genera only *Nitrospira* and *Acidobacteria*, *Subgroup 6*, uncultured *Acidobacteria* bacterium occurred in both pools (Fig. 7). Of the other 15 genera, seven were only in BR17 and eight were only in L19A. Comparing two adjacent pools with higher diversity, Hell Below Cave pools HB1 and HB2 (Fig. 8, Table 1), out of 16 genera only one, *Leptospirillum*, was found in both pools. Of the other 15 genera, seven were in HB1 and eight were in HB2. Based on the setting, HB2 likely drains into HB1 during high flow conditions. Comparing again two adjacent Carlsbad Cavern pools CC1-NMR and CC5-NMR, including the highest diversity pool, CC1-NMR (Fig. 9, Table 1), out of 31 genera only two, *Nitrospira* and *Polycyclorvorans* were present in both pools. Of the other 29 genera, 19 were in CC1-NMR and 10 were in CC5-NMR. As for the Hell Below pair, pool CC5-NMR drains into pool CC1-NMR when full (Fig. 4C), although there are no historical reports of this happening. CC1-NMR also has 33 % other minor genera, so even this plot does not fully show the diversity.

DISCUSSION

Introduction

Cave pools in an active epiphreatic zone are replenished with water and groundwater microbial assemblages on an annual basis (Shabarova et al., 2013; 2014), while pools in the vadose zone are thought to function more as “static collectors of microbial diversity” (Shabarova and Pernthaler, 2010). An alternative hypothesis, particularly for isolated vadose pools as the study pools, is that vadose pools act as incubators of diversity. Thus, the microbial community of each pool

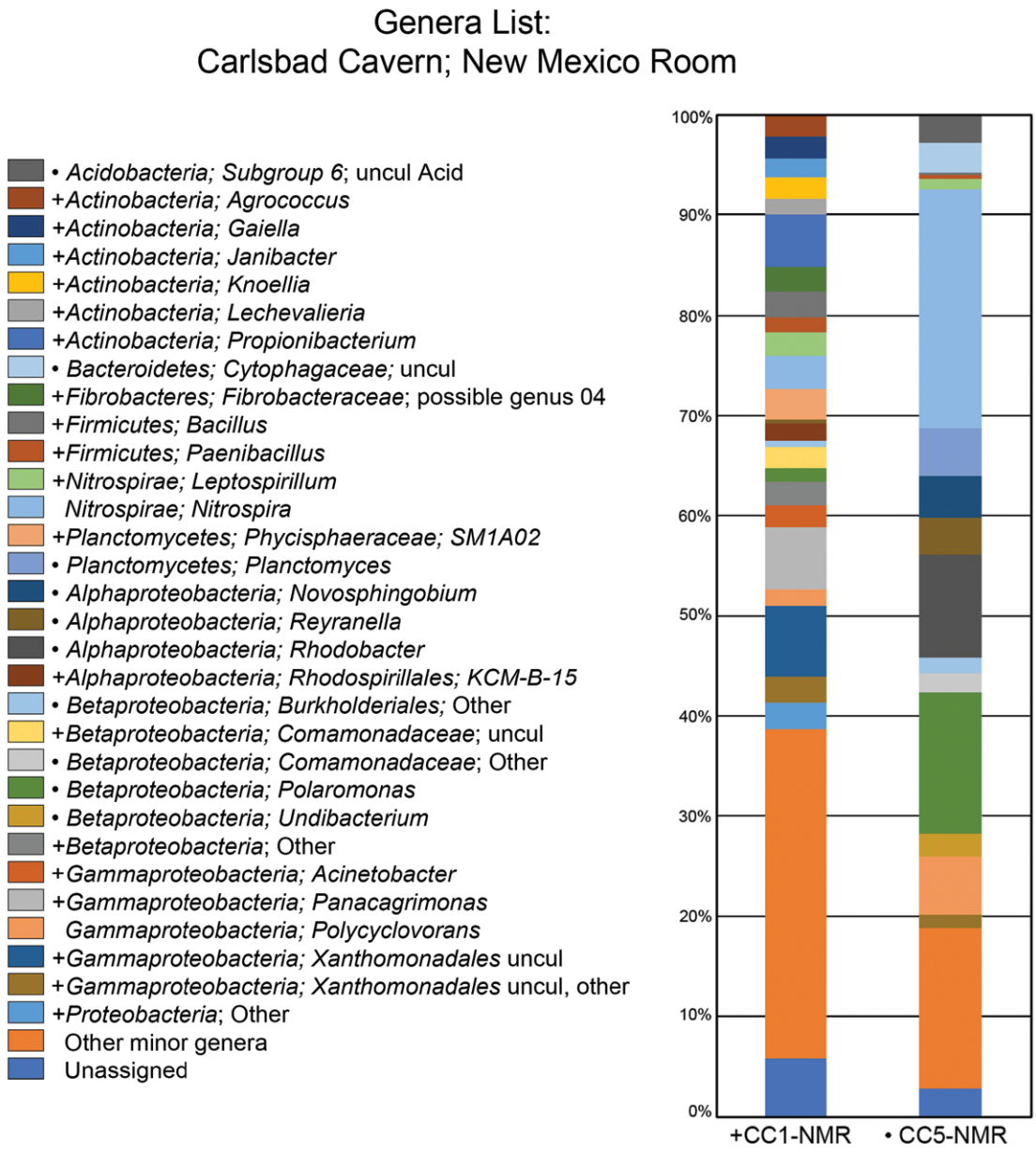

Figure 9. Comparison of genera >2 % abundance in two relatively high diversity pools, CC1-NMR (Simpson 0.981) and CC1-NMR (Simpson 0.907). CC5-NMR drains into CC1-NMR when full. Code: + genera present only in CC1-NMR; • genera present only in CC1-NMR.

should reflect not only what can survive in the pool, but also how that community has evolved over time.

Based on estimates of the last time pools in Carlsbad were full (13.5 ka; Polyak et al., 2012), most of these individual pool ecosystems have likely been isolated for thousands of years, perhaps even longer. However, the Hell Below pools and Carlsbad Cavern New Mexico Room pools (HB1 – HB2, CC1-NMR – CC2-NMR; Figs. 8 and 9), have probably been isolated from each other for a much shorter time period, perhaps decades since a large rain event overfilled the upper pools and drained into the lower pools. Since these pools share water, large differences in water chemistry are unlikely. Even so, the bacterial community differences between these paired pools are as great as between any two pools in this study (Figs. 8 and 9), so mere decades appear to be long enough for unique communities to evolve, even without significantly different chemistry. With this idea in mind, a number of topics can be addressed with this data set, including potential roles for the bacterial genera found, a comparison between examples of previously-studied cave microbial diversity and these pool results, and evaluating the possible human impact, particularly in the heavily-visited Big Room.

Potential Roles of Bacteria in Study Pools

The diversity of bacterial genera present in the study pools provides the opportunity to identify possible roles that these bacteria may play in cave pools. A predominant potential ecosystem function in the study pools is the presence of putative nitrogen cyclers. Nitrogen is often limited in caves due to their oligotrophic nature, especially in arid land caves (Levy, 2007; Ortiz et al., 2014). Research in caves over the last two decades (e.g., Holmes et al., 2001; Chen et al., 2009; Tetu et al., 2013; De Mandel et al., 2017) revealed possible key roles that microorganisms play in the cycling of nitrogen, including nitrification (ammonia and nitrite oxidation), dissimilatory nitrate reduction, and denitrification. The presence of several potential nitrogen cycling bacteria in the study pools suggests that nitrogen cycling may also be an important microbial role in cave pool ecosystems.

The most abundant genus across these pools (Fig. 6; Table 4) is the bacterial genus *Nitrospira*, a well-known nitrite oxidizer (Koch et al., 2015). *Nitrospira* is highest in Carlsbad Cavern's Big Room pool BR25 pool with 36 %, and there are four other pools in Carlsbad Cavern with high *Nitrospira* varying between 20 % to 26 %. Only one other study pool exhibited a greater than 20 % abundance (L19A in Lechuguilla Cave). Across all study pools, eight pools ranged from 10 % to 36 % and only two study pools had no *Nitrospira*. Earlier studies (Holmes et al., 2001; Tetu et al., 2013) of an unusual formation in the flooded cave passages of Weebubbie Cave located in the Nullarbor region of Australia, documented the presence of *Nitrospira*, plus some other potential nitrification and denitrification archaea and bacteria.

In addition to *Nitrospira*, *Pseudomonas*, which is the most abundant genus in CC7-LC, is known to play a role in nitrification (Daum et al., 1998). Other abundant genera in Lechuguilla Cave and Hell Below Cave also include genera known to play roles in the nitrogen cycle (Tables 3 and 4). These include *Bacillus* (highest in L5), which can be a denitrifier (Pichinoty et al., 1983), and *Leptospirillum*, (highest in HB2), which can fix nitrogen (Parro and Moreno-Paz, 2004; Tyson et al., 2005) and is an iron-oxidizing chemolithoautotroph (Tyson et al., 2005). A few of the other abundant genera also play roles in the nitrification phase of the nitrogen cycle. These include the *Nitrosomonadaceae*, a family that includes *Nitrosomonas*, which oxidizes ammonia (Zhou et al., 2007; Chen et al., 2009, Movile Cave). Additionally, about half of *Reyanella* species are able to reduce nitrate (Pagnier et al., 2011), and *Polaromonas*, present in five study pools at >1%, has been documented as a denitrifier (Wang, et al., 2014; Jang et al., 2019).

Two of the study genera are common human skin bacteria: *Propionibacterium* and *Staphylococcus* (found in three and two study pools respectively at >5 %), but can also have roles in the nitrogen cycle. Besides being known as a common human skin bacterium (Stackebrandt et al., 2006), *Propionibacterium* is also known to reduce nitrate (Allison et al., 1989; Swart et al., 1998). While *Staphylococcus* is known to be a common member of the human skin microbiome (Grice and Segre, 2011), some species of *Staphylococcus* have recently been documented to have the ability to fix nitrogen (Yousuf et al., 2020).

An interesting uncultured organism found at 13% abundance in both CC7-LC (Carlsbad Cavern) and in HB2 (Hell Below Cave), belongs to the *Candidatus Omnitrophica*, previously known as *OP3*. Sequences classified in this group were recovered from one of three cave pools studied by Shabarova and Pernthaler (2010). The pool in which *Candidatus* Omnitrophica was found by Shabarova and Pernthaler (2010) contained significantly higher NO_3^- levels and *Nitrospira*, a nitrite-oxidizing bacterium. A more recent paper by Momper et al. (2017), who studied the microbiome of deep terrestrial fluids, differentiates *OP3* from *Candidatus* Omnitrophica, describing them as two candidate phyla. However, the NCBI Taxonomy database (NCBI, 2020) only recognizes the *Omnitrophica* candidate phylum, and more recent papers utilize the *Candidatus Omnitrophica* nomenclature (Rivas-Marı and Devos, 2018; Kirs et al., 2020).

Bacillus, as previously noted, is extremely high in Lechuguilla pool L5 (69 %), but is not present in Lechuguilla Cave pool L1, 30 m from L5, which poses a mystery of why it's there and not also in pool L1. *Bacillus* is very common in soils and natural waters (Logan and De Vos, 2015). In caves, it is the most common cultured bacteria associated with calcite precipitation (Cacchio et al., 2003; Ferris et al., 2003; Dhami et al., 2018; Tredici et al., 2018). This versatile genus is often involved in the nitrogen cycle (Pichinoty et al. 1983) but can also oxidize Mn and Fe (De Vrind et al., 1986; Logan and De Vos, 2015). The oddity, therefore, is not in its presence but in its unusual abundance in Lechuguilla Cave pool L5. Although L5 is more yellow in color than most, which might suggest slightly higher iron, other pools in this study (that do not have the high *Bacillus*) are equally yellow. Lavoie and Northup (2005) found greater presence of high-temperature *Bacillus* (putatively from cavers' boots that hiked across hot desert soils) in areas of Lechuguilla Cave with high human impact, which could suggest that cavers brought *Bacillus*, or its spores, into the cave on their boots. However, because pool L5 is so far from the entrance, this seems less likely.

Polaromonas was first isolated from Antarctica (Irgens et al., 1996) and it remains best-known from glacial and periglacial settings (Vimercati et al., 2019). However, it has also been found in a number of cave settings (Northup et al., 2003; Shabarova and Pernthaler, 2010; Ortiz et al., 2013; Yun et al., 2016b). *Polaromonas* is present in five pools (>1 %) and abundant in two Carlsbad Cavern pools (BR44, 13 %, CC5-NMR 14 %), but it is not the dominant genus in any pool (Table 4). It is a metabolically diverse heterotroph, able to use a wide variety of energy sources (Vimercati et al., 2019) and survive in oligotrophic conditions (Loy et al., 2005; Ortiz et al., 2013). Its ability to denitrify nitrogen suggests it could play a role in the nitrogen cycle in Carlsbad Cavern, or its heterotrophic nature could suggest it is taking advantage of areas with enrichment from human visitation.

Haliangium is only found in higher abundance (16%) in one study pool, Lechuguilla Cave pool L1. Although the only cultured members of this genus are obligate halophiles (Ivanova et al., 2010; Albataineh and Stevens, 2018; Mohr, 2018), *Haliangium* has been found in several low-salt cave samples, including moonmilk (Engel et al., 2013) and cave sediments (de Mandel et al., 2017; Yasir, 2018). Mohr (2018) suggested that the diversity of this hard-to-culture group is larger than currently known, so it may not be as halophilic in caves as currently seen in other habitats.

Acidobacteria Subgroup 6 are uncultured isolates that are present in seven pools, ranging from 1 % to 4 % in six of the pools, and with the highest occurrence being 18 % in Lechuguilla Cave pool L19A (Table 3, Figs. 6, 7, 9). This *Aci-*

dobacteria subgroup has been characterized from a variety of soils (Barns et al., 2007; Li et al., 2019), including forest and grassland soils, with it being dominant in the latter, which are less oligotrophic (Naether et al., 2012). This subgroup has also been documented as common in Altamira Cave in Spain and Roman Catacombs (Zimmermann et al., 2005, 2006) and Lower Kane Cave (Meisinger et al., 2007).

Microbial Diversity of Caves vs. Study Cave Pools

In this study, no two pools contain the exact same set of phyla/Proteobacterial classes and no phylum/Proteobacterial class is present in all pools. (Fig. 5). Additionally, there are large variations in three commonly used diversity indices (Chao1, Shannon, and Simpson; Table 1; Fig. 10). The Chao1 values are an estimate of richness in the sample, or how many OTUs may be present in each pool. Shannon and Simpson indices are both estimates of evenness, or whether each OTU is present in an equal quantity. The Shannon index is more influenced by rare OTUs, while the Simpson is a probability value that is influenced by dominant OTUs. We chose to use both, because of the variability in evenness of the pools.

A comparison of the diversity indices from the study pools with other vadose cave pool bacteria studies is hindered by the general lack of such studies. Shabarova et al. (2010) looked at a pair of vadose pools, but did not present diversity indices. Sauro et al. (2018) included one vadose pool in their study of an orthoquartzite cave and reported higher Shannon (7.854) and Simpson (0.9916) than the carbonate pools in this study. Interestingly, despite the higher Shannon index, they detected a lower number of bacterial phyla (11 total phyla present, but only 3 phyla >2 %, Sauro et al., 2018, their Table S5; versus this study with an average of 14 phyla present, and an average of 5.3 phyla at >2 %). In addition, they have fewer genera in their one pool (6 at >2 %; Sauro et al., 2018, their Table S5) than most of our study pools (8 at >2 %, range 5−16), even though they have a higher Simpson. The dominant groups include *Alphaproteobacteria Rhizobiales* unclassified (40 %), and *Acidobacteria* (27 %), mainly *Acidobacteria Gp13* (18 %; Sauro et al., 2018, Table S5), neither of which are present in our study pools. However, this is not surprising as a silica system is very different from a carbonate system.

Results from other carbonate cave habitats are available (Ortiz et al., 2013: Alonso et al., 2019; Thompson et al., 2019). However, there are several challenges in such a comparison. These studies sampled surfaces of speleothems or cave sediment, whereas the study pool samples are planktonic. Surfaces are known to have more microbes than planktonic communities (Savio et al., 2018). In addition, some studies group samples together from similar settings, but different caves (Lavoie et al., 2017; Alonso et al., 2019; Thompson et al., 2019), whereas this study has not grouped the data, preferring to look at each pool separately. Different sequencing methods between studies also limit some comparisons.

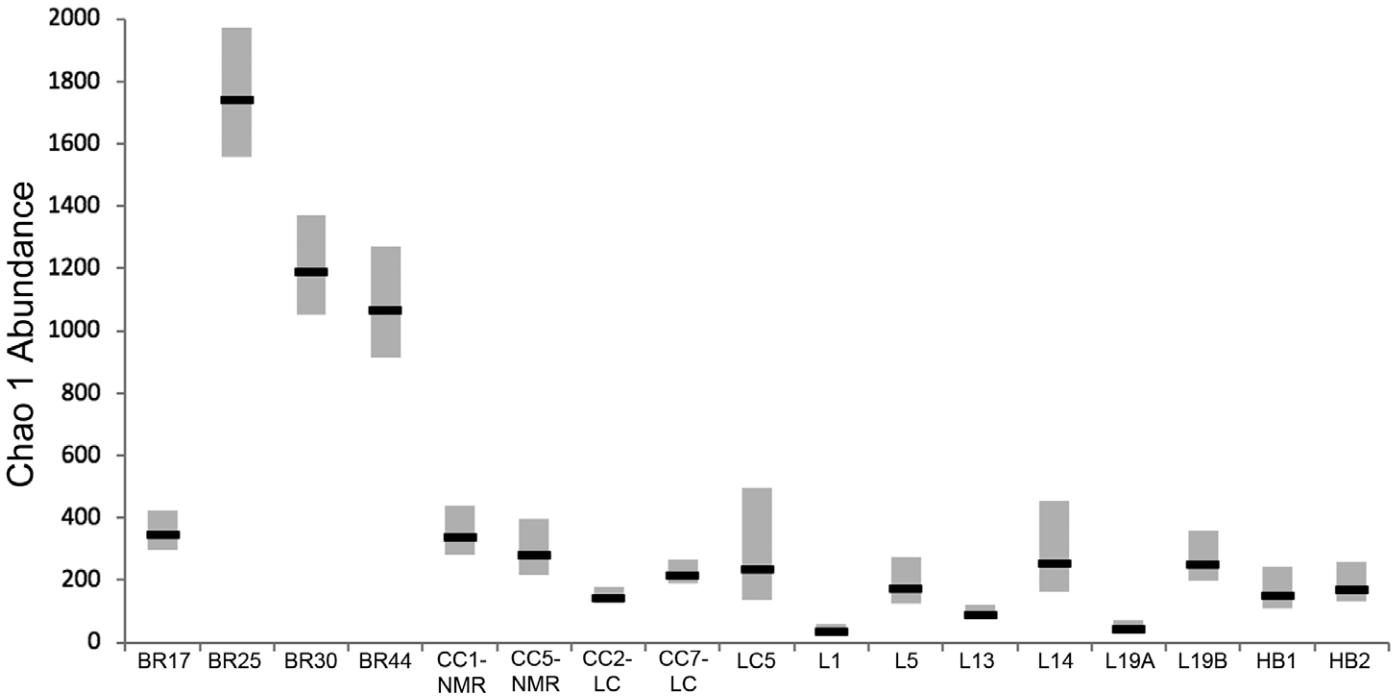

Figure 10. Chao 1 values for the sampled pools. The black line is the Chao value. The gray bars represent the upper and lower bounds of the diversity calculation.

Ortiz et al. (2013) compared speleothem surfaces with surface soil in Kartchner Caverns, an arid land cave in Arizona. The speleothems had much higher Chao1 values (2067−3693) than the study pools, but comparable Shannon (4.3−6.1; Ortiz et al., 2013, their Table 1). Interestingly, they found three separate communities based on variations in *Actinobacteria*, *Proteobacteria*, and *Acidobacteria* and interpreted this as variation in the chemical profile of the speleothems. In comparison to these studies, the study pools have much less *Actinobacteria* and *Acidobacteria*, and much more *Nitrospirae* (Fig. 5, Table 2),

Sampling different microbial mats in lava caves, Lavoie et al. (2017) report much lower diversity in both Shannon (~1.4 to 2.6, with some outliers) and Simpson (~0.40 to 0.75; Lavoie et al., 2017; their Fig. 3 and Supplemental S2) for grouped data. Their top cave groups were *Actinobacteria* (37 % to 44 %), *Gammaproteobacteria* (19 % to 24 %), *Alphaproteobacteria* (10 %), and *Nitrospirae* (4 % to 11 %). Although these groups are also found in these cave pool samples, notable differences include *Actinobacteria* and *Nitrospirae*: *Actinobacteria* are much less common (>5 % in six pools, maximum 21 % in Carlsbad Cavern pool CC1- NMR) and *Nitrospirae* is much more common (>20 % in seven pools; Fig. 5, Table 2).

Alonso et al. (2019) used cave wall samples from nine karst caves in the Dordogne region of France to compare more or less anthropized caves. Looking just at the bacterial results, their Chao1 results are higher (using a different method), their Shannon values are similar (~4.1−5.2), and their Simpson values are higher (above 0.95 except for one cave with values of ~0.82−0.95; Alonso et al., 2019, Fig. 2). The *Proteobacteria* (14 % to 56 %, undifferentiated) and *Actinobacteria* (11 % to 49 %) were their most abundant phyla, as is common on carbonate cave surfaces (Tomczyk-Żak and Zielenkiewicz, 2016).

Thompson et al. (2019) found that speleothems had lower Chao1, Shannon, and Simpson diversity than did the cave sediment and surface soils. All of their Chao1 values were much higher than the study pools. Their much higher Chao1 values may be a reflection of their different methods. Looking at Shannon and Simpson, speleothems are closest to the cave pools (Shannon ~4.7, Simpson ~0.989, Thompson et al., 2019, Fig. 1; compare to Table 1), while both cave sediment and surface soils are more diverse. The most abundant cave phyla are similar to the other studies with the top three being *Actinobacteria* (speleothems 19.47 %, cave sediment 21.91 %), *Proteobacteria* (speleothems 14.21 %, cave sediment 16.05 %), and *Acidobacteria* (speleothems 9.85 %, cave sediment 2.15 %, Thompson et al., 2019, Table 1). *Nitrospriae* were <1 % of any sample.

Thus, the diversity values of cave samples are variable, and the study cave pool samples fall within that variability. The dominant phyla, however, are notably different. Although *Proteobacteria* are abundant in most cave samples, *Actinobacteria* and *Acidobacteria* are more common in surface samples and *Nitrospirae* are more common in the cave pool samples. *Actinobacteria* are very common in caves but are known mainly from surfaces (Tomczyk-Żak and Zielenkiewicz, 2016), which likely explains their greater abundance in other studies than the cave pools. *Nitrospirae* are known to inhabit aquatic environments (Tomczyk-Żak and Zielenkiewicz, 2016), which may help explain the higher pool abundances.

The means of diversity indices, however, do not tell the whole story. Although the cave pool average values are similar to other cave samples, the range of values is much higher. Looking at the carbonate cave samples, the Kartchner speleothems have a Shannon range of values of ~1.7 (4.37 to 6.06; Ortiz et al., 2013, Table 1), the Appalachian cave speleothems range ~2.4 (~3.5 to ~5.9; Thompson et al., 2019, Fig. 1); and the French caves of ~2.2 (~3 to ~5.2, Alonso et al., 2019, Fig. 2). The study cave pools, in contrast, have a range in Shannon values of 3.9 (2.5 to 6.4, Table 1). The range in Simpson values is also higher for our cave pools (Table 1), suggesting there is a greater variation among pools than is represented just by looking at the diversity indices.

A few of the cave pools are strongly dominated by single OTUs. When looking at the distribution of the phyla/proteobacterial classes of the two pools with the lowest Simpson values, Carlsbad Cavern pool BR17 and Lechuguilla Cave pool L5, (Fig. 5), it is apparent there is not an even distribution, as both pools are dominated by a single phylum/proteobacterial class. Looking closer at these two pools, BR17's low Simpson index value is likely due to the dominance of the *Gammaproteobacteria*, *Polycyclovorans* (56 %), and L5 is dominated by *Fimicutes*, *Bacillus* (69 %; Fig. 6 and Table 3). Additional pools with relatively low Simpson values include Lechuguilla Cave pools L1 (0.809) and L19B (0.842), both also dominated by single genera, but not as strongly. Other pools have Shannon and Simpson values comparable to the speleothem data of Thompson et al. (2019). For example, Carlsbad Cavern pools CC1-NMR and CC7-LC (Shannon 6.4 and 6.0; Simpson 0.981 and 0.976, respectively) have higher Shannon values, but slightly lower Simpson values than the Appalachian speleothems. Thus, the differences of the alpha diversity index values in the seventeen pools across three cave systems indicates that sample evenness is variable, even within the same cave system.

Paired comparisons of distant vs. adjacent pools

To examine this variability, the genera from three paired pools were compared (Figs. 7, 8, and 9). Pools Carlsbad Cavern BR17 and Lechuguilla Cave L19A both have lower diversity and may be impacted by human activity. As dis-

cussed previously, BR17 is adjacent to the primary trail in the Big Room of Carlsbad Cavern. L19A was a common water and rest stop for expeditions through Lechuguilla Cave. BR17 has a moderate Chao1 value (343), but a low Simpson index value (0.677) (Table 1). L19A has a low Chao1 value (40), but a moderate Simpson index value (0.881). The two pools have the same Shannon index value (3.5). Despite the similar Shannon, only two genera are shared between the two pools at >2 %, *Nitrospira* and an uncultured *Acidobacteria* (Fig. 7). The abundance of the two genera is different, with both more common in L19A. Of the remaining genera found in greater than 2% abundance, none are shared between the two cave pools. L19A has *Pseudomonas* and *Escherichia-Shigella* present in the pool; both are known human contaminates. BR17 has 56 % *Polycyclovorans*, a hydrocarbon degrader (Gutierrez et al., 2013), which may be related to asphalt from the nearby trail. Although both pools have been impacted by human visitation, they have been impacted in different ways, which can be seen in both the alpha diversity index values and the presence of various OTUs.

The two pools in Hell Below Cave are adjacent to each other, and HB1 has likely drained into HB2 during major rainfall events within the last few decades. However, results from Shabarova et al. (2013, 2014), indicate that the distribution of bacteria within a cave pool can change within a few months after a perturbation. In Hell Below Cave, the two pools have similar Chao1, Simpson, and Shannon values, but have very few shared OTUs. These two pools are adjacent to each other and likely share water, suggesting they receive similar inputs from the vadose zone and experience similar climates. The distribution of phyla in each pool (Table 1) is not dominated by a single phylum. *Nitrospirae* is the highest at 30 % in HB1. There are 16 genera found at greater than 2 % in these pools (Fig. 8). Of these 16 genera, only three are shared between the two pools, the rest are only found in one of the pools.

In the New Mexico Room of Carlsbad Cavern, pool CC5-NMR flows into CC1-NMR when it overflows, and it was nearly full at the time of sample collection (Fig. 4C). These two pools have likely shared water during a major rainfall event within the last several decades, similar to the two pools in Hell Below Cave. However, unlike the Hell Below Cave pools, the pools in the New Mexico Room have different alpha diversity index values and genera present (Table 1, Fig. 9). CC1-NMR has the highest Shannon and Simpson index values of the seventeen pools in this study, 6.4 and 0.981 respectively (Table 1). CC5-NMR has moderate Shannon and Simpson index values of 4.7 and 0.907. There are 30 genera found between the two pools, but only six are found in both pools.

Thus, although the diversity index values of individual pools are similar to that of other cave systems (see above), each pool has its own community, indicated by the low overlap between pool genera (Figs. 6−9, Tables 3 and 4). Studies on pool water chemistry in both Carlsbad Cavern and Lechuguilla Cave have shown the pools are broadly similar, albeit with considerable minor chemical variation among pools (Chapman et al., 1992; Turin and Plummer, 2000; Levy, 2007a; Forbes, 2000). These chemical differences are likely minimal between the adjacent pools that share water in Carlsbad Cavern's New Mexico Room and Hell Below Cave, yet these pools share only a few genera (Figs. 8 and 9). Rather than a single stable cave pool community, adapted to the cave pool system, the study data show 17 different communities despite relatively similar conditions. These data support the hypothesis that each pool is a unique, isolated ecosystem, with differences likely caused as much by the isolation of each pool as by variable water chemistry. Within some of the study cave pools, however, this isolation has been affected by human impact, which can have an impact on microbial communities (see discussion below).

Effects of human visitation on pool communities

The study pools vary in terms of alpha diversity and show significant differences in microbial community structure. They also vary in terms of human visitation with the Big Room (Carlsbad Cavern) having by far the most visitors per year (300,000/year to 500,000/year), and Lechuguilla Cave and Hell Below Cave having the least (<100/year to 200/year). In a previous study of the impact of human visitation in Carlsbad Cavern, Griffin et al. (2014) reported significant human impacts of visitors on the microbiota. Collecting samples from the cave air, they reported that *Staphylococcus* spp., noted above as a common human skin inhabitant (Stackebrandt et al., 2006), were the dominant bacteria cultured along tourist trails. *Knoellia* sp. was most common off trail. *Knoellia* is a novel genus of *Actinobacteria*, first isolated from a cave in China (Groth et al., 2002), which was also found in this study in one of the Carlsbad Cavern New Mexico Room pools (CC1-NMR, Fig. 9). Griffin et al. (2014) also utilized genetic sequencing to show that *Enterobacteriaceae* dominated along the descent trail railing and in the Lunchroom, which is not unexpected given the number of fecal deposits from visitors that rangers clean up. They concluded that humans were important sources of non-indigenous microorganisms in Carlsbad Cavern.

The four pools in the Big Room of Carlsbad Cavern have the highest number of OTUs and the highest Chao values of any pools. The larger numbers of OTUs in the Big Room could be driven by a variety of factors, such as increased energy sources from the illumination, shed skin cells, or construction materials. This last item is supported by the presence of the genus *Polycyclovorans*, particularly in Big Room pools, which can facultatively use hydrocarbons for energy (Gutierrez et al., 2013; Thompson et al., 2018). The trail system in the Big Room is asphalt (Brooke, 1996, Van

der Heijde et al., 1997) and BR17, which has 56 % *Polycyclovorans*, is directly below the trail and contains debris from the trail (Fig. 4A). However, *Polycyclovorans* has been documented as a marine genus (Berry and Gutierrez, 2017); other genera isolated from marine environments are found in pools in each cave system. *Polycyclovorans* has also been documented in soils (Lu, 2018), and will probably be discovered in other environments as the knowledge of microbial communities expands. In addition, the *Polycyclovorans* genus is also found in Carlsbad Cavern's New Mexico Room pools and one pool from Hell Below Cave (Table 3), which do not have asphalt trails.

In a study by Lavoie et al. (2017) in Lava Beds National Monument (LABE) volcanic caves, there was only one *Staphylococcaeae* identified, and only 25 OTUs of *Enterbacteriacae* identified to the level of family detected at any LABE cave or surface sample. Lavoie et al. (2017) hypothesized that there is a threshold of visitors before the effects of human visitation are observed, which is greater than the 30,000/y seen in LABE. The Carlsbad Cavern Big Room pools greatly exceed this threshold with 300,000 visitors/year to 500,000 visitors/year over the last decades. However, the presence of human-associated genera such as *Staphylococcus* and *Pseudomonas* (Table 4) does not correlate with visitation numbers. *Staphylococcus* is most common in Lechuguilla Cave and absent in the Big Room. *Pseudomonas* is present in some, but not all Big Room pools, but also in four Lechuguilla Cave pools. These genera are also known to play roles in the nitrogen cycle, so perhaps they are not simply indicators of human impact in these pools.

Another recent study by Alonso et al. (2019) examined the differences in microbial and micro-eukaryotic diversity in four pristine and four anthropized caves, plus two sections of the highly visited Lascaux Cave (France). Of particular interest was differences noted in the bacterial phylum *Bacteroidetes*, which were higher in anthropized caves, and *Nitrospirae*, which were lower in anthropized caves versus pristine caves. In this study, *Bacteroidetes* were present in all Carlsbad Cavern pools, varying from 1 % to 26 %, but in only two of the Lechuguilla Cave (L1 and L5, 1 % to 2 %), and one of the Hell Below Cave pools (HB2, 3 %) (Table 2).

This study observed considerable variation in *Nitrospirae* across the study pools (Fig. 5). *Nitrospirae* were present in all Carlsbad Cavern pools, varying from 2 % to 36 %, with five of the pools having >20 % occurrence, and the highest percentage of 36 % being found in the Big Room. In Lechuguilla Cave pools, *Nitrospirae* varied from 1 % to 21 %, with only two pools at 10 % and 21 % across pools with varying visitation (but still low in comparison to Carlsbad Cavern). Hell Below Cave had 15 % and 30 % in its pools, with low visitation. Thus, both high and low impact settings can have high *Nitrospirae*, in contrast with Alonso et al. (2019) who found that *Nitrospirae* were more abundant on the walls in less anthropized caves (5 % to 10 %). The different pattern of *Nitrospirae* occurrence in the cave pools suggests further investigation into how the unique bacterial communities utilize the nitrogen cycle and what drives the community make-up of each pool.

Broader Implications

Studies of microbial diversity in caves are often trying to characterize either different caves or different sample types in the context of larger questions like human impact (Adetutu et al., 2012; Leuko et al., 2017; Alonso et al., 2019), soil contributions to cave ecosystems (Ortiz et al., 2013; Lavoie et al., 2017; Thompson et al., 2019), or variation between microbial mat types (Lavoie et al., 2017). It is common to group samples from different locations (Lavoie et al., 2017; Alonso et al., 2019; Thompson et al., 2019). Ortiz et al. (2013) instead looked at individual speleothems and found different microbial communities for adjacent stalactites. They attributed the differences to varying water and speleothem chemistry. This study of vadose pools also found unique ecosystems, even for adjacent pools that likely share water occasionally. Thus, we suggest an additional variable in the cave ecosystem may be time; communities that are isolated from each other will evolve independently over time. This contrasts with groundwater ecosystems that vary less over larger distances (Wegner et al., 2019), perhaps because of more interaction in the connected aquifer. Thus, the common habit of grouping samples, while useful for some questions, misses some of the differences in diversity present in cave ecosystems. Rather, caves may harbor a wide variety of isolated ecosystems, each one potentially containing a unique community impacted by both the local conditions and the amount of time it has been isolated. Further exploration of this hypothesis in different kinds of cave ecosystems would be useful.

Future Directions

Future studies will focus on elucidating the geochemistry of the pools, expanding the sequencing to include the Archaea and expand the Bacteria, and conducting metagenomic and transcriptomic analyses of pool water. The extensiveness of potential nitrogen cycling bacteria in the study samples points to the need to expand future studies to sequencing of the Archaea present, using Archaea-specific primers for more comprehensive recovery (Bahram et al. 2019). Metagenomic sequencing will confirm what nitrogen cycle genes, if any, are present in the pool inhabitants and transcriptomics, if successful, will confirm what nitrogen cycling is taking place. Simultaneous sampling for water chemistry is required to better test the controls on diversity. Expanding the analysis of pool water microbial analyses to other cave types and climate settings would be very beneficial as the number of cave water pool studies is very low. Also, long-term studies are needed to determine the stability of the communities. We also suggest that additional test-

ing of the impact of human activities and built environments that are installed to facilitate tourists in caves with different visitation levels is essential to understanding how to mitigate such impacts. Such studies would expand the knowledge of microbial diversity in caves substantially.

CONCLUSIONS

The 17 study pools across three caves represent unique bacterial communities, suggesting they are isolated systems. *Nitrospirae*, *Alphaproteobacteria*, *Betaproteobacteria* and *Gammaproteobacteria* were the most abundant phyla/proteobacterial classes in over half the cave pools. The most widespread genus observed was *Nitrospira*, while nine other top genera included *Polyclorovans*, *Polyclorovans*, *Propionibacterium*, *Polaromonas*, *Haliangium, Bacillus*, *Subgroup 6 uncultured Acidobacteria*, *Candidatus Omnitrophica*, and uncultured *Nitrosomonadaceae*. Prior studies of several of these genera suggest roles in the nitrogen cycle for pool bacteria. These data suggest there is some evidence of human contamination, but do not clearly support it as a major factor in the diversity observed. Although *Proteobacteria* are abundant in both settings, the dominant bacterial phyla on speleothems and other surfaces (*Actinobacteria* and *Acidobacteria*), are different than that found in the study cave pools (*Nitrospirae*). Rather than a single stable cave pool community, adapted to the cave pool system, these data show 17 different communities despite relatively similar conditions. These data support the hypothesis that each pool is a unique, isolated ecosystem, with differences likely arising from the isolation of each pool and not just from different water chemistry. These data also suggest that to accurately assess diversity present in cave ecosystems future cave studies should not group samples.

ACKNOWLEDGEMENTS

We are very grateful to our funding agencies, the National Science Foundation Geobiology and Low-Temperature for the collaborative grant EAR-0719507 to Melim, Northup, and colleagues, and to T&E, Inc. for funding for the sequencing. We thank Carlsbad Caverns National Park for our sampling permit CAVE-2008-SCI-0004 and the U.S. Forest service for sampling permit FS-2700-4 (10/09). Stan Allison, Dale Pate, and Paul Burger of the Carlsbad Caverns National Park Cave Resources Office were very supportive of our fieldwork. Pat Cicero, Ian McMillan, Thibault Datry, and Aaron Stockton did a great job of water sampling in Lechuguilla Cave. All cave photographs are courtesy of Dr. Kenneth Ingham or Pat Cicero.

REFERENCES

Adetutu, E., Thorpe, K., Shahsavari, E., Bourne, S., Cao, X., Fard, R., Kirby, G., and Ball, A., 2012, Bacterial community survey of sediments at Naracoorte Caves, Australia: International Journal of Speleology, v. 41, no. 2, p. 137−147. https://doi.org/10.5038/1827-806X.41.2.2.

Albataineh, H., and Stevens, D.C., 2018, Marine myxobacteria: A few good halophiles: Marine Drugs, v. 16, no. 6., p. 209. https://doi.org/10.3390/md16060209.

Allison, C., and Macfarlane, G.T., 1989, Dissimilatory nitrate reduction by *Propionibacterium acnes*: Applied and Environmental Microbiology, v. 55, p. 2899−2903. https://doi.org/10.1128/AEM.55.11.2899-2903.1989.

Alonso, L., Pommier, T., Kaufmann, B., Dubost, A., Chapulliot, D., Dore, J., Douady, C.J., and Moenne-Loccoz, Y., 2019, Anthropization level of Lascaux Cave microbiome shown by regional-scale comparisons of pristine and anthropized caves: Molecular Ecology, v. 28, no. 14, p. 3383−3394. https://doi.org/10.1111/mec.15144.

Bahram, M., Anslan, S., Hildebrand, F., Bork, P., and Tedersoo, L., 2019, Newly designed 16S rRNA metabarcoding primers amplify diverse and novel archaeal taxa from the environment: Environmental Microbiology Reports, v. 11, no. 4, p. 487−494. https://doi.org/10.1111/1758-2229.12684.

Barns, S.M., Cain, E.C., Sommerville, L., and Kuske, C.R., 2007, Acidobacteria phylum sequences in uranium-contaminated subsurface sediments greatly expand the known diversity within the phylum: Applied and Environmental Microbiology, v. 73, no. 9, p. 3113−3116. https://doi.org/10.1128/AEM.02012-06.

Barton, H.A., and Northup, D.E., 2007, Geomicrobiology in cave environments: Past, current and future perspectives: Journal of Cave and Karst Studies, v. 69, no. 1, p. 163−178.

Barton, H.A., Taylor, N.M., Kreate, M.P., Springer, A.C., Oehrle, S.A., and Bertog, J.L., 2007, The impact of host rock geochemistry on bacterial community structure in oligotrophic cave environments: International Journal of Speleology, v. 36, p. 93−104. https://doi.org/10.5038/1827-806X.36.2.5.

Berry, D., and Gutierrez, T., 2017, Evaluating the detection of hydrocarbon-degrading bacteria in 16S rRNA gene sequencing surveys: Frontiers in Microbiology, v. 8, p. 896. https://doi.org/10.3389/fmicb.2017.00896.

Blyth, A.J., Hartland, A., and Baker, A., 2016, Organic proxies in speleothems – New developments, advantages and limitations: Quaternary Science Reviews, v. 149, p. 1−17. https://doi.org/10.1016/j.quascirev.2016.07.001.

Brannen-Donnelly, K., and Engel, A.S., 2015, Bacterial diversity differences along an epigenic cave stream reveal evidence of community dynamics, succession, and stability: Frontiers in Microbiology, v. 6, p. 729. https://doi.org/10.3389/fmicb.2015.00729

Brewer, T.E., and Fierer, N., 2018, Tales from the tomb: the microbial ecology of exposed rock surfaces: Environmental Microbiology, v. 20, no. 3, p. 958−970. https://doi.org/10.1111/1462-2920.14024.

Brooke, M., 1996, Infiltration Pathways at Carlsbad Caverns National Park Determined by Hydrogeologic and Hydrochemical Characterization and Analysis: Colorado School of Mines, 182 p.

Budd, D.A., Frost, E.L., Huntington, K.W., and Allwardt, P.F., 2013, Syndepositional deformation features in high-relief carbonate platforms: Long-lived conduits for diagenetic fluids: Journal of Sedimentary Research, v. 83, no. 1, p. 12−36. https://doi.org/10.2110/jsr.2013.3.

Cacchio, P., Ercole, C., Cappuccio, G., and Lepidi, A., 2003, Calcium carbonate precipitation by bacterial strains isolated from a limestone cave and from a loamy soil: Geomicrobiology Journal, v. 20, p. 85−-98. https://doi.org/10.1080/01490450303883.

Caporaso, J.G., Kuczynski, J., Stombaugh, J., Bittinger, K., Bushman, F.D., Costello, E.K., et al., 2010, QIIME allows analysis of high-throughput community sequencing data: Nature Methods, v. 7, no. 5, p. 335−336. https://doi.org/10.1038/nmeth.f.303.

Carmichael, S., and Bräuer, S.L., 2015, Microbial diversity and manganese cycling: a review of Mn-oxidizing microbial cave communities, *in* Engel, A.S., ed., Microbial Life of Cave Systems: Boston, MA, USA, De Gruyter, p. 137−160.

Carmichael, M.J., Carmichael, S.K., Santelli, C.M., Strom, A., and Bräuer, S.L., 2013a, Mn(II)-oxidizing Bacteria are abundant and environmentally relevant members of ferromanganese deposits in caves of the Upper Tennessee River Basin: Geomicrobiology Journal, v. 30, no. 9, p. 779−800. https://doi.org/10.1080/01490451.2013.769651.

Carmichael, S., Carmichael, M., Strom, A., Johnson, K., Roble, L., Gao, Y., and Brauer, S., 2013b, Sustained anthropogenic impact in Carter Saltpeter Cave, Carter County, Tennessee and the potential effects on manganese cycling: Journal of Cave and Karst Studies, v. 75, no. 3, p. 189−204. https://doi.org/10.4311/2012MB0267.

Chapman, J.B., Ingraham, N.L., and Hess, J.W., 1992, Isotopic investigation of infiltration and unsaturated zone flow processes at Carlsbad Cavern, New Mexico: Journal of Hydrology, v. 133, p. 342−363. https://doi.org/10.1016/0022-1694(92)90262-T.

Chelius, M.K., and Moore, J.C., 2004, Molecular phylogenetic analysis of Archaea and Bacteria in Wind Cave, South Dakota: Geomicrobiology Journal, v. 21, p. 123−134. https://doi.org/10.1080/01490450490266389.

Chen, Y., Wu, L., Boden, R., Hillebrand, A., Kumaresan, D., Moussard, H., Baciu, M., Lu, Y., and Colin Murrell, J., 2009, Life without light: microbial diversity and evidence of sulfur- and ammonium-based chemolithotrophy in Movile Cave: International Society for Microbial Ecology Journal, v. 3, no. 9, p. 1093−1094. https://doi.org/10.1038/ismej.2009.57.

Daum, M., Zimmer, W., Papen, H., Kloos, K., Nawrath, K., and Bothe, H., 1998, Physiological and molecular biological characterization of ammonia oxidation of the heterotrophic nitrifier *Pseudomonas putida*: Current Microbiology, v. 37, p. 281−288. https://doi.org/10.1007/s002849900379,

De Mandal, S., Chatterjee, R., and Kumar, N.S., 2017, Dominant bacterial phyla in caves and their predicted functional roles in C and N cycle: BMC Microbiology, v. 17, no. 1, p. 90. https://doi.org/10.1186/s12866-017-1002-x.

De Vrind, J.P.M., De Vrind-De Jong, E.W., De Voogt, J.-W.H., Westbroek, P., Boogerd, F.C., and Rosson, R.A., 1986, Manganese oxidation by spores and spore coats of a marine *Bacillus* species: Applied and Environmental Microbiology, v. 52, p. 1096−1100. https://doi.org/10.1128/AEM.52.5.1096-1100.1986.

Dhami, N.K., Mukherjee, A., and Watkin, E.L.J., 2018, Microbial Diversity and Mineralogical-Mechanical Properties of Calcitic Cave Speleothems in Natural and in Vitro Biomineralization Conditions: Frontiers in Microbiology, v. 9, p. 40. https://doi.org/10.3389/fmicb.2018.00040.

Dunham, R.J., 1972, Capitan Reef, New Mexico and Texas: Facts and Questions to Aid Interpretation and Group Discussion, Permian Basin Section-SEPM Publication 72-14: Midland, TX, Permian Basin Section-SEPM Publication 72-14, 291 p.

Edgar, R.C., 2010, Search and clustering orders of magnitude faster than BLAST: Bioinformatics, v. 26, no. 19, p. 2460-2461. https://doi.org/10.1093/bioinformatics/btq461.

Engel, A.S., 2010, Microbial diversity of cave ecosystems, *in* Barton, L.L., Mandl, M., and Loy, A., eds., Geomicrobiology: Molecular and Environmental Perspective: Dordrecht, Springer, p. 219−238. https://doi.org/10.1007/978-90-481-9204-5_10

Engel, A.S., Paoletti, M., Beggio, M., Dorigo, L., Pamio, A., Gomiero, T., Furlan, C., Brilli, M., Dreon, A.L., Bertoni, R., and Squartini, A., 2013, Comparative microbial community composition from secondary carbonate (moonmilk) deposits: implications for the Cansiliella servadeii cave hygropetric food web: International Journal of Speleology, v. 42, no. 3, p. 181−192. https://doi.org/10.5038/1827-806X.42.3.2.

Engel, A.S., Porter, M.L., Stern, L.A., Quinlan, S., and Bennett, P.C., 2004b, Bacterial diversity and ecosystem function of filamentous microbial mats from aphotic (cave) sulfidic springs dominated by chemolithoautotrophic "Epsilonproteobacteria": FEMS Microbiology Ecology, v. 51, no. 1, p. 31−53. https://doi.org/10.1016/j.femsec.2004.07.004.

Engel, A.S., Stern, L.A., and Bennett, P.C., 2004a, Microbial contributions to cave formation: New insights into sulfuric acid speleogenesis: Geology, v. 32, p. 369−372. https://doi.org/10.1130/G20288.1.

Estes, E.R., Andeer, P.F., Nordlund, D., Wankel, S.D., and Hansel, C.M., 2017, Biogenic manganese oxides as reservoirs of organic carbon and proteins in terrestrial and marine environments: Geobiology, v. 15, no. 1, p. 158−172. https://doi.org/10.1111/gbi.12195.

Even, H., Carmi, I., Magaritz, M., and Gerson, R., 1986, Timing the transport of water through the upper vadose zone in a karstic system above a cave in Israel: Earth Surface Processes and Landforms, v. 11, p. 181−191. https://doi.org/10.1002/esp.3290110208.

Fairchild, I.J., and Baker, A., 2012, Speleothem Science: From Process to Past Environments: Oxford, UK, Wiley-Blackwell, 432 p. https://doi.org/10.1002/9781444361094.

Farnleitner, A.H., Wilhartitz, I., Ryzinska, G., Kirschner, A.K., Stadler, H., Burtscher, M.M., Hornek, R., Szewzyk, U., Herndl, G., and Mach, R.L., 2005, Bacterial dynamics in spring water of alpine karst aquifers indicates the presence of stable autochthonous microbial endokarst communities: Environmental Microbiology, v. 7, no. 8, p. 1248−59. https://doi.org/10.1111/j.1462-2920.2005.00810.x.

Ferris, F.G., Phoenix, V.R., Fujita, Y., and Smith, R.W., 2003, Kinetics of calcite precipitation induced by ureolytic bacteria at 10 to 20°C in artificial groundwater: Geochimica et Cosmochimica Acta, v. 67, p. 1701−1722. https://doi.org/10.1016/S0016-7037(03)00503-9.

Forbes, J.R., 2000, Geochemistry of Carlsbad Cavern pool waters, Guadalupe Mountains, New Mexico: Journal of Cave and Karst Studies, v. 62, no. 2, p. 127−134.

Frost, E.L., Budd, D.A., and Kerans, C., 2013, Syndepositional deformation in a high-relief carbonate platform and its effect on early fluid flow as revealed by dolomite patterns: Journal of Sedimentary Research, v. 82, no. 12, p. 913−932. https://doi.org/10.2110/jsr.2012.74.

Genty, D., Labuhn, I., Hoffmann, G., Danis, P.A., Mestre, O., Bourges, F., Wainer, K., Massault, M., Van Exter, S., Régnier, E., Orengo, P., Falourd, S., and Minster, B., 2014, Rainfall and cave water isotopic relationships in two South-France sites: Geochimica et Cosmochimica Acta, v. 131, p. 323−343. https://doi.org/10.1016/j.gca.2014.01.043.

Giovannoni, S.J., DeLong, E.F., Schmidt, T.M., and Pace, N.R., 1990, Tangential flow filtration and preliminary phylogenetic analysis of marine picoplankton: Applied and Environmental Microbiology, v. 56, p. 2572−2575. https://doi.org/10.1128/AEM.56.8.2572-2575.1990.

Goldscheider, N., Hunkeler, D., and Rossi, P., 2006, Review: Microbial biocenoses in pristine aquifers and an assessment of investigative methods: Hydrogeology Journal, v. 14, no. 6, p. 926−941. https://doi.org/10.1007/s10040-005-0009-9.

Grice, E.A., and Segre, J.A., 2011, The skin microbiome: Nature Reviews Microbiology, v. 9, no. 4, p. 244−253. https://doi.org/10.1038/nrmicro2537.

Griebler, C., and Lueders, T., 2009, Microbial biodiversity in groundwater ecosystems: Freshwater Biology, v. 54, no. 4, p. 649−677. https://doi.org/10.1111/j.1365-2427.2008.02013.x.

Griffin, D.W., Gray, M.A., Lyles, M.B., and Northup, D.E., 2014, The transport of nonindigenous microorganisms into caves by human visitation: A case study at Carlsbad Caverns National Park: Geomicrobiology Journal, v. 31, no. 3, p. 175−185. https://doi.org/10.1080/01490451.2013.815294.

Groth, I., Schumann, P., Schütze, B., Augsten, K., and Stackebrandt, E., 2002, *Knoellia sinensis* gen. nov., sp. nov. and *Knoellia subterranea* sp. nov., two novel actinobacteria isolated from a cave: International Journal of Systematic and Evolutionary Microbiology, v. 52, p. 77−84. https://doi.org/10.1099/00207713-52-1-77

Gulden, B, 2020, Worlds longest caves, http://www.caverbob.com/wlong.htm, [accessed July 20, 2020].

Gutierrez, T., Green, D.H., Nichols, P.D., Whitman, W.B., Semple, K.T., and Aitken, M.D., 2013, *Polycyclovorans algicola* gen. nov., sp. nov., an aromatic-hydrocarbon-degrading marine bacterium found associated with laboratory cultures of marine phytoplankton: Applied and Environmental Microbiology, v. 79, no. 1, p. 205−214. https://doi.org/10.1128/AEM.02833-12.

Hershey, O.S., Kallmeyer, J., Wallace, A., Barton, M.D., and Barton, H.A., 2018, High microbial diversity despite extremely low biomass in a deep karst aquifer: Frontiers in Microbiology, v. 9, p. 2823. https://doi.org/10.3389/fmicb.2018.02823.

Hill, C.A., 1987, Geology of Carlsbad Cavern and Other Caves in the Guadalupe Mountains, New Mexico and Texas: Socorro, New Mexico, New Mexico Bureau of Mines and Mineral Resources, 150 p.

Hill, C.A., 1990, Sulfuric acid speleogenesis of Carlsbad Cavern and its relationship to hydrocarbons, Delaware Basin, New Mexico and Texas: American Association of Petroleum Geologists Bulletin, v. 74, p. 1685−1694.

Holmes, A.J., Tujula, N.A., Holley, M., Contos, A., James, J.M., Rogers, P., and Gillings, M.R., 2001, Phylogenetic structure of unusual aquatic microbial formations in Nullarbor cavees, Australia: Environmental Microbiology, v. 3, no. 4, p. 256−264. https://doi.org/10.1046/j.1462-2920.2001.00187.x.

Hose, L.D., and Macalady, J.L., 2006, Observations from active sulfidic karst systems: is the present the key to understanding Guadalupe Mountain speleogenesis, *in* Land, L., Lueth, V., Raatz, B., Boston, P.J., and Love, D., eds., Caves and Karst of Southeastern New Mexico, New Mexico Geological Society, p. 185−194.

Hose, L.D., Palmer, A.N., Palmer, M.V., Northup, D.E., Boston, P.J., and DuChene, H.R., 2000, Microbiology and geochemistry in a hydrogen-sulphide-rich karst environment: Chemical Geology, v. 169, p. 399−423. https://doi.org/10.1016/S0009-2541(00)00217-5

Hose, L.D., and Rosales-Lagarde, L., 2017, Sulfur-rich caves of southern Tabasco, Mexico, *in* Klimchouk, A.B., Palmer, A.N., DeWaele, J., Auler, A.S., and Audra, P., eds., Hypogene Karst Regions and Caves of the World, Springer International Publishing, p. 803−814. https://doi.org/10.1007/978-3-319-53348-3_54

Ikner, L.A., Toomey, R.S., Nolan, G., Neilson, J.W., Pryor, B.M., and Maier, R.M., 2007, Culturable microbial diversity and the impact of tourism in Kartchner Caverns, Arizona: Microbial Ecology, v. 53, no. 1, p. 30−42. https://doi.org/10.1007/s00248-006-9135-8

Ingraham, N.L., Chapman, J.B., and Hess, J.W., 1990, Stable isotopes in cave pool systems: Carlsbad Cavern, New Mexico, U.S.A.: Chemical Geology, v. 86, p. 65−74. https://doi.org/10.1016/0168-9622(90)90006-X.

Irgens, R.L., Gosink, J.J., and Staley, J.T., 1996, *Polaromonas vacuolata* gen. nov., sp. nov., a psychrophilic, marine, gas vacuolate bacterium from Antarctica: International Journal of Systematic Bacteriology, v. 46, p. 822−826. https://doi.org/10.1099/00207713-46-3-822.

Ivanova, N., Daum, C., Lang, E., Abt, B., Kopitz, M., Saunders, E., Lapidus, A., Lucas, S., Glavina Del Rio, T., Nolan, M., Tice, H., Copeland, A., Cheng, J.F., Chen, F., Bruce, D., Goodwin, L., Pitluck, S., Mavromatis, K., Pati, A., Mikhailova, N., Chen, A., Palaniappan, K., Land, M., Hauser, L., Chang, Y.J., Jeffries, C.D., Detter, J.C., Brettin, T., Rohde, M., Goker, M., Bristow, J., Markowitz, V., Eisen, J.A., Hugenholtz, P., Kyrpides, N.C., and Klenk, H.P., 2010, Complete genome sequence of *Haliangium ochraceum* type strain (SMP-2): Standards in Genomic Sciences, v. 2, no. 1, p. 96−106. https://doi.org/10.4056/sigs.69.1277.

Jagnow, D.H., 1979, Cavern Development in the Guadalupe Mountains: Columbus, Ohio, Cave Research Foundation, 55 p.

Jagnow, D.H., Hill, C.A., Davis, D.G., DuChene, H.R., Cunningham, K.I., Northup, D.E., and Queen, J.M., 2000, History of sulfuric acid theory of speleogenesis in the Guadalupe Mountains, New Mexico and west Texas: Journal of Cave and Karst Studies, v. 62, no. 2, p. 54−59.

Jang, J., Anderson, E.L., Venterea, R.T., Sadowsky, M.J., Rosen, C.J., Feyereisen, G.W., and Ishii, S., 2019, Denitrifying bacteria active in woodchip bioreactors at low-temperature conditions: Frontiers in Microbiology, v. 10, p. 635. https://doi.org/10.3389/fmicb.2019.00635.

Jones, A.A., and Bennett, P.C., 2017, Mineral Ecology: Surface specific colonization and geochemical drivers of biofilm accumulation, composition, and phylogeny: Frontiers in Microbiology, v. 8, p. 491. https://doi.org/10.3389/fmicb.2017.00491.

Jones, D.S., Schaperdoth, I., and Macalady, J.L., 2016, Biogeography of sulfur-oxidizing *Acidithiobacillus* populations in extremely acidic cave biofilms: ISEM Journal, v. 10, p. 2879−2891. https://doi.org/10.1038/ismej.2016.74.

Karwautz, C., Kus, G., Stockl, M., Neu, T.R., and Lueders, T., 2018, Microbial megacities fueled by methane oxidation in a mineral spring cave: International Society for Microbial Ecology Journal, v. 12, no. 1, p. 87−100. https://doi.org/10.1038/ismej.2017.146.

Kaufman, A., Bar-Matthews, M., Ayalon, A., and Carmi, I., 2003, The vadose flow above Soreq Cave, Israel: a tritium study of the cave waters: Journal of Hydrology, v. 273, p. 155−163. https://doi.org/10.1016/S0022-1694(02)00394-3.

Kim, B.R., Shin, J., Guevarra, R., Lee, J.H., Kim, D.W., Seol, K.H., Lee, J.H., Kim, H.B., and Isaacson, R., 2017, Deciphering Diversity Indices for a Better Understanding of Microbial Communities: Journal of Microbiology and Biotechnology, v. 27, no. 12, p. 2089−2093. https://doi.org/10.4014/jmb.1709.09027.

Kirkland, D.W., 2014, Role of Hydrogen Sulfide in the Formation of Cave and Karst Phenomena in the Guadalupe Mountains and Western Delaware Basin, New Mexico and Texas, National Cave and Karst Research Institute, 77 p.

Kirs, M., Kisand, V., Nelson, C.E., Dudoit, T., and Moravcik, P.S., 2020, Distinct bacterial communities in tropical island aquifers: PLOS One, v. 15, no. 4, p. e0232265. https://doi.org/10.1371/journal.pone.0232265.

Koch, H., Lucker, S., Albertsen, M., Kitzinger, K., Herbold, C., Spieck, E., Nielsen, P.H., Wagner, M., and Daims, H., 2015, Expanded metabolic versatility of ubiquitous nitrite-oxidizing bacteria from the genus Nitrospira: Proceedings of the National Academy of Sciences of the United States of America, v. 112, no. 36, p. 11371−11376. https://doi.org/10.1073/pnas.1506533112.

Kumaresan, D., Stephenson, J., Doxey, A.C., Bandukwala, H., Brooks, E., Hillebrand-Voiculescu, A., Whiteley, A.S., and Murrell, J.C., 2018, Aerobic proteobacterial methylotrophs in Movile Cave: genomic and metagenomic analyses: Microbiome, v. 6, no. 1, p. 1. https://doi.org/10.1186/s40168-017-0383-2.

Land, L., and Burger, P., 2008, Rapid recharge events in a karstic aquifer: An example from Lake of the White Roses, Lechuguilla Cave, New Mexico, *in* 11th Multidisciplinary Conference on Sinkholes and the Engineering and Environmental Impacts of Karst, Tallahassee, Florida, ASCE Geotechnical Special Publication no. 183, p. 396–403 https://doi.org/10.1061/41003(327)37.

Lane, D.J., 1991, 16S/23S rRNA sequencing, *in* Stackebrandt, E., and Goodfellow, M, eds, Nucleic Acid Techniques in Bacterial Systematics, p. 115−175.

Lavoie, K.H., and Northup, D.E., 2005, Bacteria as indicators of human impact in caves, *in* Rea, G.T., ed., 17th National Cave and Karst Management Symposium, NICKMS Steering Committee, p. 40−47.

Lavoie, K.H., Winter, A.S., Read, K.J., Hughes, E.M., Spilde, M.N., and Northup, D.E., 2017, Comparison of bacterial communities from lava cave microbial mats to overlying surface soils from Lava Beds National Monument, USA: PLOS One, v. 12, no. 2, p. e0169339.

Lechleitner, F.A., Dittmar, T., Baldini, J.U.L., Prufer, K.M., and Eglinton, T.I., 2017, Molecular signatures of dissolved organic matter in a tropical karst system: Organic Geochemistry, v. 113, p. 141−149. https://doi.org/10.1016/j.orggeochem.2017.07.015.

Legatzki, A., Ortiz, M., Neilson, J.W., Casavant, R.R., Palmer, M.W., Rasmussen, C., Pryor, B.M., Pierson, L.S., and Maier, R.M., 2012, Factors influencing observed variations in the structure of bacterial communities on calcite formations in Kartchner Caverns, AZ, USA: Geomicrobiology Journal, v. 29, no. 5, p. 422−434. https://doi.org/10.1080/01490451.2011.581326.

Legatzki, A., Ortiz, M., Neilson, J.W., Dominguez, S., Andersen, G.L., Toomey, R.S., Pryor, B.M., Pierson, L.S., and Maier, R.M., 2011, Bacterial and Archaeal community structure of two adjacent calcite speleothems in Kartchner Caverns, Arizona, USA: Geomicrobiology Journal, v. 28, no. 2, p. 99−117. https://doi.org/10.1080/01490451003738465.

Leuko, S., Koskinen, K., Sanna, L., D'Angeli, I.M., De Waele, J., Marcia, P., Moissl-Eichinger, C., and Rettberg, P., 2017, The influence of human exploration on the microbial community structure and ammonia oxidizing potential of the Su Bentu limestone cave in Sardinia, Italy: PLOS One, v. 12, no. 7, p. e0180700. https://doi.org/10.1371/journal.pone.0180700.

Levy, D.B., 2007a, Geochemical trends in selected Lechuguilla Cave pools: Journal of Cave and Karst Studies, v. 69, no. 3, p. 342−350.

Levy, D.B., 2007b, Oxidation-reduction chemistry of Lechuguilla Cave seepage: Journal of Cave and Karst Studies, v. 69, no. 3, p. 351−358.

Levy, D.B., and Amrhein, C., 2011, Geochemical evolution of hypersaline cave pools, Guadalupe Mountains, New Mexico: Chemical Geology, v. 290, no. 1-2, p. 60−66. https://doi.org/10.1016/j.chemgeo.2011.08.012.

Li, W., Liu, X., and Niu, S., 2019, Differential responses of the acidobacterial community in the topsoil and subsoil to fire disturbance in *Pinus tabulaeformis* stands: PeerJ – Life & Environment, v. 7, p. e8047. https://doi.org/10.7717/peerj.8047.

Logan, N.A., and De Vos, P., 2015, *Bacillus*, *in* Whitman, W.B., ed., Bergey's Manual of Systematics of Archaea and Bacteria, p. 1−163. https://doi.org/10.1002/9781118960608.gbm00530.

Loy, A., Beisker, W., and Meier, H., 2005, Diversity of bacteria growing in natural mineral water after bottling: Applied and Environmental Microbiology, v. 71, no. 7, p. 3624−3632. https://doi.org/10.1128/AEM.71.7.3624-3632.2005.

Lu, X., 2018, Distribution and Function of Soil *Thaumarchaeota*: University of Waterloo, 159 p.

Macalady, J.L., Dattagupta, S., Schaperdoth, I., Jones, D.S., Druschel, G.K., and Eastman, D., 2008, Niche differentiation among sulfur-oxidizing bacterial populations in cave waters: International Society for Microbial Ecology Journal, v. 2, no. 6, p. 590−601. https://doi.org/10.1038/ismej.2008.25.

Macalady, J.L., Jones, D.S., and Lyon, E.H., 2007, Extremely acidic, pendulous cave wall biofilms from the Frasassi cave system, Italy: Environmental Microbiology, v. 9, p. 1402-1414. https://doi.org/10.1111/j.1462-2920.2007.01256.x.

Macalady, J.L., Lyon, E.H., Koffman, B., Albertson, L.K., Meyer, K., Galdenzi, S., and Mariani, S., 2006, Dominant microbial populations in limestone-corroding stream biofilms, Frasassi cave system, Italy: Applied and Environmental Microbiology, v. 72, no. 8, p. 5596−5609.https://doi.org/10.1128/AEM.00715-06.

McDonald, D., Price, M.N., Goodrich, J., Nawrocki, E.P., DeSantis, T.Z., Probst, A., Andersen, G.L., Knight, R., and Hugenholtz, P., 2012, An improved Greengenes taxonomy with explicit ranks for ecological and evolutionary analyses of bacteria and archaea: International Society for Microbial Ecology Journal, v. 6, no. 3, p. 610−618. https://doi.org/10.1038/ismej.2011.139.

McMurdie, P.J., and Holmes, S., 2013, Phyloseq: an R package for reproducible interactive analysis and graphics of microbiome census data: PLOS One, v. 8, no. 4, p. e61217. https://doi.org/10.1371/journal.pone.0061217.

Meisinger, D.B., Zimmermann, J., Ludwig, W., Schleifer, K.H., Wanner, G., Schmid, M., Bennett, P.C., Engel, A.S., and Lee, N.M., 2007, *In situ* detection of novel Acidobacteria in microbial mats from a chemolithoautotrophically based cave ecosystem (Lower Kane Cave, WY, USA): Environmental Microbiology, v. 9, no. 6, p. 1523−34. https://doi.org/10.1111/j.1462-2920.2007.01271.x.

Melim, L.A., Brehm, A., Rust, G., Shannon, N., and Northup, D.E., 2006, The unknown crust beneath your feet: Cave pool precipitates of Lower Cave, Carlsbad Cavern, New Mexico, *in* Raatz, W., Land, L., and Boston, P.J., eds., Caves and Karst of Southeastern New Mexico, New Mexico Geological Society Guidebook, 57th Field Conference, p. 38−40.

Melim, L.A., and Scholle, P.A., 2002, Dolomitization of the Capitan Formation forereef facies (Permian, West Texas and New Mexico): Seepage reflux revisited: Sedimentology, v. 49, no. 6, p. 1207−1228. https://doi.org/10.1046/j.1365-3091.2002.00492.x.

Melim, L.A., and Spilde, M.N., 2018, A New Unified Model For Cave Pearls: Insights from cave pearls in Carlsbad Cavern, New Mexico, U.S.A: Journal of Sedimentary Research, v. 88, no. 3, p. 344−364. https://doi.org/10.2110/jsr.2018.21.

Mercier, C., Boyer, F., Bonin, A., and Coissac, E., 2013, SUMATRA and SUMACLUST: fast and exact comparison and clustering of sequences, SeqBio Invited talks, p. 27−29.

Mischel, S.A., Scholz, D., and Spötl, C., 2015, δ18O values of cave drip water: a promising proxy for the reconstruction of the North Atlantic Oscillation?: Climate Dynamics, v. 45, no. 11−12, p. 3035-3050. https://doi.org/10.1007/s00382-015-2521-5.

Mohr, K.I., 2018, Diversity of Myxobacteria-We only see the tip of the iceberg: Microorganisms, v. 6, no. 3., 23 p. https://doi.org/10.3390/microorganisms6030084.

Momper, L., Jungbluth, S.P., Lee, M.D., and Amend, J.P., 2017, Energy and carbon metabolisms in a deep terrestrial subsurface fluid microbial community: International Society for Microbial Ecology Journal, v. 11, no. 10, p. 2319−2333. https://doi.org/10.1038/ismej.2017.94.

Naether, A., Foesel, B.U., Naegele, V., Wust, P.K., Weinert, J., Bonkowski, M., et al., 2012, Environmental factors affect Acidobacterial communities below the subgroup level in grassland and forest soils: Applied and Environmental Microbiology, v. 78, no. 20, p. 7398−7406. https://doi.org/10.1128/AEM.01325-12

NCBI, 2020, Nucleotide, https://www.ncbi.nlm.nih.gov/nucleotide?cmd=search [Accessed July 10, 2020].

Northup, D.E., Barnes, S.M., Yu, L.E., Spilde, M.N., Scheble, R.T., Dano, K.E., Crossey, L.J., Connolly, C.A., Boston, P.J., Natvig, D.O., and Dahm, C.N., 2003, Diverse microbial communities inhabiting ferromanganese deposits in Lechuguilla and Spider Caves: Environmental Microbiology, v. 5, p. 1071−1086. https://doi.org/10.1046/j.1462-2920.2003.00500.x.

Northup, D.E., Snider, J.R., Spilde, M.N., Porter, M.L., van de Kamp, J.L., Boston, P.J., Nyberg, A.M., and Bargar, J.R., 2010, Diversity of rock varnish bacterial communities from Black Canyon, New Mexico, Journal of Geophysical Research, v. 115, p. G02007, doi:10.1029/2009JG001107

Ortiz, M., Legatzki, A., Neilson, J.W., Fryslie, B., Nelson, W.M., Wing, R.A., Soderlund, C.A., Pryor, B.M., and Maier, R.M., 2014, Making a living while starving in the dark: metagenomic insights into the energy dynamics of a carbonate cave: International Society for Microbial Ecology Journal, v. 8, p. 478−491. https://doi.org/10.1038/ismej.2013.159.

Ortiz, M., Neilson, J.W., Nelson, W.M., Legatzki, A., Byrne, A., Yu, Y., Wing, R.A., Soderlund, C.A., Pryor, B.M., Pierson, L.S., 3rd, and Maier, R.M., 2013, Profiling bacterial diversity and taxonomic composition on speleothem surfaces in Kartchner Caverns, AZ: Microbial Ecology, v. 65, no. 2, p. 371−383. https://doi.org/10.1007/s00248-012-0143-6.

Oster, J.L., Montañez, I.P., and Kelley, N.P., 2012, Response of a modern cave system to large seasonal precipitation variability: Geochimica et Cosmochimica Acta, v. 91, p. 92−108. https://doi.org/10.1016/j.gca.2012.05.027.

Palmer, A.N., 2006, Support for a sulfuric acid origin for caves in the Guadalupe Mountains, New Mexico, *in* Land, L., Lueth, V., Raatz, B., Boston, P.J., and Love, D., eds., Caves and Karst of Southeastern New Mexico, New Mexico Geological Society, p. 195−202.

Palmer, A.N., 2007, Cave Geology: Dayton, Ohio, Cave Books, 454 p.

Palmer, A.N., and Palmer, M.V., 2000, Hydrochemical interpretation of cave patterns in the Guadalupe Mountains, New Mexico: Journal of Cave and Karst Studies, v. 62, no. 2, p. 91−108.

Palmer, M., and Palmer, A., 2012, Petrographic and isotopic evidence for late-stage processes in sulfuric acid caves of the Guadalupe Mountains, New Mexico, USA: International Journal of Speleology, v. 41, no. 2, p. 231−250. https://doi.org/10.5038/1827-806X.41.2.10.

Pagnier, I., Raoult, D., and La Scola, B., 2011, Isolation and characterization of *Reyranella massiliensis* gen. nov., sp. nov. from freshwater samples by using an amoeba co-culture procedure: International Journal of Systematic and Evolutionary Microbiology, v. 61, no. Pt 9, p. 2151−2154. https://doi.org/10.1099/ijs.0.025775-0.

Parro, V., and Moreno-Paz, M., 2004, Nitrogen fixation in acidophile iron-oxidizing bacteria: the *nif* regulon of *Leptospirillium ferrooxidans*: Research in Microbiology, v. 155, p. 703−709. https://doi.org/10.1016/j.resmic.2004.05.010.

Pichinoty, F., de Barjac, H., Mandel, M., and Asselineau, J., 1983, Description of *Bacillus azotoformans* sp. nov.: International Journal of Systematic Bacteriology, v. 33, p. 660−662. https://doi.org/10.1099/00207713-33-3-660.

Plese, B., Pojskic, N., Ozimec, R., Mazija, M., Cetkovic, H., and Lukic-Bilela, L., 2016, Molecular characterization of aquatic bacterial communities in Dinaric Range caves: Water Environment Research, v. 88, p. 617−630. https://doi.org/10.2175/106143016X14609975746488.

Polyak, V.J., Asmerom, Y., Burns, S.J., and Lachniet, M.S., 2012, Climatic backdrop to the terminal Pleistocene extinction of North American mammals: Geology, v. 40, no. 11, p. 1023−1026. https://doi.org/10.1130/G33226.1.

Polyak, V.J., McIntosh, W.C., Güven, N., and Provencio, P., 1998, Age and origin of Carlsbad Cavern and related caves from $^{40}Ar/^{39}Ar$ of alunite: Science, v. 279, p. 1919−1922. https://doi.org/10.1126/science.279.5358.1919.

Porca, E., Jurado, V., Zgur-Bertok, D., Saiz-Jimenez, C., and Pasic, L., 2012, Comparative analysis of yellow microbial communities growing on the walls of geographically distinct caves indicates a common core of microorganisms involved in their formation: FEMS Microbiology Ecology, v. 81, no. 1, p. 255−266. https://doi.org/10.1111/j.1574-6941.2012.01383.x.

Porter, M.L., Engel, A.S., Kane, T.C., and Kinkle, B.K., 2009, Productivity-diversity relationships from chemolithoautotrophically based sulfidic karst systems: International Journal of Speleology, v. 38, p. 27−40. https://doi.org/10.5038/1827-806X.38.1.4.

Pronk, M., Goldscheider, N., and Zopfi, J., 2009, Microbial communities in karst groundwater and their potential use for biomonitoring: Hydrogeology Journal, v. 17, no. 1, p. 37−48. https://doi.org/10.1007/s10040-008-0350-x.

R Development Core Team, 2012, R: A language and environment for statistical computing. Vienna: R Foundation for Statistical Computing. Available: http://www.R-project.org

Rivas-Marin, E., and Devos, D.P., 2018, The paradigms they are a-changin': Past, present and future of PVC bacteria research: Antonie Van Leeuwenhoek, v. 111, no. 6, p. 785−799. https://doi.org/10.1007/s10482-017-0962-z.

Rusterholtz, K.J., and Mallory, L.M., 1994, Density, activity, and diversity of bacteria indigenous to a karst aquifer: Microbial Ecology, v. 28, p. 79−99. https://doi.org/10.1007/BF00170249

Sarbu, S.M., Kane, T.C., and Kinkle, B.K., 1996, A Chemoautotrophically based cave ecosystem: Science, v. 272, p. 1953−1955. https://doi.org/10.1126/science.272.5270.1953.

Sauro, F., Cappelletti, M., Ghezzi, D., Columbu, A., Hong, P.Y., Zowawi, H.M., Carbone, C., Piccini, L., Vergara, F., Zannoni, D., and De Waele, J., 2018, Microbial diversity and biosignatures of amorphous silica deposits in orthoquartzite caves: Scientific Reports, v. 8, no. 1, p. 17569. https://doi.org/10.1038/s41598-018-35532-y.

Savio, D., Stadler, P., Reischer, G.H., Demeter, K., Linke, R.B., Blaschke, A.P., Mach, R.L., Kirschner, A.K.T., Stadler, H., and Farnleitner, A.H., 2019, Spring water of an alpine karst aquifer is dominated by a taxonomically stable but discharge-responsive bacterial community: Frontiers in Microbiology, v. 10, p. 28. https://doi.org/10.3389/fmicb.2019.00028.

Savio, D., Stadler, P., Reischer, G.H., Kirschner, A.K.T., Demeter, K., Linke, R., et al., 2018, Opening the black box of spring water microbiology from alpine karst aquifers to support proactive drinking water resource management: WIREs Water, v. 5, no. 3, p. e1282. https://doi.org/10.1002/wat2.1282.

Shabarova, T., and Pernthaler, J., 2010, Karst pools in subsurface environments: Collectors of microbial diversity or temporary residence between habitat types: Environmental Microbiology, v. 12, p. 1061−1074. https://doi.org/10.1111/j.1462-2920.2009.02151.x.

Shabarova, T., Villiger, J., Morenkov, O., Niggemann, J., Dittmar, T., and Pernthaler, J., 2014, Bacterial community structure and dissolved organic matter in repeatedly flooded subsurface karst water pools: FEMS Microbiology Ecology, v. 89, no. 1, p. 111−26. https://doi.org/10.1111/1574-6941.12339.

Shabarova, T., Widmer, F., and Pernthaler, J., 2013, Mass effects meet species sorting: transformations of microbial assemblages in epiphreatic subsurface karst water pools: Environmental Microbiology, v. 15, no. 9, p. 2476−2488. https://doi.org/10.1111/1462-2920.12124.

Shen, Y., Chapelle, F.H., Strom, E.W., and Benner, R., 2015, Origins and bioavailability of dissolved organic matter in groundwater: Biogeochemistry, v. 122, no. 1, p. 61−78. https://doi.org/10.1007/s10533-014-0029-4.

Simon, K.S., Pipan, T., and Culver, D.C., 2007, A conceptual model of the flow and distribution of organic carbon in caves: Journal of Cave and Karst Studies, v. 69, p. 279−284.

Spilde, M.N., Northup, D.E., Boston, P.J., Schelble, R.T., Dano, K.E., Crossey, L.J., and Dahm, C.N., 2005, Geomicrobiology of cave ferromanganese deposits; a field and laboratory investigation: Geomicrobiology Journal, v. 22, p. 99-116. https://doi.org/10.1080/01490450590945889.

Spötl, C., Fairchild, I.J., and Tooth, A.F., 2005, Cave air control on dripwater geochemistry, Obir Caves (Austria): Implications for speleothem deposition in dynamically ventilated caves: Geochimica et Cosmochimica Acta, v. 69, p. 2451−2468. https://doi.org/10.1016/j.gca.2004.12.009.

Stackebrandt, E., Cummins, C.S., and Johnson, J.L., 2006, Family Propionibacteriaceae: The Genus *Propionibacterium*, *in* Dworkin, M., Falkow, S., Rosenberg, E., Schleifer, K.H., and Stackebrandt, E., eds., The Prokaryotes: New York, NY, Springer, p. 400−418. https://doi.org/10.1007/0-387-30743-5_19.

Swart, R., Riedel, K.-H., and Britz, T., 1998, Optimized standard conditions for determination of nitrate reduction in *Propionibacteria*: Lait, v. 78, p. 217−226. https://doi.org/10.1051/Lait:1998224.

Tetu, S.G., Breakwell, K., Elbourne, L.D., Holmes, A.J., Gillings, M.R., and Paulsen, I.T., 2013, Life in the dark: metagenomic evidence that a microbial slime community is driven by inorganic nitrogen metabolism: International Society For Microbial Ecology Journal, v. 7, no. 6, p. 1227−1236. https://doi.org/10.1038/ismej.2013.14.

Thompson, B., Richardson, D., Vangundy, R., and Cahoon, A.B., 2019, Metabarcoding comparison of prokaryotic microbiomes from Appalachian karst caves to surface soils in southwest Virginia, USA: Journal of Cave and Karst Studies, p. 244−253. https://doi.org/10.4311/2019MB0112

Thompson, H.F., Lesaulnier, C., Pelikan, C., and Gutierrez, T., 2018, Visualisation of the obligate hydrocarbonoclastic bacteria *Polycyclovorans algicola* and *Algiphilus aromaticivorans* in co-cultures with micro-algae by CARD-FISH: Journal of Microbiological Methods, v. 152, p. 73−79. https://doi.org/10.1016/j.mimet.2018.07.016.

Tomczyk-Żak, K., and Zielenkiewicz, U., 2015, Microbial diversity in caves: Geomicrobiology Journal, v. 33, no. 1, p. 20−38. https://doi.org/10.1080/01490451.2014.1003341.

Tredici, S.M., Buccolieri, A., Tanini, L., Calcagnile, M., Manno, D., and Alifano, P., 2018, Calcite-forming *Bacillus licheniformis* thriving on underwater speleothems of a hydrothermal cave: Geomicrobiology Journal, v. 35, no. 9, p. 804−817. https://doi.org/10.1080/01490451.2018.1476626.

Turin, H.J., and Plummer, M.A., 1995, Tritium in Lechuguilla Cave pool water: Implications for recharge processes: Geological society of America Abstracts with Programs, v. 27, p. 95.

Turin, H.J., and Plummer, M.A., 2000, Lechuguilla Cave pool chemistry, 1986−1999: Journal of Cave and Karst Studies, v. 62, p. 135−143.

Turin, H.J., and Plummer, M.A., 2001, Isotope profiles from three deep western U.S. caves: Insights into arid-region vadose-zone processes: Geological Society of America, Abstracts with Program, v. 33, p. A-110.

Turin, H.J., Plummer, M.A., Phillips, F.M., and Thompson, M.L., 2001, Vadose-zone infiltration velocities: Evidence from Lechuguilla cave pool radioisotopes: Geological Society of America Abstracts with Programs, v. 33, p. 60.

Tyson, G.W., Lo, I., Baker, B.J., Allen, E.E., Hugenholtz, P., and Banfield, J.F., 2005, Genome-directed isolation of the key nitrogen fixer *Leptospirillum ferrodiazotrophum* sp. nov. from an acidophilic microbial community: Applied and Environmental Microbiology, v. 71, no. 10, p. 6319−6324. https://doi.org/10.1128/AEM.71.10.6319-6324.2005.

van der Heijde, P.K.M., Kolm, K.E., Dawson, H.E., and Brooke, M., 1997, Determining Water Infiltration Routes from Structures Located Above Carlsbad Cavern, Carlsbad Caverns National Park, Carlsbad, New Mexico: International Ground Water Modeling Center, Colorado School of Mines, 90 p.

Vimercati, L., Darcy, J.L., and Schmidt, S.K., 2019, The disappearing periglacial ecosystem atop Mt. Kilimanjaro supports both cosmopolitan and endemic microbial communities: Scientific Reports, v. 9, no. 1, p. 10676. https://doi.org/10.1038/s41598-019-46521-0.

Wang, Z., Chang, X., Yang, X., Pan, L., and Dai, J., 2014, Draft genome sequence of *Polaromonas glacialis* strain R3-9, a psychrotolerant bacterium isolated from arctic glacial foreland: Genome Announcements, v. 2, no. 4, p. e00695-14. https://doi.org/10.1128/genomeA.00695-14.

Wegner, C.-E., Gaspar, M., Geesink, P., Herrmann, M., Marz, M., and Küsel, K., 2019, Biogeochemical regimes in shallow aquifers reflect the metabolic coupling of the elements nitrogen, sulfur, and carbon: Applied and Environmental Microbiology, v. 85, p. e02346-18. https://doi.org/10.1128/AEM.00502-19.

Wickham, H., 2009, ggplot2: Elegant Graphics for Data Analysis: New York, NY, Springer, 212 p. https://doi.org/10.1007/978-0-387-98141-3.

Williams, P.W., 1983, The role of the subcutaneous zone in karst hydrology: Journal of Hydrology, v. 61, p. 45−67. https://doi.org/10.1016/0022-1694(83)90234-2.

Williams, P.W., and Fowler, A., 2002, Relationship between oxygen isotopes in rainfall, cave percolation waters and speleothem calcite at Waitomo, New Zealand: Journal of Hydrology (New Zealand), v. 41, p. 53−70.

Wu, Y., Tan, L., Liu, W., Wang, B., Wang, J., Cai, Y., and Lin, X., 2015, Profiling bacterial diversity in a limestone cave of the western Loess Plateau of China: Frontiers in Microbiology, v. 6, p. 244. https://doi.org/10.3389/fmicb.2015.00244.

Yasir, M., 2018, Analysis of bacterial communities and characterization of antimicrobial strains from cave microbiota: Brazilian Journal Microbiology, v. 49, no. 2, p. 248−257. https://doi.org/10.1016/j.bjm.2017.08.005.

Yousuf, J., Thajudeen, J., P.A, Aeesa., Joseph, A., Divya, P.S, Varghese, A., and Mohamed Hatha, A.A, 2020, Diversity and activity of culturable nitrogen fixing heterotrophic bacteria from estuarine and coastal environments of Southeastern Arabian Sea (SEAS): Regional Studies in Marine Science, v. 33, p. 100973. https://doi.org/10.1016/j.rsma.2019.100973.

Yun, Y., Wang, H., Man, B., Xiang, X., Zhou, J., Qiu, X., Duan, Y., and Engel, A.S., 2016, The Relationship between pH and bacterial communities in a single karst ecosystem and its implication for soil acidification: Frontiers in Microbiology, v. 7, p. 1955. https://doi.org/10.3389/fmicb.2016.01955.

Yun, Y., Xiang, X., Wang, H., Man, B., Gong, L., Liu, Q., Dong, Q., and Wang, R., 2015, Five-year monitoring of bacterial communities in dripping water from the Heshang Cave in Central China: Implication for Paleoclimate Reconstruction and Ecological Functions: Geomicrobiology Journal, v. 33, no. 7, p. 1−11. https://doi.org/10.1080/01490451.2015.1062062.

Zhou, J., Gu, Y., Zou, C., and Mo, M., 2007, Phylogenetic diversity of bacteria in an earth-cave in Guizhou Province, Southwest of China: Journal of Microbiology, v. 45, p. 105−112.

Zimmermann, J., Gonzalez, J.M., and Saiz-Jimenez, C., 2006, Epilithic biofilms in Saint Callixtus Catacombs (Rome) harbour a broad spectrum of Acidobacteria: Antonie Van Leeuwenhoek, v. 89, no. 1, p. 203−208. https://doi.org/10.1007/s10482-005-9020-3.

Zimmermann, J., Gonzalez, J.M., Saiz-Jimenez, C., and Ludwig, W., 2005, Detection and phylogenetic relationships of highly diverse uncultured acidobacterial communities in Altamira Cave using 23S rRNA sequence analyses: Geomicrobiology Journal, v. 22, no. 7-8, p. 379−388. https://doi.org/10.1080/01490450500248986.

GUIDE TO AUTHORS

The *Journal of Cave and Karst Studies* is a multidisciplinary journal devoted to cave and karst research. The *Journal* is seeking original, unpublished manuscripts concerning the scientific study of caves or other karst features. Authors do not need to be members of the National Speleological Society, but preference is given to manuscripts of importance to North American speleology.

LANGUAGES: The *Journal of Cave and Karst Studies* uses American-style English as its standard language and spelling style, with the exception of allowing a second abstract in another language when room allows. In the case of proper names, the *Journal* tries to accommodate other spellings and punctuation styles. In cases where the Editor-in-Chief finds it appropriate to use non-English words outside of proper names (generally where no equivalent English word exist), the *Journal* italicizes them. However, the common abbreviations i.e., e.g., et al., and etc. should appear in roman text. Authors are encouraged to write for our combined professional and amateur readerships

CONTENT: Each paper will contain a title with the authors' names and addresses, an abstract, and the text of the paper, including a summary or conclusions section. Acknowledgments and references follow the text. Manuscripts should be limited to 6,000 words and no more than 10 figures and 5 tables. Larger manuscripts may be considered, but the *Journal* reserves the right to charge processing fees for larger submissions.

ABSTRACTS: An abstract stating the essential points and results must accompany all articles. An abstract is a summary, not a promise of what topics are covered in the paper.

STYLE: The *Journal* consults The Chicago Manual of Style on most general style issues.

REFERENCES: In the text, references to previously published work should be followed by the relevant author's name and date (and page number, when appropriate) in brackets. All cited references are alphabetical at the end of the manuscript with senior author's last name first, followed by date of publication, title, publisher, volume, and page numbers. Geological Society of America format should be used (see http://www.geosociety.org/documents/gsa/pubs/GSA_RefGuide_Examples.pdf). Please do not abbreviate periodical titles. Web references are acceptable when deemed appropriate. The references should follow the style of: Author (or publisher), year, Webpage title: Publisher (if a specific author is available), full URL (e.g., http://www.usgs.gov/citguide.html), and the date the website was accessed in brackets. If there are specific authors given, use their name and list the responsible organization as publisher. Because of the ephemeral nature of websites, please provide the specific date. Citations within the text should read: (Author, Year).

SUBMISSION: Manuscripts are to be submitted via the PeerTrack submission system at http://www.edmgr.com/jcks/. Instructions are provided at that address. At your first visit, you will be prompted to establish a login and password, after which you will enter information about your manuscript and upload your manuscript, tables, and figure files. Manuscript files can be uploaded as DOC, WPD, RTF, TXT, or LaTeX. Note: LaTeX files should not use any unusual style files; a LaTeX template and BiBTeX file may be obtained from the Editor-in-Chief. Table files can be uploaded as DOC, WPD, RTF, TXT, or LaTeX files and figure files can be uploaded as TIFF, AI, EPS, or CDR files. Extensive supporting data may be placed on the Journal's website as supplemental material at the discretion of the Editor-in-Chief. The data that are used within a paper must be made available upon request. Authors may be required to provide supporting data in a fundamental format, such as ASCII for text data or comma-delimited ASCII for tabular data.

DISCUSSIONS: Critical discussions of papers previously published in the *Journal* are welcome. Authors will be given an opportunity to reply. Discussions and replies must be limited to a maximum of 1000 words and discussions will be subject to review before publication. Discussions must be within 6 months after the original article appears.

MEASUREMENTS: All measurements will be in Systeme Internationale (metric) except when quoting historical references. Other units will be allowed where necessary if placed in parentheses and following the SI units.

FIGURES: Figures and lettering must be neat and legible. Figure captions should be on a separate sheet of paper and not within the figure. Figures should be numbered in sequence and referred to in the text by inserting (Fig. x). Most figures will be reduced, hence the lettering should be large. Photographs must be sharp and high contrast. Figures must have a minimum resolution of 300 dpi for acceptance. Please do not submit JPEG images.

TABLES: See http://caves.org/pub/journal/PDF/Tables.pdf to get guidelines for table layout.

COPYRIGHT AND AUTHOR'S RESPONSIBILITIES: It is the author's responsibility to clear any copyright or acknowledgement matters concerning text, tables, or figures used. Authors should also ensure adequate attention to sensitive or legal issues such as land owner and land manager concerns or policies and cave location disclosures.

PROCESS: All submitted manuscripts are sent out to at least two experts in the field. Reviewed manuscripts are then returned to the author for consideration of the referees' remarks and revision, where appropriate. Revised manuscripts are returned to the appropriate Associate Editor who then recommends acceptance or rejection. The Editor-in-Chief makes final decisions regarding publication. Upon acceptance, the senior author will be sent one set of PDF proofs for review. Examine the current issue for more information about the format used.

Journal of Cave and Karst Studies

Volume 83 Number 4 December 2021

CONTENTS